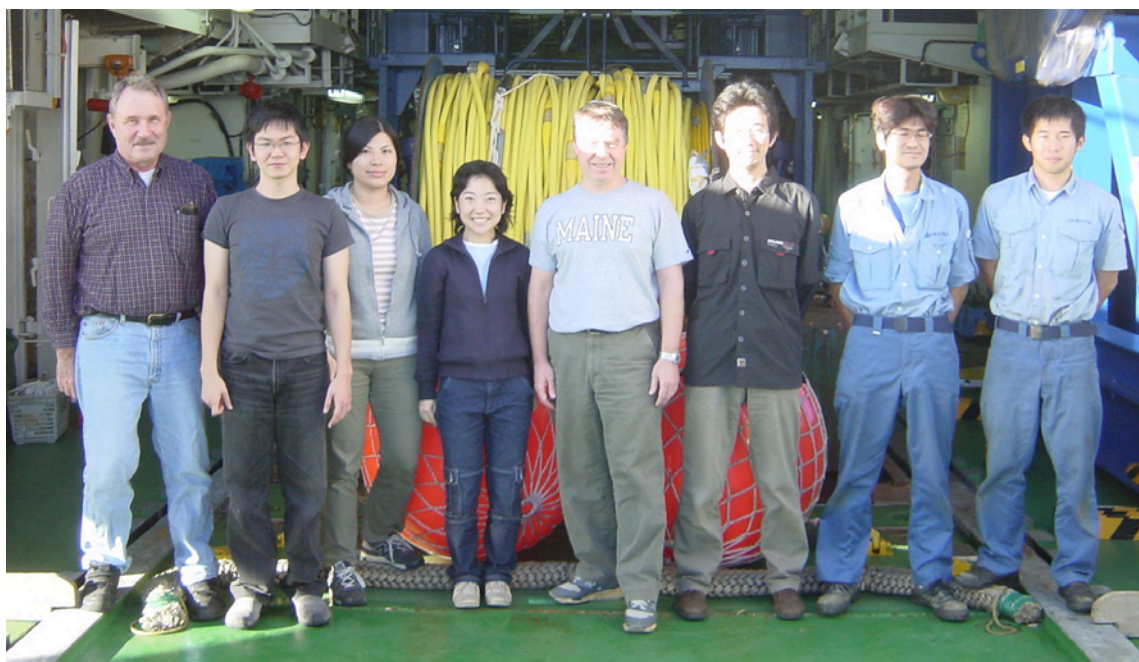# Cruise Report

R/V *Kairei* KR05-01

Origin of the Ontong Java Plateau

5-25 January 2005

Millard F. Coffin
Yasuyuki Nakamura
Hiroyuki Inoue
Mizuki Watanabe
Ocean Research Institute, University of Tokyo

Junko Sarayama
Chiba University

Loren Kroenke
University of Hawaii

Yuki Ohwatari
Mamoru Sano
Nippon Marine Enterprises

KR05-01 Shipboard Scientific Party Contact Details

Prof. Millard F. Coffin (Chief scientist and Representative of the Science Party)
Ocean Research Institute
University of Tokyo

Mr. Hiroyuki Inoue
Ocean Research Institute
University of Tokyo

Dr. Loren Kroenke
School of Ocean & Earth Science & Technology
University of Hawaii at Manoa

Dr. Yasuyuki Nakamura
Ocean Research Institute
University of Tokyo

Ms. Junko Sarayama
Graduate School of Science and Technology
Chiba University

Ms. Mizuki Watanabe
Ocean Research Institute
University of Tokyo

総端艇部署表 LIFEBOAT STATION

乗組員 Crew

1号艇（右舷）No.1 lifeboat (starb'd)				2号艇（左舷）No.2 lifeboat (port)			
職名 Rank	氏名 Name	任務 Duty	携行品 Goods	職名 Rank	氏名 Name	任務 Duty	携行品 Goods
船長 Captain	漁野 伸哉	総指揮 General Com.	重要書類 双眼鏡 時計 Important Brief, Binocular, Clock	一航士 C/O	須佐美智嗣	艇指揮 Boat Com.	重要書類 双眼鏡 時計 Important Brief, Binocular, Clock
二航士 2/O	青木 高文	艇長 Skipper	双方向無線電話 海図 航海日誌 航海用具 Transceiver,Chart,Log-book,Nav'equip.	三航士 3/O	大川 輝将	艇長 Skipper	双方向無線電話 海図 航海用具 信号用具 Transceiver,Chart,Nav'&Signal Equip.
一機士 1/E	金田 和彦	船長補佐 Assist. Capt.	重要書類 応急用具チェック Important Brief	機関長 C/E	坂口 栄次	艇指揮補佐 Assist. Com.	重要書類 機関日誌 応急用具チェック Important Brief,Eng'log-book
三機士 3/E	黒瀬 航	艇機関始動 Starting Eng.	応急用具 Emergency Tools	二機士 2/E	野口 和徳	艇機関始動 Starting Eng.	応急用具 Emergency Tools
電子長 C/Op	赤間 英之	通信連絡 Radio Operation	重要書類 救急医薬品 レーダートランスポンダ Important Brief , Medical Goods , SART	二電士 2/Op	髙楠 憲二	通信連絡 Radio Operation	重要書類 救急医薬品 レーダートランスポンダ Important Brief , Medical Goods , SART
三電士 3/Op	梅谷 有一	通信連絡 Radio Operation	重要書類 Important Brief	甲板長 Boatswain	安部 正市	降下準備指揮 S/B Lowering Boat Leader	救命索発射器 Line-Throwing Appliance
甲板部員（A） Able Seaman(A)	佐々木 栄	降下準備指揮 S/B Lowering Boat Leader	遭難信号煙 ボートコンパス Distress Signals,Boat Compass	甲板部員（B） Able Seaman(B)	徳永 藏	降下準備 S/B Lowering Boat	ライフブイ 毛布2枚 Life Buoy,2 Blankets
甲板部員（C） Able Seaman(C)	小田 初男	降下準備 S/B Lowering Boat	ライフブイ 毛布2枚 Life Buoy,2 Blankets	甲板部員（D） Able Seaman(D)	大端 正則	降下準備 S/B Lowering Boat	手旗 国旗 信号用具 毛布2枚 Signal Equip.,National Frag,2 Blankets
甲板部員（E） Able Seaman(E)	白山 哲男	降下準備 S/B Lowering Boat	メガホン 毛布2枚 Megaphon,2 Blankets	甲板部員（F） Able Seaman(F)	大石 英明	艇機関始動補助 Starting Eng. Assistant	応急用具 艇機関燃料積込 毛布2枚 Emergency Tools,F.O, 2 Blankets
操機長 No1Oiler	益永 政幸	艇機関始動補助 Starting Eng. Assistant	応急用具 艇機関燃料積込 毛布2枚 Emergency Tools,F.O, 2 Blankets	機関部員（A） Oiler(A)	張本 恒雄	艇機関始動補助 Starting Eng. Assistant	応急用具 艇機関燃料積込 毛布2枚 Emergency Tools,F.O, 2 Blankets
機関部員（B） Oiler(B)	毛利 淳司	降下準備 S/B Lowering Boat	応急用具 毛布2枚 Emergency Tools, 2 Blankets	機関部員（C） Oiler(C)	大石 洋之	降下準備 S/B Lowering Boat	応急用具 毛布2枚 Emergency Tools, 2 Blankets
機関部員（D） Oiler(D)	上田 政実	降下準備 S/B Lowering Boat	応急用具 毛布2枚 Emergency Tools, 2 Blankets	司厨長 C/S	高島 香	食料積込 Loading Foods	食料 救急医薬品 毛布2枚 Foods, Medical Goods,2 Blankets
司厨部員（A） Cook(A)	尼崎 新一	食料積込指揮 Loading Foods Leader.	食料 救急医薬品 毛布2枚 Foods, Medical Goods,2 Blankets	司厨部員（B） Cook(B)	福村 秀夫	食料積込 Loading Foods	食料 毛布2枚 Foods,2 Blankets
司厨部員（C） Cook(C)	白石 豊徳	食料積込 Loading Foods	食料 毛布2枚 Foods,2 Blankets	司厨部員（D） Cook(D)	佐藤 健	食料積込 Loading Foods	食料 毛布2枚 Foods,2 Blankets

・乗組員 Crews :28per.

1号艇（右舷）No.1 lifeboat (starb'd)				2号艇（左舷）No.2 lifeboat (port)			
所属 Organization	名前 Name	任務 Duty	携行品 Goods	所属 Organization	名前 Name	任務 Duty	携行品 Goods
東京大学海洋研究所	Millard F. Coffin	研究員総指揮 Scientist Com.	重要データ、毛布2枚 Important Data、2 Blankets	東京大学海洋研究所	中村 恭之	研究員指揮 Scientist Leader	重要データ、毛布2枚 Important Data、2 Blankets
東京大学海洋研究所	井上 博之	乗艇待機 Board'g&Wait'g	毛布2枚 2 Blankets	東京大学海洋研究所	渡邊 みずき	乗艇待機 Board'g&Wait'g	毛布2枚 2 Blankets
ハワイ大学	Loren W. Kroenke	乗艇待機 Board'g&Wait'g	毛布2枚 2 Blankets	千葉大学	更山 順子	乗艇待機 Board'g&Wait'g	毛布2枚 2 Blankets
日本海洋事業	大渡 祐樹	乗艇待機 Board'g&Wait'g	毛布2枚 2 Blankets	日本海洋事業	佐野 守	乗艇待機 Board'g&Wait'g	毛布2枚 2 Blankets

・研究者等 Scientists :08per.

・1号艇 No.1 lifeboat :18per.　　　　　・2号艇 No.2 lifeboat :18per.　　　・総員 Total :36per.

5th,Jan,2005～25th,Jan,2005

※船体傾斜等により一艇のみの退船の場合には、船長の指定する救命艇に総員乗艇とする。

○発令信号：一般非常警報による短7長1（・・・・・・・－）及び口頭またはスピーカーによる「総員端艇部署につけ」の号令（船長の命令により発令）

○部署が発令されたら、各員は、厚着、救命胴衣を着用、所定物品携行の上、指定場所に集合。艇指揮者は人員、携行品を確認し船長に報告する。

○船長は部署発令時または召集場所において使用救命艇等の降ろし方準備を命ずる。

○船体放棄の命令は船長の「退船、降ろし方始め！」の命令による。

○船長が指揮を取れない場合は、一等航海士が代行する。

○救命いかだ使用の場合の任務は救命艇の任務をそのまま準用する。

○衛星イーパブの積み込みは、二等航海士または三等航海士が担当すること。

Master

ii

24 January 2005

Captain Shinya Ryono
R/V *Kairei*

Dear Captain Ryono-san:

On behalf of the entire geoscientific party aboard *Kairei* KR05-01, I wish to commend you, C/O Susami-san, C/E Sakaguchi-san, 1/E Kaneda-san, C/EO Akama-san, C/S Takashima-san, and the rest of your officers and crew, as well as fellow NME staff Ohwatari-san and Sano-san, for your vital contributions to the successful outcome of the cruise. Your crew has been wonderfully cooperative, conscientious, good-humored, diligent, perceptive, and professional. It has been a pleasure to work aboard this well-maintained and operated vessel, especially with such geophysically knowledgeable shipmates imbued with a highly positive, 'can-do' attitude. We look forward to future opportunities to sail with you aboard *Kairei* and other fine JAMSTEC vessels.

Yours sincerely,

Prof. Millard F. Coffin
Dr. Yasuyuki Nakamura
Mr. Hiroyuki Inoue
Ms. Mizuki Watanabe
Ocean Research Institute, University of Tokyo
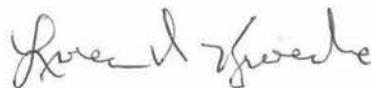
Dr. Loren Kroenke
University of Hawaii

Ms. Junko Sarayama
Chiba University

cc: Kiyoshi Suyehiro, JAMSTEC

東京大学
THE UNIVERSITY OF TOKYO

KR05-01 Cruise Track
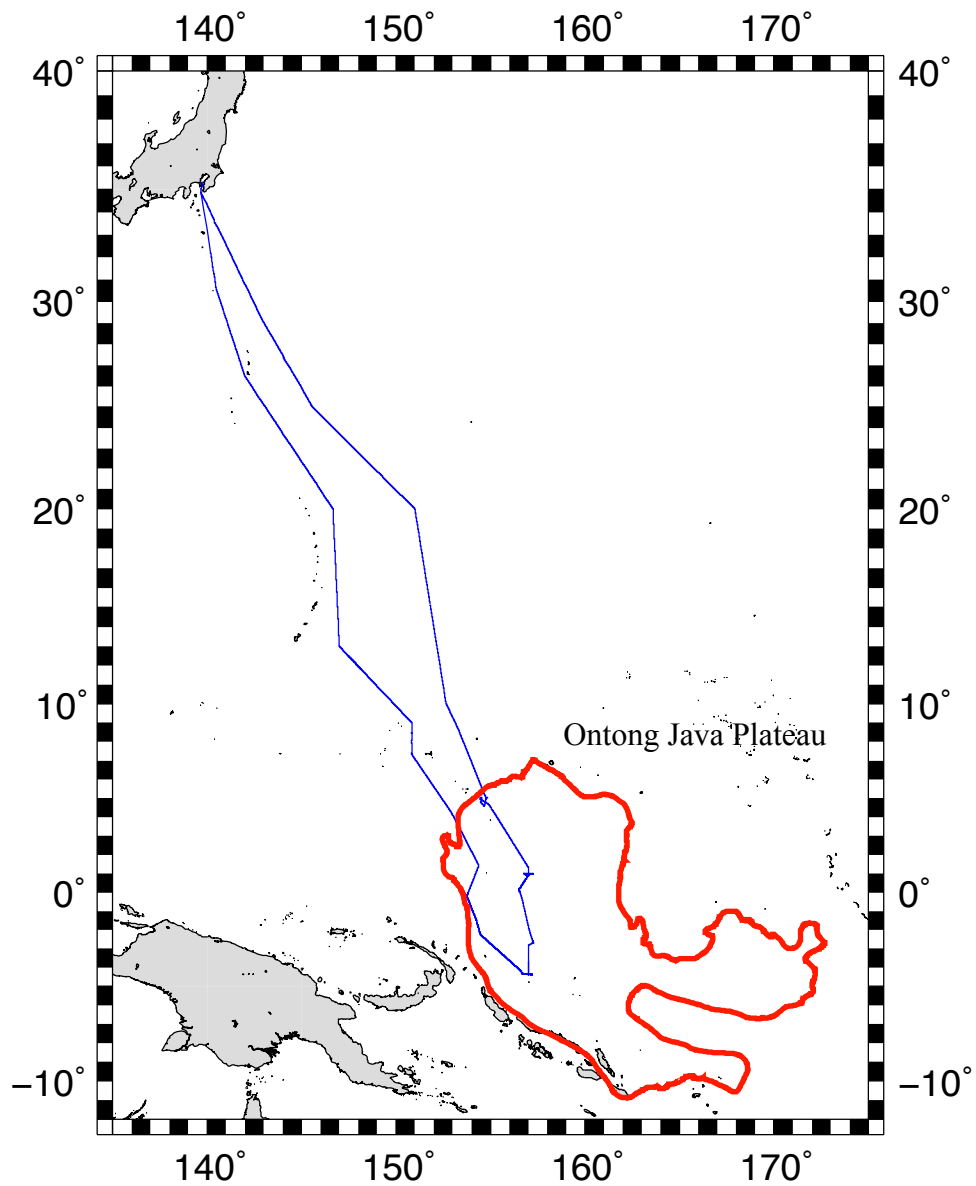
5-25 January 2005

Yokosuka - Yokosuka

Table of Contents

Executive Summary

The origin of the Ontong Java Plateau, a large igneous province (LIP) in the western equatorial Pacific, was the research objective of R/V *Kairei* cruise KR05-01. The first north-south geophysical transect of the plateau was completed, including the first multichannel seismic reflection data acquired from the plateau's crestal region. Two geophysical transects, including MCS data, of the transition between the plateau and the adjoining Lyra Basin were undertaken, and the first multibeam data along the plateau's western flank were acquired. All of these data, when processed and interpreted, should contribute to understanding how the Ontong Java Plateau formed. Complementary to the large-scale geophysical studies of the plateau and its margins, more detailed site surveys for four proposed Integrated Ocean Drilling Program (IODP Proposal 623) sites were completed. In total, ~1100 km of multichannel seismic reflection data, and ~2000 km of coincident and additional geophysical data (SeaBeam 2112 and 4 kHz subbottom profiler, shipboard gravity, proton precession magnetometer, and shipboard three-component magnetometer) data were acquired over the Ontong Java Plateau and its transition to the adjacent Lyra Basin. Integration of geophysical, petrological, geochemical, and geodynamic work should advance our knowledge of the Ontong Java Plateau's nature and development specifically, and those of LIPs in general, significantly.

Origin of the Ontong Java Plateau
(M. Coffin)

Intra-oceanic plateaus, continental flood basalts, and volcanic rifted continental margins comprise the most voluminous group of large igneous provinces (LIPs; Coffin & Eldholm, 1993). They are important to a variety of earth-science disciplines because they represent cataclysmic production of magma at rates that, in the case of the Early Cretaceous OJP, may have exceeded the contemporary worldwide ocean-ridge production rate (e.g. Tarduno et al., 1991; Coffin & Eldholm, 1994). Thus, oceanic and continental flood basalt events, which were especially prevalent during Cretaceous time, can provide critical insights into dynamic mantle processes and associated phenomena (such as the long Cretaceous Normal Superchron) (e.g. McNutt et al., 1996).

Since the late 1980s, the predominant hypothesis for the origin of LIPs has been the plume-head model (e.g., Griffiths et al., 1989; Campbell & Griffiths, 1990; Duncan & Richards, 1991; Campbell, 1998), in which the bulbous head of a new mantle plume ascending from deep in the mantle melts extensively for approximately 1-5 Myr beneath preexisting lithospheric thin spots and/or as a result of lithospheric extension caused by the buoyant plume head or other changes in a plate's stress field (Fig. 1). Following the plume-head stage, melting is theorized to continue at much-reduced rates in a narrow tail that follows the plume head; in oceanic areas, prolonged plume-tail volcanism is postulated to have produced major island and seamount chains (e.g. Richards et al., 1989).

Recent work on several fronts, however, challenges various aspects of the plume model. One of the more serious challenges comes from recent drilling (ODP Leg 192) and related studies of the OJP. With a Greenland-size area of $\sim 2 \times 10^6$ km^2 and maximum crustal thickness >30 km (Gladczenko et al., 1997; Richardson et al., 2000; Miura et al., 2004), the OJP is the largest documented flood basalt province; yet it fails to exhibit several key characteristics expected from a plume-head origin (see below and Neal et al., 1997; Mahoney, Fitton, Wallace et al., 2001; Tejada et al., 2002, 2004; Ingle & Coffin, 2004). Therefore, alternatives to plume-head models for the OJP are receiving increased attention (Ingle & Coffin, 2004; Tejada et al., 2004;), but cannot be evaluated sufficiently with existing samples and data. These include (1) an eclogite-rich rather than a purely peridotitic plume head (Yasuda et al., 1997; Cordery et al., 1997), (2) meteorite impact on the seafloor (Rogers, 1982; Isley & Abbott, 2002; Jones et al., 2002), (3) and plate separation above extensive, near-solidus, but non-plume regions of the uppermost asthenosphere ("perisphere") (e.g. Anderson, 1995; Smith & Lewis, 1999) (Fig. 1).

The primary goal of KR05-01 is to investigate the origin of the OJP, in close conjunction and collaboration with proposed Integrated Ocean Drilling Program (IODP) investigations involving the drilling of ten sites on the OJP and seven off-plateau sites. In combination, KR05-01 and IODP investigations will provide critical geophysical data and sections of igneous basement and Cretaceous sedimentary rocks needed to help test various models for the OJP's origin.
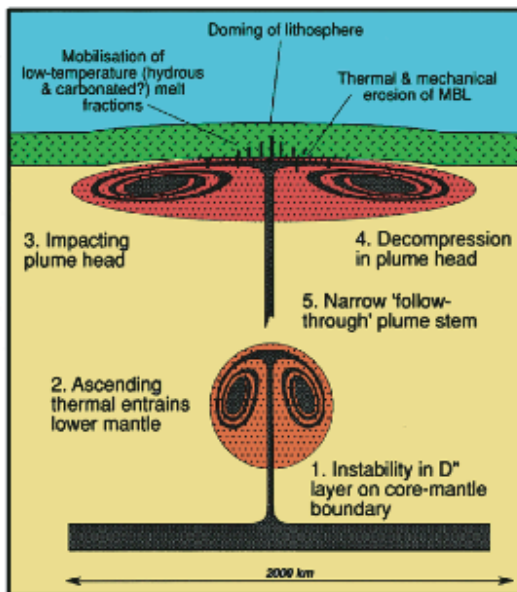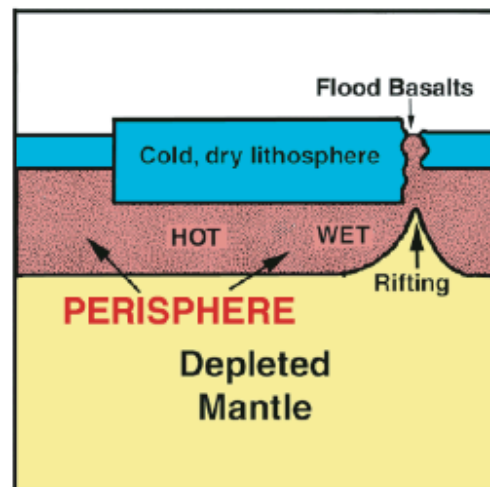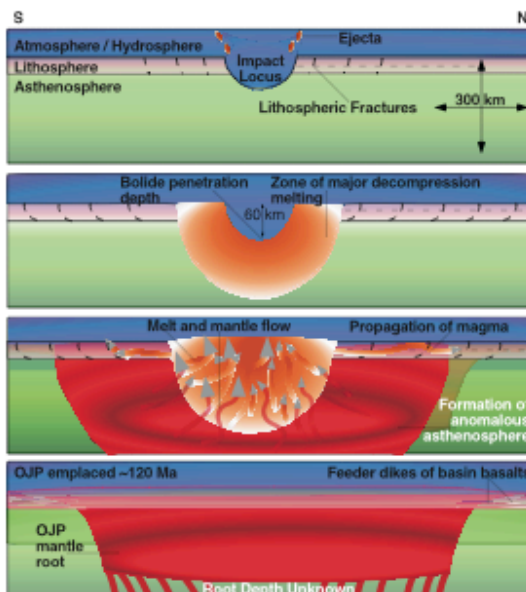
Figure 1. Cartoons of mantle plume (upper left; Saunders et al., 1992), bolide impact (lower left; Ingle and Coffin, 2004), and perisphere (lower right; Anderson, 1995) models for the origin of the Ontong Java Plateau.

Physiography, Setting, and Crustal Structure

The *in situ* OJP encompasses two major physiographic provinces, the high plateau and the eastern salient (Fig. 2; Kroenke, 1972). Much of the high plateau lies in water depths <3,000 m, culminating at depths of ~1,600 m, and several islands and atolls of undetermined age surmount it. The eastern salient comprises northern and southern arms separated by the undated Stewart Basin. Along the convergent plate boundary zone between the OJP's southern flank and the Solomon Islands, fragments of OJP crust have been obducted onto several islands (Fig. 2). Deep ocean basins abut the OJP in other directions: the Lyra Basin to the west, the East Mariana and Pigafetta basins to the north, the Nauru Basin to the northeast, and the Ellice Basin to the southeast. In at least three of these basins, the Nauru, East Mariana, and Pigafetta (Fig. 2), Lower Cretaceous flood basalts overlie older oceanic crust (Abrams et al., 1993; Shipley et al., 1993; Nakanishi & Winterer, 1998; Mochizuki et al., submitted).

The crustal structure of the OJP's high plateau has been investigated using wide-angle seismic analyses (Furumoto et al., 1976; Hussong et al., 1979; Gladczenko et al., 1997; Miura et al., 2004), gravity modeling (Gladczenko et al., 1997), and surface wave tomography (Richardson et al., 2000). The maximum crustal thickness of ~30-35 km corresponds to the shallowest portions of the high plateau. Beneath a typical 1 km-thick sediment layer on the high plateau, three layers comprise the OJP's igneous crust: a ~5.4 km/s extrusive upper crust with an average (maximum) thickness of ~4 (8) km, a ~6.1 km/s middle crust with an average (maximum) thickness of ~7 (16) km, and a 7.1 km/s lower crust with an average (maximum) thickness of ~15 (19) km (Gladczenko et al., 1997; Miura et al., 2004).

Basement Age and Composition

Seven drill sites have reached basement on the northern half of the OJP's high plateau (Fig. 2), penetrating the average 26-km-thick igneous crust to depths of 9 m to 217 m. Basement has not been recovered from the eastern salient or the southern half of the OJP's high plateau, except for extreme southern margin where subaerial exposures of OJP basement crop out on the Solomon Islands. From these drill sites and subaerial exposures, the upper levels of OJP basement are known to be tholeiitic submarine basalt. Dating by ^{40}Ar-^{39}Ar and Re-Os yields a cluster of early Aptian ages around 122 Ma for most lavas (Mahoney et al., 1993; Parkinson, 1996; 2001; Tejada et al., 1996, 2002). However, basalt flows at Site 803 and some from the Solomon Islands, although geochemically similar to other OJP basement flows (Mahoney et al., 1993; Parkinson et al., 1996; Tejada et al., 1996), yield ^{40}Ar/^{39}Ar ages clustering around 90 Ma. Current data suggest that the ~90 Ma event is volumetrically rather minor, especially in light of the discrepancy between ages from microfossils in the overlying sediment (Aptian) and ^{40}Ar-^{39}Ar ages of ~90 Ma for underlying lavas at Site 803. Presently, it appears the great bulk of the OJP formed rapidly in early Aptian time.

Three chemically different types of isotopically ocean-island-like basalt have been identified thus far (see Fitton & Godard, 2004; Tejada et al., 2004, and refs. therein). One of these chemical types (Singgalo) is isotopically distinct from the other two, the voluminous Kwaimbaita and the more primitive Kroenke basalts, which are isotopically indistinguishable. Despite their presence in areas as far apart as 1,600 km, both the Singgalo and the Kwaimbaita basalts cover only a small range of isotopic values (e.g. the total ε_{Nd} range for the Kwaimbaita (and Kroenke) types is only 1.3 units). Assuming a peridotite
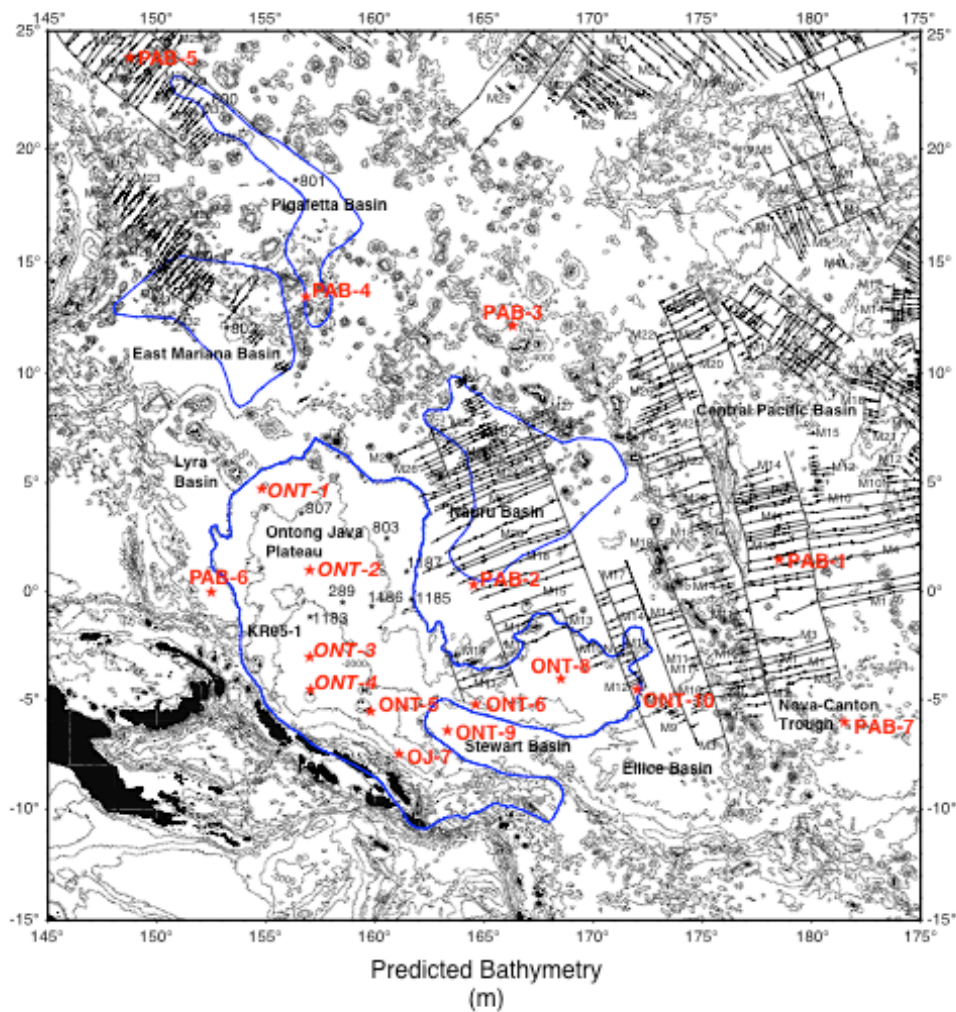
Figure 2. Proposed IODP drill sites (red) on the Ontong Java Plateau (outlined in blue), in adjacent ocean basins, and on older seamounts. Previous basement drill sites are indicated in plain smaller black font. Predicted bathymetry (1000 m contour interval) from Smith and Sandwell (1997); magnetic isochrons and fracture zones (both light black lines) from Nakanishi and Winterer (1998).

source, modeling indicates the Kroenke and Kwaimbaita types are the products of ~30% partial melting (higher than for most ocean-ridge basalts) whereas the Singgalo basalts appear to be formed by slightly smaller, though still impressively large amounts of partial melting. Kwaimbaita-type volcanism, in particular, extends well beyond the plateau proper; basement

sections in drill sites in the surrounding Nauru and East Mariana basins (e.g. Saunders, 1986; Castillo et al., 1991, 1994) are composed entirely of Kwaimbaita-type basalts.

Geodynamics

Total uplift and subsidence of the OJP are estimated from the lack of subaerial and shallow water basalts (Mahoney, Fitton, Wallace, et al., 2001), basalt emplacement depths derived from vapor saturation pressures calculated from CO_2 contents of basalt glasses (Michael, 1999; Roberge et al., 2004; Roberge et al., in prep.), and paleodepths interpreted from microfossils in sediment overlying basalt (Andrews, Packham, et al., 1975; Sliter and Leckie, 1993; Mahoney, Fitton, Wallace, et al., 2001; Sikora and Bergen, 2004). Combined isostatic and dynamic crustal uplift was significantly less for the OJP than for active hotspots today, and total subsidence is anomalously less (e.g. Neal et al., 1997; Ito and Clift, 1998) than that of any other known oceanic lithosphere (Parsons and Sclater, 1977; Stein and Stein, 1992).

Mantle Root

A "root" extending for ≥300 km into the mantle beneath the OJP (Richardson et al., 2000; Klosko et al., 2001) is the first such observation from a LIP or anywhere else in an oceanic intraplate setting. Shear wave splitting studies suggest that ambient Pacific asthenosphere flows around the root, implying the root is rheologically strong and attached to the crust of the OJP (Klosko et al., 2001). Centered beneath the OJP's thickest crust, but not extending beneath the Nauru or East Mariana Basin flood basalts, the root is cylindrical with a diameter of ~1,200 km, and is characterized by anomalously slow (≤5%) shear wave velocities. Richardson et al. (2000) estimated that if such velocities were entirely thermal in origin, the root would be ~350-700°K hotter than surrounding mantle, hot enough to cause continuing volcanism. However, the OJP shows no evidence of active volcanism, and lower than average shear attenuation rules out a thermal origin as its source (Gomer and Okal, 2003). Instead, the keel more likely represents a chemical or mineralogical heterogeneity, perhaps the "fossil" head of a plume that failed to remain anchored in the deep mantle. Mantle roots characterized by slow seismic velocities have also been detected beneath the Deccan Traps (Kennett & Widiyantoro, 1999) and Paraná flood basalts (VanDecar et al., 1995), but the roots of these much smaller continental LIPs are significantly smaller (~300 km vs. ~1,200 km diameter) and are associated with smaller velocity anomalies (maximum of 1.5% and 2.4% vs. 5%, respectively) than the root beneath the OJP (Richardson et al., 2000).

Models for the Origin of the OJP: Predictions, Observations, and Discrepancies

We consider three primary models for the formation of the OJP: surfacing plume head, bolide impact, and perisphere.

Surfacing Plume Head (Fig. 1). Surfacing of a bulbous head, signaling a new mantle plume ascending from deep in the mantle, can produce the high degree of partial melting required to generate LIPs over 1-5 Myr (Saunders et al., 1992; Campbell, 1998). Following the plume-head stage, melting is theorized to continue at much-reduced rates in the narrow tail thought to follow the plume head; in oceanic areas, prolonged plume-tail volcanism is postulated to have produced major island and seamount chains (e.g. Richards et al., 1989; Campbell & Griffiths, 1990).

Significantly, results of recent models of plume formation in the lower mantle are consistent with the isotopic and incompatible-element homogeneity exhibited by the voluminous Kwaimbaita (and Kroenke) magma type in that they predict large peridotitic plume heads should be well mixed, should entrain relatively little non-plume mantle during their ascent, and thus should be significantly more homogeneous than plume tails (Van Keken, 1997; Farnetani et al., 2002). More generally, the ocean-island-like isotopic signature, the evidence for high-degree partial melting, and the apparently rapid formation of most of the OJP are consistent with predictions of this type of model (e.g. Duncan & Richards, 1991; Campbell, 1998).

There are, however, significant discrepancies between observation and model. The most important include: (1) All OJP basement basalt flows sampled thus far were erupted well below sea level, yet standard plume-head models predict that much of the surface should originally have been shallow or even subaerial; (2) The mantle root's dimensions and anomalously low velocities do not agree with estimates of melt residue remaining from emplacement of the plateau, whereas the estimated residual heat from a fossil plume head should be enough to even now cause volcanism; (3) Post-eruptive subsidence of the plateau appears to have been much less than expected for oceanic lithosphere and instead, normal faults around the margins of the high plateau indicate the adjoining seafloor has subsided relative to the OJP (Hagen et al., 1993); (4) No post-plateau seamount chain corresponding to the plume-tail stage of hotspot development is present, nor can any known hotspot be linked unambiguously to the plateau; (5) After an apparent eruptive hiatus of ~30 Myr, the ~90 Ma volcanic episode produced basalts in several widespread locations with compositions closely similar to those of the ~122 Ma Kwaimbaita magma type. Each of these discrepancies is discussed in detail below.

(1) The arrival of hot, buoyant, ascending plume material at the base of oceanic lithosphere, accompanied by voluminous decompression melting, should result in a combination of thermal expansion, buoyant uplift, and crustal growth capable of initially maintaining the plateau above sea level (e.g. Griffiths et al., 1989; Hill, 1991; Farnetani & Richards, 1994; Ito & Clift, 1998). Both general isostatic (e.g. Detrick & Crough, 1978) and experimental dynamic plume models (e.g. Olson & Singer, 1985; Olson & Nam, 1986; Griffiths et al., 1989) predict that seafloor is uplifted by 1,000 to 2,000 m as a result of the arrival of a 1,000-2,000-km-diameter plume head at the base of the lithosphere, in agreement with observations of seafloor swells associated with major hotspots that are assumed to correspond to the spread-out tops of plume tails (e.g. Hawaii, Cape Verde). Specific OJP plume models, both dynamic (Farnetani & Richards, 1994) and isostatic (Ito & Clift, 1998), predict elevation of the seafloor by 3,000-4,000 m, and 1,000-3,000 m, respectively. Extrapolation of Mesozoic marine magnetic anomalies in the neighboring Nauru Basin (Fig. 2; Nakanishi & Winterer, 1998) suggests that most of the ~122 Ma OJP formed on ~130 to ~155 Ma (Gradstein et al., 1994) oceanic crust. Global age-depth curves (Stein & Stein, 1992) predict that 10 to 35 Myr old oceanic crust should lie at depths of ~3,600 to ~4,700 m, assuming it was formed at an average ridge-crest depth of 2,500 m. Therefore, according to Farnetani & Richards's (1994) and Ito & Clift's (1998) plume models for the OJP, oceanic crust should have been uplifted ~1,000 to ~4,000 m, therefore to between ~400 m above sea level to ~3,700 m below sea level, prior to most constructional magmatism.

According to simple isostasy, and assuming magmatism was overwhelmingly mafic, emplacement of the OJP's up to ~35-km-thick crust following uplift of preexisting ~7- km-thick (White et al., 1992) oceanic crust should have resulted in major, widespread subaerial

volcanism, culminating in (minimum) elevations of ~700 m to ~4,000 m on the central OJP. Although no present analogs on such a scale exist, the Earth's six most active hotspots in the ocean basins, characterized by magma fluxes orders of magnitude smaller than the OJP's, all feature large-scale subaerial volcanism. Similarly, most oceanic plateaus, submarine ridges, and seamount chains attributed to mantle plumes, and sampled by drilling, have experienced significant subaerial volcanism during construction (e.g. Detrick et al., 1977; Coffin, 1992). Yet all OJP basalt flows, either drilled or sampled from obducted Solomon Islands sections, erupted well below sea level, and sediments deposited just above this basement are marine (Neal et al., 1997; Michael, 1999; Mahoney, Fitton, Wallace et al., 2001; Tejada et al., 2002). Presently, the only evidence for any shallow volcanism on the plateau is the 338-m-thick basaltic volcaniclastic sequence drilled at Site 1184 (the age of which is not well constrained), and thin Aptian vitric tuff layers at Sites 288, 289, and 1183. Interestingly, evidence for significant pre- and syn-volcanic uplift is also lacking in several large continental flood basalt provinces (e.g. Menzies et al., 1997; Czamanske et al., 1998; Sheth, 2000).

(2) The 300-km-thick mantle root is too large to simply be the residue of melting that formed Kwaimbaita-, Kroenke-, and Singgalo-type magmas: assuming a peridotite mantle source and that such magmas compose the entire plateau, Neal et al. (1997) estimated that a residual mantle root would be less than 100 km thick. Also, the root is seismically slow; yet melt-depleted olivine-rich mantle, such as that beneath cratons, is seismically faster than ambient asthenosphere (e.g. Zhang & Tanimoto, 1993). One likely possibility is that the root retains some of the excess heat from the original plume head. However, Richardson et al.'s (2000) estimate that in such a case the root would presently have to be 350-700° hotter than the ambient upper mantle does not necessarily agree with the conclusion of both Chazey & Neal (2004) and Fitton & Godard (2004) that the *initial* potential temperature of the Kwaimbaita/Kroenke-type mantle source could have been as low as 1500°.

(3) Plateaus within oceanic lithosphere should subside via either thermal conduction (Detrick & Crough, 1978) or continuous viscous spreading of the plume head mantle following plateau emplacement (Griffiths et al., 1989). Many oceanic plateaus and submarine ridges have subsided similarly to normal oceanic crust (Detrick et al., 1977; Coffin, 1992). Predicted total subsidence of ~122 Ma oceanic crust ranges from ~3,000 m to ~3,800 m (Parsons & Sclater, 1977; Stein & Stein, 1992). However, paleoenvironments interpreted from sedimentary strata immediately overlying basalt at five out of six OJP drill sites (Andrews, Packham, et al., 1975; Sliter & Leckie, 1993; Mahoney, Fitton, Wallace et al., 2001) show that the crust, when reconstructed to account for sediment loading, subsided only 1,000-2,800 m, significantly less than either typical oceanic lithosphere or other well-studied oceanic plateaus and submarine ridges. Previous geodynamic inferences and models involving subsidence rates typical of most oceanic crust (Michael, 1999) and multiple stages of crustal growth (Ito & Clift, 1998; Ito & Taira, 2000), respectively, are inconsistent with subsidence estimated from sedimentary paleoenvironments, and a single major episode of constructional magmatism at ~122 Ma.

(4) Following the plume-head event, plumes may have a 'tail' that remains 'fixed' to a mantle boundary layer and that continues to feed the surface, allowing the plume to create long-lived volcanic expressions on the surface referred to as hotspots (e.g. Morgan, 1972; Richards et al., 1989). Although subduction has removed seafloor that was to the southwest of the OJP, no OJP-related, post-plateau volcanic chain is present on the surrounding seafloor in other directions. Likewise, although the Louisville hotspot has been suggested as the

source of the plateau (e.g. Richards et al., 1989; Phinney et al., 2000), the OJP cannot be linked definitively to it or any other hotspot track or currently active hotspot on the basis of geochemistry (Mahoney et al., 1993), plate reconstructions (Neal et al., 1997), paleomagnetic data (Riisager et al., 2004), geochronology (Koppers et al., 2004), or combined hotspot motion and true polar wander (Antretter et al., 2004).

(5) The ~90 Ma volcanic episode documented in some of the Solomon Islands, characterized by lavas with isotopic and chemical compositions closely resembling those of the ~122 Ma Kwaimbaita magma type, challenges plume models, particularly to explain an apparent eruptive hiatus of ~30 Myr. Bercovici & Mahoney (1994) proposed a "double plume head" model to account for this bimodal volcanism, whereby the starting mantle plume head is separated from its trailing conduit at the ~660 km discontinuity resulting in a second plume head surfacing 20-30 Myrs later. However, the compositional similarity between the ~122 Ma and ~90 Ma OJP lavas is still difficult to reconcile.

A recent variant of the plume-head model posits that many flood basalts may have been formed from plume heads that, rather than being composed solely of peridotite, contained substantial amounts of eclogite (e.g., Yasuda et al., 1997; Cordery et al., 1997; Takahashi et al., 1998). An eclogite-rich plume head would melt extensively at significantly lower temperatures than required if it were peridotite. A lower-temperature, eclogite-rich plume-head would probably be less buoyant; hence, the resulting dynamic uplift of the lithosphere may be significantly less than for a purely peridotitic head (Campbell, 1998). In comparison to a peridotite plume-head model, an eclogite-rich plume head model also predicts differences in magma composition, especially in maximum MgO and minimum SiO_2 contents, which would be lower and higher, respectively, than the observed compositions of the tholeiitic basalts (e.g. Klemme et al., 2002). In most other respects, however, its predictions appear rather similar to those of peridotite plume-head models.

Bolide Impact (Fig. 1). This model posits that an impacting bolide would vaporize the entire lithosphere and uppermost asthenosphere, and high degree melting in the instantly decompressed upper mantle would result in formation of the OJP (e.g., Rogers, 1982; Jones et al., 2002; Ingle & Coffin, 2004). Emplacement of the OJP in this way would be geologically instantaneous, and presumably some signature of the impact would be recorded in proximal, if not global, Lower Aptian sediments.

A bolide impact model (Ingle & Coffin, 2004) can account for the lack of significant pre- and syn-emplacement uplift and post-emplacement subsidence of OJP lithosphere, because melt and the underlying mantle would ascend adiabatically, with buoyancy generated solely by thermal expansion of ambient mantle. Catastrophic mixing would result in homogeneous geochemical and isotopic signatures of OJP lavas (Jones et al., 2002; Ingle & Coffin, 2004; Tejada et al., 2004). This model can also account for the lack of both a post-OJP seamount chain and any presently active hotspot that can be linked unambiguously with the plateau.

As with the plume models, however, several discrepancies exist between observation and model. Some of the most significant are: (1) The mantle root's size and anomalously low velocities do not agree with estimates of melt residue remaining from emplacement of the plateau. (2) The ocean-island-type isotopic signature of the basalts is not expected based upon the widely held view that the upper mantle is predominantly normal MORB-source-type mantle. (3) Effects on the Earth's environment typically attributable to a large bolide impact have not yet been found. (4) After an apparent eruptive hiatus of ~30 Myr, the puzzling ~90 Ma volcanic episode produced basalts in several widespread locations with

isotopic and chemical compositions closely similar to those of the ~122 Ma Kwaimbaita magma type. We discuss each of these discrepancies below.

(1) The root is seismically slow, yet melt-depleted olivine-rich mantle, such as that beneath cratons, is seismically faster than ambient asthenosphere (e.g. Zhang & Tanimoto, 1993). As the underlying mantle would presumably have had little or no (pre-impact) excess potential temperature, it seems unlikely that the root's low velocities are thermal in origin. One possibility is that the root is 'replacement mantle' (i.e. mantle that formed at lower pressure-temperature conditions than ambient mantle) and has retained physical properties resulting in lower seismic velocities since ~122 Ma.

(2) OJP basalts studied thus far have an ocean-island-type isotopic signature. The bolide impact model requires that the upper ~300 km of Pacific mantle in the vicinity of the impact at ~122 Ma have such a signature, rather than the normal MORB-type signature expected of typical upper mantle. Mantle heterogeneity seems to exist on many scales (e.g. Fitton & Dunlop, 1985; Allegre & Turcotte, 1986, etc.), however, and the most straightforward possibility is that the ambient upper mantle near the impact site at ~122 Ma contained a larger than usual amount of ocean-island-type mantle.

(3) An impacting bolide ~20 km in diameter would presumably cause major environmental effects that should be recorded in marine and terrestrial Lower Aptian sediments: e.g. major extinctions of flora and fauna; shocked minerals; spherules; Ir, Os, and other siderophile element and isotopic anomalies; tsunami deposits, etc. To date, only some extinctions are known to correlate with OJP emplacement at ~122 Ma (e.g., Larson & Erba, 1999); OJP basalts show a slight enrichment in platinum-group elements relative to model primitive mantle (Ely & Neal, 2003; Chazey & Neal, 2004); and OJP emplacement correlates temporally with an oceanic anoxic event (OAE1A, the 'Selli' event) (see Fig.1 of Leckie et al., 2002) and Hf and Sr excursions in marine sediments (Jones & Jenkyns, 2001; Godfrey et al., 1997). The first numerical modeling of a bolide impact in 4000 m water depth is currently in progress, and may provide insight into potential environmental effects.

(4) Most of the ~90 Ma lavas in the Solomon Islands show marked isotopic and chemical similarities to the ~122 Ma Kwaimbaita magma type. A 30 Myr hiatus in eruptions is difficult to explain by the bolide impact model, unless the initial impact induced a plume to rise beneath the impact site, which surfaced ~30 Myr later (Alt et al., 1988; Glikson, 1996, 1999). Alternatively, lithospheric extension at this time induced melting of some regions of the catastrophically mixed mantle that failed to melt by decompression during the ~122 Ma event. In either case, the compositional similarity between OJP lavas erupted at ~122 and ~90 Ma would be difficult to explain.

Perisphere (Fig. 1). "Perisphere" was defined by Anderson (1995) as weak, shallow, incompatible element enriched, near solidus mantle that is an extensive source and sink of elements most prone to recycling. Therefore, plate separation above these enriched, but non-plume regions of the uppermost asthenosphere would result in formation of the OJP (e.g. Anderson et al. 1992; Anderson, 1995; Smith & Lewis 1999). This model, although less developed than the plume head or bolide impact models for oceanic LIPs, nevertheless makes certain predictions.

As the perisphere model does not involve a plume, the lack of either a present-day OJP hotspot or a post-OJP seamount chain is no longer a problem. The model postulates that the

relatively thin perisphere lies above normal MORB-source upper mantle. Rifting of the lithosphere (e.g. a ridge jump) causes the perisphere to melt extensively. The only expected dynamic lithospheric uplift would probably be due to expansion of the underlying mantle during decompression and melting. In the later stages of volcanism, the model predicts that as the perisphere layer is depleted of melt, it will be replaced progressively by upwelling normal MORB-source mantle.

Despite some predictions consistent with some OJP observations, a number of discrepancies are also apparent. The most intractable of these include: (1) the model is typically utilized to explain flood basalt provinces at the edges of cratons (Anderson, 1995, 1996; King and Anderson, 1995). No ~122 Ma Pacific plate reconstruction places the OJP near the edge of a craton, and contrary to the Kerguelen Plateau and volcanic passive margins, OJP lavas show no evidence for containing a component of continental crust (Mahoney, 1987; Mahoney & Spencer, 1991). (2) Magmatism would be somewhat protracted, lasting as long as the lithosphere extended or plates diverged, but the OJP appears to have been emplaced relatively quickly. The processes of lithospheric extension and plate divergence typically last >10 Myr. To date, all radiometric and biostratigraphic ages indicate that most of the OJP was formed in ≤5 Myr. (3) Ocean-island-type isotopic characteristics would gradually give way to MORB-type isotopic signatures; however, no OJP basement lavas to date have a MORB character. (4) As with the other models, the 300-km-thick mantle root is significantly larger than that expected to be the residue of melting that formed Kwaimbaita-, Kroenke-, and Singgalo-type magmas. (5) Crustal subsidence following emplacement would resemble that of normal oceanic lithosphere, but evidence to date suggests the OJP has subsided significantly less than typical oceanic lithosphere since ~122 Ma.

Tests of the Models for the Origin of the OJP

Igneous basement in vast regions of the OJP has not been imaged using modern seismic techniques or sampled, including both northern and southern arms of the eastern salient, and the western and, except for the obducted southern margin now exposed in the Solomon Islands, the southern half of the high plateau (Fig. 2). Where basement has been drilled, only the uppermost 9 m to 217 m has been penetrated. In addition, the relationship between the OJP and the volcanoes that now support some of the largest atolls in the world is unknown. The proposed geophysical surveying and drilling will provide the data and samples needed for more detailed evaluation of the plume head (and variants thereof), bolide impact, and perisphere models. In addition, heat-flow determinations at on-plateau sites (Sites ONT-1 through 10 and OJ-7) and surrounding off-plateau sites in the abyssal basins (Sites PAB-1, 2, 4, 6), including the Nova-Canton trough (PAB-7; Fig. 2) will establish whether the seismic characteristics of the OJP's immense, enigmatic mantle root are at least partly thermal in origin, especially as no downhole temperature measurements were performed during previous OJP drilling. The root poses challenges for all models, and a better understanding of its nature is essential.

Surfacing Plume Head. Arguably the strongest support for the standard plume-head model, especially in concert with negative indications for other models (see below), would come from the discovery of evidence for the significant crustal uplift predicted by plume theory (e.g. Detrick & Crough, 1978; Griffiths et al., 1989; Farnetani & Richards, 1994), as well as total subsidence comparable to other oceanic lithosphere of similar age. The crestal plateau transects, and the western and southern high plateau, and eastern salient sites (ONT-2, 3, 4, 5, 8; OJ-7) will address these questions. Better age control for OJP basement (ONT-1 through

10; OJ-7) and the surrounding basins (PAB-2, 4, 6) is also required to evaluate this model as it predicts massive, short-lived volcanism. In addition, drilling into the basement and accumulated sediments of the Nova Canton Trough (NCT) will constrain the age of this structure, to determine whether or not it is linked to the hypothesized spreading of the OJP and Manihiki plumes (the "drain-off" hypothesis of Larson, 1997). The recovery of ~122–115 Ma, geochemically OJP-type basalts from PAB-7 would strongly support the model proposed by Larson (1997) for the origin of the NCT, and would also point towards a plume model for the origin of the OJP.

Melting of eclogite will not produce high-MgO magmas (e.g. Yasuda et al., 1997; Klemme et al., 2002). Melting of eclogite-fertilized peridotite, on the other hand, may produce primary magmas that are Fe-enriched relative to their SiO_2 contents (e.g. Yaxley & Green, 1998), but the OJP lavas sampled to date do not appear to have had unusually Fe-rich primary magmas. The Kroenke-type basalts discovered during Leg 192 appear to be parental to the voluminous Kwaimbaita basalt type (Fitton & Godard, 2004). They contain 9-11 wt% MgO, which does not rule out eclogite as a source, but does require that it melt very extensively. However, discovery of significant amounts of isotopically similar basalt with still higher MgO contents would make an eclogite-rich plume head untenable. This question will be addressed by sampling over broad regions of the plateau (ONT-1 through 10; OJ-7).

Bolide Impact. In concert with negative evidence for the other models, the strongest support for a bolide impact model would come from evidence such as shocked minerals, spherules, and Ir, Os, and other siderophile element/isotope (Os, W) anomalies in both marine and terrestrial syn-OJP sedimentary sections. Discovery in these sedimentary records from neighboring basins of impact ejecta (e.g. microspherules) and/or a characteristic pattern of siderophile element/isotope signatures distinct from those characteristic of purely volcanic activity would provide strong evidence for a bolide impact origin. Such evidence has not yet been found in late Barremian-early Aptian sediments, but relatively few well-preserved sections are available for, or have been subject to, detailed analysis for highly siderophile elements (as accorded the Cretaceous-Tertiary boundary sections), whereas identification of microspherules and other textural evidence is highly dependent on preservation. Therefore, recovery of syn-OJP sedimentary records in the neighboring Pacific Ocean basins (Sites PAB-1, 2, 4, 6, 7) and atop older seamounts (PAB-3, 5) is critical. Several holes at each PAB site will be required to ensure the complete syn-OJP sedimentary record is recovered.

Some OJP basalts might preserve a signature from an impacting body in the PGEs (platinum-group elements) and Os isotope ratios, by analogy with some known impact sites like Chicxulub (e.g. Schuraytze et al., 1996); W isotope anomalies might also be found, depending upon the nature of the impactor (cf. Lee & Halliday, 1996; Halliday & Lee, 1999). Ely & Neal (2003) and Chazey & Neal (2004) have shown that the PGE are slightly enriched in existing OJP samples relative to model primitive mantle, but this interpretation is non-unique at present. PGE and Os and possibly W isotope measurements of lavas from the proposed plateau drill sites (ONT-1 through 10 and OJ-7) will more fully define the characteristics of and reasons for the PGE enrichment. An important caveat to all of the above, however, is that little work has been undertaken on the processes associated with large, abyssal-ocean bolide impacts, although numerical modeling of such impacts is currently in progress (Coffin et al., in prep.) For example, how 4,000 m of water surrounding the impact site would affect ejecta (*sensu lato,* including PGE, W, etc.) distribution is currently unknown.

Perisphere. Thus far, there is no evidence for involvement of MORB-type mantle in the OJP (e.g. Tejada et al., 2002) as predicted by the perisphere model. Discovery of such an influence, particularly if found at more than one site, would greatly strengthen a perisphere model for the plateau. More extensive basement sampling (ONT-1 through 10, OJ-7, as well as from the off-plateau sites PAB-1, 2, 4, 6, 7) will address this question.

Post-Cruise Research

Our research will address the origin of the OJP from two major perspectives: 1) structural and stratigraphic understanding of the OJP, and 2) preparatory (site survey) work for IODP expeditions. Future integration of geophysical, petrological, geochemical, and geodynamic work should advance our understanding of the OJP specifically, and of LIPs in general, significantly.

Multichannel seismic data will be processed and interpreted at the University of Tokyo Ocean Research Institute's (ORI) Seismic Research Center under the overall direction of Coffin and Nakamura. Multibeam, sub-bottom profiler, and gravity data will also be interpreted at ORI. Inoue intends to complete his M.Sc. degree at ORI using the KR05-01 data set. Magnetics data will be processed and interpreted at Chiba University under the direction of Nakanishi.

Drilling of large igneous provinces (LIPs), of which the OJP is an outstanding example for study, is one of eight major initiatives in *Earth, Oceans, and Life*, the Integrated Ocean Drilling Program's (IODP) Initial Science Plan (2003-2013). KR05-01 is closely related to IODP proposal 623, *Origin of the Ontong Java Plateau and Associated Effects on the Earth System*, contributing to the scientific site surveys required for drilling.

LIP research in Japan is at a young, but growing stage. LIPs, mantle plumes, and bolide impacts are first-order problems in earth sciences, and we hope that our work will help stimulate national research on the topics as well as foster more interdisciplinary research among solid earth scientists.

References

Abrams L.J., Larson R.L., Shipley T.H., and Lancelot Y. (1993) Late Jurassic-Early Cretaceous oceanic crust and Early Cretaceous volcanic sequences of the Nauru Basin, western Pacific. In: *The Mesozoic Pacific: Geology, Tectonics, and Volcanism* (M.S. Pringle, W.W. Sager, W.V. Sliter, and S. Stein, eds.) *Geophys. Monogr.* **77**, 103-119, AGU, Washington D.C.

Allegre C.J. and Turcotte D.L. (1986) Implications of a two-component marble-cake mantle. *Nature* **323**, 123-127.

Allen, R.M., G. Nolet, W.J. Morgan and others, (2002) Imaging the mantle beneath Iceland using integrated seismological techniques, *J. Geophys. Res.* **107, B12**, 2325, doi:10.1029/2001JB000595.

Alt D., Sears M., and Hyndman D.W. (1988) Terrestrial maria: The origins of large basalt plateaus hotspot tracks and spreading ridges. *J. Geology* **96**, 647-662.

Anderson D.L. (1995) Lithosphere, asthenosphere, and perisphere. *Rev. Geophys.* **33**, 125-149.

Anderson D.L. (1996) Enriched asthenosphere and depleted plumes. Inter, Geol. Rev. 38, 1-21.

Anderson D.L.*, Zhang Y-S., and Tanimoto T. (1992) Plume heads, continental lithosphere, flood basalts, and tomography. In Storey B.C., Alabaster T., and Pankhurst R.J., (eds) *Magmatism and the Causes of Continental Break-up*, *Geol. Soc. Lond. Spec. Pub*. **68**, 99-124.

Andrews J. E., Packham G. H., et al. (1975) *Proceedings of the Deep Sea Drilling Project, Initial Reports,* **30,** 753 pp.

Antretter M., Riisager P., Hall S., Zhao X., and Steinberger B. (2004) Modeled paleolatitudes for the Louisville hotspot and the Ontong Java Plateau. *Geol. Soc. Lond. Spec. Pub*. **229**, 21-30.

Barrera E. and Savin S. M. (1999) Evolution of late Campanian-Maastrichtian marine climates and oceans Evolution of the Cretaceous ocean-climate system, *Special Paper - Geological Society of America* **332**, 245-282.

Bercovici D. and Mahoney J.J. (1994) Double flood-basalt events and the separation of mantle-plume heads at the 660 km discontinuity, *Science*, **266**, p.1,367-1,369.

Bralower T. J., Fullagar P. D., Paull C. K., Dwyer G. S., and Leckie R. M. (1997) Mid-Cretaceous strontium-isotope stratigraphy of deep-sea sections. *Geological Society of America Bulletin*, **109**, 1421-1442

Bralower T.J., CoBabe E., Clement B., Sliter W.V., Osburn C.L., and Longoria J. (1999) The record of global change in Mid-Cretaceous (Barremian-Albian) sections from the Sierra Madre, northeastern Mexico *Journal of Foraminiferal Research* **29**, 418-437.

Bralower T.J., Silva I.P., Malone M.J. and the Shipboard Participants of Leg 198 (2002) New evidence for abrupt climate change in the Cretaceous and Paleogene. *GSA Today, November*, 4-10.

Campbell I.H. (1998) The mantle's chemical structure: Insights from the melting products of mantle plumes. In *The Earth's Mantle: Composition, Structure, and Evolution* (ed. I.N.S. Jackson), pp. 259-310. Cambridge University Press.

Campbell I.H. and Griffiths R.W. (1990) Implications of mantle plume structure for the evolution of flood basalts. Earth Planet. Sci. Lett. 99, 79-93.

Castillo P. R., Carlson R. W., and Batiza R. (1991) Origin of Nauru Basin igneous complex: Sr, Nd, and Pb isotopes and REE constraints. *Earth and Planetary Science Letters* **103**, 200-213.

Castillo P., Pringle M.S., and Carlson R.W. (1994) East Mariana Basin tholeiites: Jurassic ocean crust or Cretaceous rift basalts related to the Ontong Java plume? *Earth and Planetary Science Letters* **123**, 139-154.

Chambers L. M., Pringle M. S. & Fitton J. G. (2002) Age and duration of magmatism on the Ontong Java Plateau: ^{40}Ar-^{39}Ar results from ODP Leg 192. Abstract V71B-1271, *Eos, Transactions American Geophysical Union* **83**: F47.

Chambers L. M., Pringle M. S. & Fitton J. G. (2004) Phreatomagmatic eruptions on the Ontong Java Plateau: an Aptian ^{40}Ar/^{39}Ar age for volcaniclastic rocks at ODP Site 1184. *Geol. Soc. Lond. Spec. Pub*. **229**, 325-332.

Chazey,W.J.. III and Neal C.R. (2004) Large igneous province magma petrogenesis from source to surface: platinum-group element evidence from Ontong Java Plateau basalts recovered during ODP Legs 130 and 192. *Geol. Soc. Lond. Spec. Pub*. **229**, 219-238.

Coffin M.F. (1992) Emplacement and Subsidence of Indian Ocean Plateaus and Submarine Ridges. *Geophysical Monograph.* **70**, 115-125.

Coffin M.F. and Eldholm O. (1993) Scratching the surface: Estimating the dimensions of large igneous provinces. *Geology* **21**, 515-518.

Coffin M. F. and Eldholm O. (1994) Large igneous provinces: Crustal structure, dimensions, and external consequences. *Reviews of Geophysics* **32**, 1-36.

Cordery M.J., Davies G.F., and Campbell I.H. (1997) Genesis of flood basalts from eclogite-bearing mantle plumes. J. *Geophys. Res.* **102**, 20,179-20,197.

Courtillot V. E. and Renne P. R. (2003) On the ages of flood basalts, *C. R. Geoscience* **335**, 113-140.

Czamanske G.K., Gurevitch A.B., FedorenkoV., and Simonov O. (1998) Demise of the Siberian plume; paleogeographic and paleotectonic reconstruction from the prevolcanic and volcanic record, north-central Siberia. *Int. Geol. Rev.* **40**, 95-115.

Detrick R.S. and Crough S.T. (1978) Island subsidence, hot spots, and lithospheric thinning. *J. Geophys. Res.* **83**, 1235-1244.

Detrick R.S., Sclater J.G., and Thiede J. (1977) The subsidence of aseismic ridges. *Earth Planet. Sci. Lett.* **34**, 185-196.

Duncan R.A. (2002) Thermal and compositional effects of oceanic plateau form ation: consequences mfor the Cretaceoius anoxic events. Abstract volume of the *Workshop on Cretaceous Climate and Ocean Dynamics*, Florissant, Colorado, July 14-18, 2002, p. 18.

Duncan R.A. and Rchards M.A. (1991) Hotspots, mantle plumes, flood basalts, and true polar wander. Reviews of Geophysics, 29, 31-50.

Ely J.C. and Neal C.R. (2003) Using platinum-group elements to investigate the origin of the Ontong Java Plateau, SW Pacific. *Chem. Geol.* **196**, 235-257.

Erba E. (1994) Nannofossils and superplumes; the early Aptian "nannoconid crisis". *Paleoceanography* **9**, 483-501.

Farnetani C.G. and Richards M.A. (1994) Numerical investigations of the mantle plume initiation model for flood basalt events. *J. Geophys. Res.* **99**, 13,813-13,833.

Farnetani C. G., Legras B. and Tackley P. J. (2002) Mixing and deformations in mantle plumes. *Earth and Planetary Science Letters,* **196,** 1-15.

Fitton J.G. and Dunlop H.M. (1985) The Cameroon Line, West Africa, and its bearing on the origin of oceanic and continental alkali basalt. *Earth Planet. Sci. Lett.* **72**, 23-38.

Fitton J.G. and Godard M. (2004) Origin and evolution of magmas on the Ontong Java Plateau. *Geol. Soc. Lond. Spec. Pub.* **229**, 151-178.

Forsyth, D.W., S.C. Webb, L.M. Dorman, and Y. Shen (1998) Phase velocities of Rayleigh waves in the vicinity of the MELT experiment on the East Pacific Rise, *Science* **280**, 1235-1238.

Furomoto A.S., Webb J.P., Odegard M.E., and Hussong D.M. (1976) Seismic studies on the Ontong Java Plateau, 1970. Tectonophysics 34, 71-90.

Gaherty, J.B. (2001) Seismic evidence for hotspot-induced buoyant flow beneath the Reykjanes Ridge, *Science* **293**, 1645-1647.

Gladczenko T.P., Coffin M., and Eldholm O. (1997) Crustal structure of the Ontong Java Plateau: modeling of new gravity and existing seismic data, *J. Geophys. Res.* **102**, 22,711-22,729.

Glikson A.Y. (1996) Mega-impacts and mantle-melting episodes: Tests of possible correlations. *J. Australian Geol. Geophys.* **16**, 587-607.

Glikson A. Y. (1999) Oceanic mega-impacts and crustal evolution. *Geology,* **27,** 387-390.

Godfrey L. V., Lee D. C., Sangrey W. F., Halliday A. N., Salters V. J. M., Hein J. R., and White W. M. (1997) The Hf isotopic composition of ferromanganese nodules and crusts and hydrothermal manganese deposits; implications for seawater Hf. *Earth Planet. Sci. Lett.,* **151**, 91-105.

Gomer B.M. and Okal E.A. (2003) Multiple-ScS probing of the Ontong-Java Plateau. *Phys. Earth Planet. Int.,* **138**, 317-331.

Gradstein F.M., Agterberg F.P., Ogg J.G., Hardenbol J.; van Veen P. (1994) A Mesozoic time scale. *J. Geophys. Res.* **99**, 24,051-24,071.

Griffiths R.W., Gurnis M., and Eitelberg G. (1989) Holographic measurements of surface topography in laboratory models of mantle hotspots. geophysical Journal 96, 477-495.

Hagen R.A., Mayer L.A., Mosher D.C., Kroenke L.W., Shipley T.H., and Winterer E.L. (1993) *Proc. Ocean Drilling Prog. Sci. Results*, **130**, 23-31.

Hall, P., and Kincaid, C. (2003) Melting, dehydration, and the dynamics of off-axis plume-ridge interaction, *Geochem. Geophys. Geosys.* **4 (9).**

Halliday A.N. and Lee D-C. (1999) Tungsten isotopes and the early development of the Earth-Moon system. *Geochim. Cosmochim. Acta* **63**, 4157-4179.

Hill R.I. (1991) Starting plumes and continental break-up. *Earth Planet. Sci. Lett.* **104**, 398-416.

Hirth, G., and D.L. Kohlstedt (1996) Water in the oceanic upper mantle: implications for rheology, melt extraction, and the evolution of the lithosphere, *Earth Planet. Sci. Lett.* **144**, 93-108.

Hussong D.M., Wipperman L.K., and Kroenke L.W. (1979) The crustal structure of the Ontong Java and Manihiki oceanic plateaus. *J. Geophys. Res*. **84**, 6003-6010.

Ingle S. and Coffin M.F. (2004) Impact origin for the Greater Ontong Java Plateau? *Earth Planet. Sci. Lett*. **218**, 123-134.

Isley A.E. and Abbott D.H. (2002) Implications of the temporal distribution of high-Mg magmas for mantle plume volcanism through time. *J. Geology* **110**, 141-158.

Ito G. and Clift P. (1998) Subsidence and growth of Pacific Cretaceous plateaus. *Earth Planet. Sci. Lett.,* **161**, 85-100.

Ito, G., Y. Shen, G. Hirth, C.J. Wolfe (1999) Mantle flow, melting, and dehydration of the Iceland mantle plume, *Earth Planet. Sci. Lett.* **165**, 81-96.

Ito G. and Taira A. (2000) Compensation of the Ontong Java Plateau by surface and subsurface loading. *J. Geophys. Res.,* **105***, 11,171-11,183.

Jahren A. H., Amundson R., Arens N. C., Sarmiento G., and Guerrero J. (2001) Terrestrial record of methane hydrate dissociation in the Early Cretaceous. *Geology* **29**, 159-162.

Jahren A. H. (2002) The biogeochemical consequences of the mid-Cretaceous superplume, *Journal of Geodynamics* **34**, 177-191.

Janney P.E. and Castillo P.R. (1997) Geochemistry of Mesozoic Pacific mid-ocean ridge basalt: Constraints on melt generation and the evolution of the Pacific upper mantle. *J. Geophys. Res*. **102**, 5207-5229.

Jenkyns H.C. (1995) Carbon-isotope stratigraphy and paleoceanographic significance of the Lower Cretaceous shallow-water carbonates of Resolution Guyot, Mid-Pacific Mountains *Proceedings of the Ocean Drilling Program, Scientific Results*, **143**, 99-104.

Jones A.P., Price G.D., Price N.J., DeCarli P.S., and Clegg R.A. (2002) Impact induced melting and the development of large igneous provinces. *Earth Planet. Sci. Lett*. **202**, 551-561.

Jones C.E. and Jenkyns H.C. (2001) Seawater strontium isotopes, Oceanic Anoxic Events, and seafloor hydrothermal activity in the Jurassic and Cretaceous. *Amer. J. Sci*. **301**, 112-149.

Jordan, T.H. (1979) Mineralogies, densities and seismic velocities of garnet lherzolites and their geophysical implications, in The mantle sample: Inclusions in kimberlites and other volcanics, edited by F.R. Boyd, and H.O. Meyer, pp. 1-14, AGU, Washington, D.C.

Kennett B.L.N. and Widiyantoro S. (1999) A low seismic wave speed anomaly beneath northwestern India; a seismic signature of the Deccan Plume? *Earth Planet. Sci. Lett.* **165**, 145-155.

Kerr A.C. (1998) Oceanic plateau formation; a cause of mass extinction and black shale deposition around the Cenomanian-Turonian boundary? *J. Geol. Soc. Lond.* **155**, 619-626.

King S.D. and Anderson D.L. (1995) An alternative mechanism of flood basalt formation. *Earth Planet. Sci. Lett.* **136**, 269-279.

Klemme S., Blundy J.D., and Wood B.J. (2002) Experimental constraints on major and trace element partitioning during partial melting of eclogite. *Geochim. Cosmochim. Acta* **66**, 3109-3123.

Klosko E.R., Russo R.M., Okal E.A., and Richardson W.P. (2001) Evidence for a rheologically strong chemical mantle root beneath the Ontong-Java Plateau. *Earth Planet. Sci. Lett.*, **186**, 347-361.

Koppers A., Staudigel H., Wijbrans J.R., and Pringle M. (1998) The Magellan seamount trail: Implications for Cretaceous hotspot volcanism and absolute Pacific plate motion. *Earth Planet. Sci. Lett.* **163**, 53-68.

Koppers A., Staudigel H., Pringle M.S., and Wijbrans J.R. (2003) Short-lived and discontinuous intra-plate volcanism in the South Pacific: Hotspots or extensional volcanism? *Geology, Geophysics, Geosystems* **4(10)**, 1089, doi:10.1029/2003GC000533.

Koppers, A., Duncan, R.A., and Steinberger, B. (2004) Implications of a non-linear $^{40}Ar/^{39}Ar$ age progression along the Louisville seamount trail for models of fixed and moving hotspots. *Geology, Geophysics, Geosystems* (submitted).

Kroenke L.W. (1972) Geology of the Ontong Java Plateau. *Hawaii Inst. Geophys. Rpt.*, *HIG-72-5*, 119 pp.

Kyte F.T., Leinen M., Heath G.R., and Zhou L. (1993) Cenozoic sedimentation history of the central North Pacific; inferences from the elementary geochemistry of core LL44-GPC3. *Geochim. Cosmochim. Acta* **57**, 1719-1740.

Larson R. L. (1997) Superplumes and ridge interactions between Ontong Java and Manihiki plateaus and the Nova-Canton trough. *Geology* **25**, 779-782.

Larson R. L. and Erba E. (1999) Onset of mid-Cretaceous greenhouse in the Barremian-Aptian: igneous events and the biological, sedimentary, and geochemical consequences. *Paleoceanography* **14**, 663-678.

Leckie R.M., Bralower T.J., and Cashman R.(2002) Oceanic anoxic events and plankton evolution; biotic response to tectonic forcing during the Mid-Cretaceous, *Paleoceanography*, **17**, 29-40.

Lee D-C. and Halliday A.N. (1996) Hf-W isotopic evidence for rapid accretion and differentiation in the early solar system. *Science* **274**, 1876-1879.

Li L. and Keller G. (1999) Variability in Late Cretaceous climate and deep waters; evidence from stable isotopes, *Marine Geology* **161**, 171-190.

Mahoney J.J. (1987) An isotopic survey of Pacific oceanic plateaus: Implications for their nature origin. In Seamounts, Islands, and Atolls (Keating B., Fryer P., Batiza R., and Boehlert G. eds.), Amer. Geophys. Union Monograph 43, 207-220.

Mahoney J.J. and Spencer K.J. (1991) Isotopic evidence for the origin of the Manihiki and Ontong Java oceanic plateaus. Earth Planet. Sci. Lett. 104, 196-210.

Mahoney, J.J, Fitton, J.G., Wallace, P.J. et al. 2001. Basement drilling of the Ontong Java Plateau, Sites 1183-1187, 8 September- 7 November, 2000. *Proc. ODP Init. Rpts.*, **192**, 75p.

Mahoney J.J., Storey M., Duncan R.A., Spencer K.J., and Pringle M. (1993) Geochemistry and age of the Ontong Java Plateau, In: *The Mesozoic Pacific: Geology, Tectonics, and Volcanism* (M.S. Pringle, W.W. Sager, W.V. Sliter, and S. Stein, eds.) *Geophys. Monogr.* **77**, 233-262, AGU, Washington D.C.

Mann P., Coffin M., Shipley T., Cowley S., Phinney E., Teagan A., Suyehiro K., Takahashi N., Araki E., Shinohara M., and Miura S. (1996) Researchers investigate fate of oceanic plateaus at subduction zones. *Eos Trans. AGU,* **77**, 282-283.

Mayer L.A., Shipley T.H., Winterer E.L., Mosher D., and Hagen R.A. (1991) Deabeam and seismic reflection surveys on the Ontong Java Plateau. In: L.W. Kroenke, W.H. Berger, T.R. Janacek et al., *Proc. ODP Init. Rpts. 130*: College Station, TX (Ocean Drilling Program), 45-75.

McNutt M.K., Sichoix L., and Bonneville A. (1996) Modal depths from shipboard bathymetry; there is a South Pacific Superswell. *Geophys. Res. Lett.* **23**, 3397-3400.

Menegatti A. P., Farrimond P., Strasser A., Caron M., Weissert H., Brown R. S., and Tyson R. V. (1998) High-resolution δ13C stratigraphy through the early Aptian 'Livello Selli' of the Alpine Tethys, *Paleoceanography* **13**, 530-545.

Menzies M., Gallagher K., Yelland A., and Hurford A.J. (1997) Volcanic and nonvolcanic rifted margins of the Red Sea and Gulf of Aden; crustal cooling and margin evolution in Yemen. *Geochim. Cosmochim. Acta* **61**, 2511-2527.

Michael P. J. (1999) Implications for magmatic processes at Ontong Java Plateau from volatile and major element contents of Cretaceous basalt glasses. *Geochemistry, Geophysics, Geosystems* **1**, 1999GC000025.

Mitchell, B.J. (1995) Anelastic structure and evolution of the continental crust and upper mantle from seismic surface wave attenuation, *Rev. Geophys. Space Phys.* **33**, 441-462.

Miura S., Suyehiro K., Shinohara M., Takahashi N., Araki E., and Taira A. (2004) Seismological structure and implications of double convergence and oceanic plateau collision of Ontong Java Plateau and Solomon Island arc from ocean bottom seismometer-airgun data. *Tectonophysics* **389**, 191-220.

Mochizuki, K., Coffin, M.F., Eldholm, O., and Taira, A. (submitted) Massive Early Cretaceous volcanic activity in the Nauru basin related to emplacement of the Ontong Java Plateau, *Geochemistry Geophysics Geosystems (G^3)*.

Morgan J.W. (1972) Plate motions and deep mantle convection. *Mem. Geol. Soc. Am.* **132**, 7-22.

Mosher D.C., Mayer L.A., Shipley T.H., Winterer E.L., Hagen R.A., Marsters J.C., Bassinot F., Wilkens R.H., and Lyle M. (1993) Seismic stratigraphy of the Ontong Java Plateau. *Proc. Ocean Drilling Prog. Sci. Res.* **130**, 33-49.

Nakanishi M. and Winterer E.L. (1998) Tectonic history of the Pacific-Farallon-Phoenix triple junction from Late Jurassic to Early Cretaceous; an abandoned Mesozoic spreading system in the Central Pacific Basin. *J. Geophys. Res.* **103**, 12,453-12,468.

Nakanishi M., Tamaki K. and Kobayashi K. (1992) Magnetic anomaly lineations from Late Jurassic to Early Cretaceous in the west-central Pacific Ocean. *Geophysical Journal International,* **109,** 701-719.

Neal C.R., Mahoney J.J., Kroenke L.W., Duncan R.A., and Petterson M.G. (1997) The Ontong Java Plateau. In: Mahoney, J. J. and Coffin, M. F. (eds.) *Large Igneous Provinces: Continental, Oceanic, and Planetary Flood Volcanism. Geophysical Monograph, American Geophysical Union,* **100,** 183-216.

Olson P. and Nam I.S. (1986) Formation of seafloor swells by mantle plumes. *J. Geophys. Res.* **91**, 7181-7191.

Olson P. and Singer H.A. (1985) Creeping plumes. *J. Fluid Mech.* **158**, 511-531.

Olsson R. K., Wright J. D., and Miller K.G. (2001) Paleobiogeography of Pseudotextularia elegans during the latest Maastrichtian global warming event, *Journal of Foraminiferal Research* **31**, 275-282.

Parkinson I.D., Arculus R.J. and Duncan R.A. (1996) Geochemistry of Ontong Java Plateau basalt and gabbro sequences, Santa Isabel, Solomon Islands. *Eos, Trans. Amer. Geophys. Union* **77**, 715.

Parkinson I.J., Schaefer B.F. & the ODP Leg 192 Shipboard Scientific Party, (2001) A lower mantle origin for the world's biggest LIP? A high precision Os isotope isochron from Ontong Java Plateau basalts drilled on ODP Leg 192. Abstract No. V51C-1030, *Eos, Transactions American Geophysical Union,* **82:** F47.

Parsons B. and Sclater J.G. (1977) An analysis of the variation of ocean floor bathymetry and heat flow with age. *J. Geophys. Res*. **82**, 803-827.

Phinney E. J., Mann P., Coffin M.F., and Shipley T.H. (1999) Sequence stratigraphy, structure, and tectonic history of the southwestern Ontong Java Plateau adjacent to the North Solomon Trench and Solomon Islands arc. *J. Geophys. Res*. **104**, 20,449-20,466.

Richards M.A., Duncan R.A., and Courtillot V.E. (1989) Flood basalts and hot-spot tracks: Plume heads and tails. *Science* **246**, 103-107.

Richardson W.P., Okal E.A., and van der Lee S. (2000) Rayleigh-wave tomography of the Ontong Java Plateau, *Phys. Earth Planet. Int.,* **118**, 29-51.

Riisager P., Hall S., Antretter M., and Zhao X. (2004) Early Cretaceous Pacific paleomagnetic pole from Ontong Java Plateau basement rocks. *Geol. Soc. Lond. Spec. Pub*. **229**, 31-44.

Roberge, J., White, R. & Wallace, P., 2004. Volatiles in basaltic magmas from the Ontong Java Plateau (ODP Leg 192): implications for magmatic processes and source region compositions. *Geol. Soc. Lond. Spec. Pub*. **229**, 239-258.

Rogers, G. C. (1982) Oceanic plateaus as meteorite impact signatures. *Nature*, **299,** 341-342.

Roth, E.G., D.A. Wiens, L.M. Dorman, J. Hildebrand, and S.C. Webb (1999) Seismic attenuation tomography of the Tonga-Fiji region using phase-pair methods, *J. Geophys. Res*. **104**, 4795-4809.

Russo, R.M., V. Mocanu, M. Radulian, M. Popa, and K.-P. Bonjer (2004) Seismic attenuation in the Carpathian bend zone and surroundings, *Earth Planet.Sci. Lett.,* submitted.

Sandwell D.T. and Smith W.H.F. (1997) Marine gravity anomaly from GEOSAT and ERS 1 satellite altimetry. *J. Geophys. Res*. **102**, 10,039-10,054.

Saunders A.D. (1986) Geochemistry of basalts from the Nauru Basin, Deep Sea Drilling Project Legs 61 and 89: implications for the origin of oceanic flood basalts, *Init. Repts. Deep Sea Drill. Proj.,* **89,** 499-518.

Saunders, A.D., Storey M., Kent R.W., and Norry M.J. (1992) Consequences of plume-lithosphere interactions. In Storey, B. C., Alabaster, T., and Pankhurst, R. J. (eds.) *Magmatism and the Causes of Continental Break-Up*, Geol. Soc. Lond. Spec. Pub., **68,** 41-59.

Scholle P.A. and Arthur M.A. (1980) Carbon isotope fluctuations in Cretaceous pelagic limestones: Potential stratigraphic and petroleum exploration tool: AAPG Bull. **64**, 67–87.

Schuraytze B. C., Lindstrom D. J., Marin L. E., Martinez R. R., Mittlefehldt D. W., et al. (1996) Iridium metal in Chicxulub impact melt; forensic chemistry on the K-T smoking gun. *Science,* **276,** 1573-1576.

Shen, Y., S.C. Solomon, I. Th. Bjarnason, and C.J. Wolfe (1998) Seismic evidence for a lower mantle origin of the Iceland mantle plume, *Nature* **395**, 62-65.

Sheth H.C. (2000) The timing of crustal extension, diking, and eruption of the Deccan flood basalts. *Int. Geol. Rev*. 42, 1007-1016.

Shipley T.H., Abrams L.J., Lancelot Y., and Larson R.L. (1993) Late Jurassic – Early Cretaceous oceanic crust and Early Cretaceous volcanic sequences of the Nauru Basin, western Pacific, In: *The Mesozoic Pacific: Geology, Tectonics, and Volcanism* (M.S. Pringle, W.W. Sager, W.V. Sliter, and S. Stein, eds.) *Geophys. Monogr.* **77**, 103-119, AGU, Washington, D.C.

Sikora P.J. and Bergen J.A. (2004) Lower Cretaceous planktonic and nannofossil biostratigraphy of Ontong Java sites from DSDP Leg 30 and ODP Leg 192. *Geol. Soc. Lond. Spec. Pub.* **229**, 83-112.

Silver, P.G. (1996) Seismic anisotropy beneath the continents: Probing the depth of geology, *Ann. Rev. Earth Planet. Sci.* **24**, 385-432.

Sliter W.V. and Leckie R.M. (1993) Cretaceous planktonic foraminifers and depositional environments from the Ontong Java Plateau with emphasis on Sites 803 and 807, *Proc. Ocean Dril. Prog. Sci. Results* **130**, 63-84.

Smith A. D. and Lewis C. (1999) The planet beyond the plume hypothesis. *Earth-Science Reviews,* **48,** 135-182.

Stein C.A. and Stein S. (1992) A model for the global variation in oceanic depth and heat flow with lithospheric age. *Nature* **359**, 123-129.

Takahashi E., Nakajima K., and Wright T.L. (1998) Origin of the Columbia River basalts: melting of a heterogeneous plume head. *Earth Planet. Sci. Lett.* **162**, 63-80.

Tarduno J.A., Sliter W.V., Kroenke L., Leckie M., Mayer H., Mahoney J.J., Musgrave R., Storey M., and Winterer E.L. (1991) Rapid formation of Ontong Java Plateau by Aptian mantle plume volcanism. Science 254, 399-403.

Tarduno J.A., Brinkman D.B., Renne P.R., Cottrell R.D., Scher H., and Castillo P. (1998) Evidence for extreme climatic warmth from late Cretaceous Arctic vertebrates. *Science* **282**, 2241-2244.

Tejada M.L.G., Mahoney J.J., Duncan R.A., and Hawkins M.P. (1996) Age and geochemistry of basement and alkalic rocks of Malaita and Santa Isabel, Solomon Islands, southern margin of the Ontong Java Plateau, *J. Petrol.* **37**, 361-394.

Tejada M.L.G., Mahoney J.J., Neal C.R., Duncan R.A., and Petterson M.G.(2002) Basement geochemistry and geochronology of Central Malaita, Solomon Islands, with implications for the origin and evolution of the Ontong Java Plateau. *J. Petrol.,* **43,** 449-484.

Tejada M.L.G., Mahoney J.J., Castillo P.R., Ingle S.P., Sheth H.C., and Weis D. (2004) Pin-pricking the elephant: evidence on the origin of the Ontong Java Plateau from Pb-Sr-Hf-Nd isotopic characteristics of ODP Leg 192 basalts. *Geol. Soc. Lond. Spec. Pub.* **229**, 133-150.

VanDecar J.C., James D.E., and Assumpcao M. (1995) Seismic evidence for a fossil mantle plume beneath South America and implications for plate driving forces. *Nature* **378**, 25-31.

Van Keken P. (1997) Evolution of starting mantle plumes; a comparison between numerical and laboratory models. *Earth Planet. Sci. Lett.* **148**, 1-11.

Wallace P., Roberge J., White R.V., and Coffin M.F. (in prep) Anomalous subsidence of the Ontong Java Plateau inferred from CO_2 contents of submarine basaltic glasses. *Geology*.

White R.S. (1993) Melt production rates in mantle plumes. *Phil. Trans. Roy. Soc London* **342**, 137-153.

White R.S., McKenzie D., and O'Nions R.K. (1992) Oceanic crustal thickness from seismic measurements and rare earth element inversions. *J. Geophys. Res.* **97**, 19,683-19,715.

Wignall P.B. (2001) Large igneous provinces and mass extinctions. *Earth Sci. Rev.* **53**, 1-33.

Wilson P.A. and Opdyke B.N. (1996) Equatorial sea-surface temperatures for the Maastrichtian revealed through remarkable preservation of metastable carbonate, *Geology* **24**, 555-558.

Wolfe, C.J., and S.C. Solomon (1998) Shear wave splitting measurements and implications for mantle flow beneath the MELT region of the East Pacific Rise, *Science* **280**, 1230-1232.

Yasuda A., Fujii T., and Kurita K. (1997) A composite diapir model for extensive basaltic volcanism: Magmas from subducted oceanic crust entrained within mantle plumes. **Proc. Jpn. Acad. Ser. 73**, 201-204.

Yaxley G.M. and Green D.H. (1998) Reactions between eclogite and peridotite: mantle refertilisation by subduction of oceanic crust. *Schweiz Mineral. Petrogr. Mitt.* **78**, 243-255.

Zhang Y.S. and Tanimoto T. (1993) High-resolution global upper mantle structure and plate tectonics. *J. Geophys. Res.* **98**, 9793-9823.

Zhou L. and Kyte F.T. (1992) Sedimentation history of the South Pacific pelagic clay province over the last 85 million years inferred from the geochemistry of Deep Sea Drilling Project Hole 596. *Paleoceanography* **7**, 441-465.

KR05-01 Cruise Narrative

(L. Kroenke)

At 1000 JST (0100 UTC), 5 January, the R/V *Kairei* departed the JAMSTEC dock at Yokosuka, first headed east into Tokyo Bay, and then began the long transit southward to the survey area. The survey area, extending from 25º N to about 5º S and from 145º E to about 160º E, focused on a north-south multichannel seismic transect of the Ontong Java Plateau (OJP), including site surveys for proposed IODP ONT- sites 1 – 4, on the OJP, and PAB site 5, north of the OJP. Pending entry clearance from Papua New Guinea, the four ONT sites were considered to be the highest priority. On 6 January, notification of entry clearance was received. At 0705 JST, 7 January, as the R/V *Kairei* approached the survey area, the proton precession magnetometer was deployed. After deployment at 25º 08.3 N, 145º 29.8 E, SeaBeam swath mapping and 4 kHz subbottom profiling, gravity, and magnetic data collection commenced as the *Kairei* advanced southward into the survey area.

From entry into the survey area until arrival at the northernmost OJP site ONT-1, on 11 January, data acquisition was routine. However, in order to provide as much survey time as possible, a high transit speed had to be maintained enroute to to the start of the north-south OJP transect near proposed IODP site ONT-1. During the approach to ONT-1, the planned survey trackline was repositioned to avoid a seamount in close proximity to the site and additional short survey lines were added to better define the downfaulted block and fault scarp, which were targeted for drilling at the site. At 0000 JST, 10 January, shipboard time was advanced one hour to 0100 LST (1500 UTC, 9 January).

At 0500 LST, 11 January, the magnetometer was retrieved and the ERI air guns and the ORI multichannel solid streamer hydrophone array were deployed. Problems with a streamer bird required the streamer to be partially retrieved and the forward bird replaced. The MCS streamer was redeployed and, as SeaBeam swath mapping, SeaBeam 4 kHz, and gravity data continued to be collected, MCS surveying commenced at 0859 LST at the northern end of Eastport, the first survey line into the ONT-1 survey area. Eastport, an incoming dip line to the SSW, which crossed Leg 130 profile G-G' and passed west of ONT-1, was oriented perpendicular to the structure. This was followed by three more lines to the west over key structural components: Moosehorn, a short strike line along the crest of the structure, roughly orthogonal to Eastport; Lubec, a short connecting dip line to the NNE, parallel to the first line, and Quoddy, another strike line along the top of the fault block, which also crossed Leg 130 profile G-G' and passed over proposed site ONT 1. At the end of line Lubec, prior to the start of line Quoddy, 2 streamer birds had to be replaced, which slightly delayed the start of Quoddy. At 0151 LST, 12 Jan., the *Kairei* arrived at the end of line Quoddy and turned southward toward ONT-2, at the beginning of survey line Roque.

Line Roque, a long survey line connecting ONT-1 (through line Quoddy) to ONT-2 (through line Jonesport), along which SeaBeam swath mapping, SeaBeam 4 kHz, gravity, and MCS data continued to be acquired, extended south-southeastward along the crest of the northern OJP. An undulating, irregular seafloor topography accompanied by a somewhat rough acoustic basement terrain characterized the northern end of Roque. To the south, the seafloor became smoother, gradually decreasing in depth, as sediment thickness increased and acoustic basement roughness

decreased. The southern end of the line was characterized by a very smooth seafloor and very thick sedimentary section, with only minor basement relief.

At the end of line Roque, at 2319 LST, 13 Jan., *Kairei* changed course to the south to begin line Jonesport of the ONT-2 site survey. At 0257 LST, 14 Jan., *Kairei* crossed site ONT-2 and, after continuing another 10 km along this line, turned to the west-northwest, at 0412 LST, and stopped recording MCS data. At 0739 LST, *Kairei* turned to the east onto cross line Beals and again began recording MCS data. At 0900 LST, a leak occurred in the high pressure air line near the port airgun, requiring the airgun to be retrieved. At 0928 LST, speed was reduced to 3.6 kts and the port airgun was retrieved, while the starboard airgun continued to fire and MCS data continued to be acquired.

At 1000 LST, *Kairei* again crossed ONT-2. At 1030 LST, with the port airgun on board, speed was increased back to 5.5 kts. At this time, the port high pressure air and firing lines were replaced and the airgun refurbished. At 1227 LST, after extending line Beals 25 km past ONT-2, *Kairei* turned to the west-southwest, and again stopped recording MCS data. After the turn, the starboard airgun was also retrieved and checked for similar problems. During the transit to the southern end of line Jonesport, both port and starboard airguns were redeployed and tested. At 1624 LST, *Kairei* turned to the southwest along line Wass and again began recording MCS data and, at 1633 LST, line Jonesport was crossed, as *Kairei* headed toward the Hakuho Maru KH98-1 Leg 2 MCS profile 501.

During the survey across ONT-2, both the N-S and E-W MCS profiles collected were of high quality and were almost indistinguishable, each characterized by a very flat sea floor above a very thick well stratified sedimentary section overlying a smooth acoustic basement reflector.

At 0119 LST, 15 Jan., another leak developed in the high pressure air line near the port airgun and at 0126 LST, the port airgun was shut down. The starboard airgun, however, was still properly functioning and, with the MCS records still very acceptable, data acquisition continued. At 0143 LST, profile 501 was crossed about 10 km from the northern end of the profile. After continuing another 10 km to the southwest, at 0259 LST, the end of the line Wass was reached and speed was reduced to retrieve the MCS streamer and air guns. At 0415 LST, the airguns and MCS streamer were retrieved, the magnetometer fish was deployed and, at 0450 LST, after completing a short figure eight gravity meter calibration run, speed was increased to 14 kts, at the start of the transit line to the southern end of profile 501. This high transit speed was maintained enroute to the next 501 crossing line, in order to provide as much time as possible for finishing the north-south OJP transect, including the IODP site surveys.

At the end of the transit line, at 1606 LST, speed was reduced, at 1703 LST, the magnetometer was retrieved, and, at 1839 LST, the airguns and MCS streamer were redeployed. MCS data acquisition began again, at 1929 LST, 10 km from profile 501, as *Kairei*, headed west-southwest along line Split, toward profile 501. At 2029 LST, profile 501 was crossed about 10 km from its southern end, after which *Kairei* continued on the west-southwest heading until 2202 LST when the northern end of line Schoodic was reached and *Kairei* changed course to the south onto line Schoodic, a north-south survey line aligned along 157º E, heading toward sites ONT-3 and 4.

At 2358 LST *Kairei* crossed site ONT-3 and continued to head south on Schoodic toward ONT-4. At 1432 LST, 16 Jan., as *Kairei* approached site ONT 4, the most distant Tauu volcanic flows became clearly discernible in the MCS record, above the middle of the sedimentary section. At 1640 LST, *Kairei* reached the southern end of line Schoodic and, well before the flows breached the seafloor to form the northern submarine flank of Tauu, turned to the east-northeast and headed along Prospect toward the eastern end of cross line Machias, which was positioned 25 km from line Schoodic. Cross line Machias, a 50 km long east-west survey line, was aligned along 4º 20'S.

At 1909 LST, *Kairei* began a wide turn to the west and, at after completing the turn, at 1934 LST, began acquiring data along line Machias. During the cross line survey, the intermittent presence of very strong, sub bottom reflectors in the upper sedimentary section, obscured the presence of underlying reflectors along the eastern half of line Machias and resulted in the discontinuous appearance of coherent deep sediment and acoustic basement reflectors. At 2204 LST, line Schoodic was crossed. These same strong reflectors, believed to be sediment covered, outlying lava flows from Tauu, appeared to be relatively continuous across the western half of line Machias.

At 0037 LST, 17 Jan., *Kairei* reached the end of line Machias and speed was reduced to retrieve the air guns and MCS streamer. At 0147 LST, with the air guns and streamer back on board and the magnetometer fish deployed, speed was increased to 15.5 kts, as *Kairei*, continuing to acquire SeaBeam swath mapping, SeaBeam 4 kHz, gravity, and magnetic data, headed northwest at the start of a survey line to the western edge of the OJP.

At 1407 LST, the first waypoint (WP), WP 1, was reached on the southwestern edge of the OJP and *Kairei* turned to the north-northwest toward WP 2, beginning the survey of the western edge of the OJP. At 2240 LST, *Kairei* arrived at WP 2 and turned to the north-northeast toward WP 3, positioned to the northwest of Kapingamaragi Atoll. At 0727 LST, 18 Jan., *Kairei* arrived at WP 3 and turned to the north-northwest toward WP 4. At 1823 LST, WP 4 on the northwestern edge of the OJP was reached and *Kairei*, continuing to collect SeaBeam swath mapping, SeaBeam 4 kHz, gravity, and magnetic data, headed, on a slightly more northwesterly course, off the OJP toward WP 5, positioned south of the Caroline Islands.

At 0836 LST, 19 Jan., after passing south of the Nomoi, Namoluk, Losap and Chuk islands, *Kairei* arrived at WP 5 and turned due north toward WP 6, positioned between the Hall Islands and Namonuito Atoll at the western end of the Caroline Islands. The 15.5 kt speed that was maintained enroute, however, coupled with the moderately rough seas being encountered, forced repetitive rebooting of the SeaBeam system, which necessitated termination of 4 kHz subbottom profiling at 1150 LST.

At 1500 LST, WP 6 was reached and *Kairei* turned to the northwest to head into the East Mariana Basin. At 1626 LST, speed was reduced to retrieve the magnetometer fish, and at 1848 LST, after a new drogue line replaced the missing one on the fish and the fish was redeployed, speed was increased to 14 kts. At 0000 LST, shipboard time was set back one hour to 2300 JST (1400 UTC, 19 January). At 0640 JST, 20 Jan., speed was reduced to retrieve the magnetometer fish and, at 0710 JST after the fish was back on board, the *Kairei* increased speed toward WP 7.

At 0714 JST, 20 Jan., all data acquisition was terminated, concluding the departure survey off the OJP.

At the end of the survey line, *Kairei* continued to head northwest, beginning the transit back to Yokosuka. At 1410 JST, after completing the crossing of the southern East Mariana Basin, *Kairei* arrived at WP 7 on the Mariana Trench outer rise, about 300 km east of Guam, and headed north across the Mariana Trench. After crossing the trench, *Kairei* continued to head north, skirting the Mariana Forearc, east of the Mariana Islands, enroute to WP 8. At 1927 JST, 21 Jan., at WP 8, *Kairei* changed course to the west of north-northwest and headed toward WP 9, which was positioned due west of the Bonin Trench – Ogasawara Plateau collision zone. At, 0800 JST, 23 Jan., upon arrival at WP 9, *Kairei* changed course again to the north, to pass west of the Bonin Islands: Haha Jima, Chichi Jima, and Muko Jima. As of 1900 on 24 Jan., *Kairei* was approaching a waypoint near Oshima Island, with the intention of achieving Tokyo Bay late in the evening of 24 Jan, and then heaving to near the entrance to Yokosuka Harbor overnight. Docking at JAMSTEC in Yokosuka Harbor was planned for the morning of 25 Jan., thereby completing cruise KR05-1 to the Ontong Java Plateau.

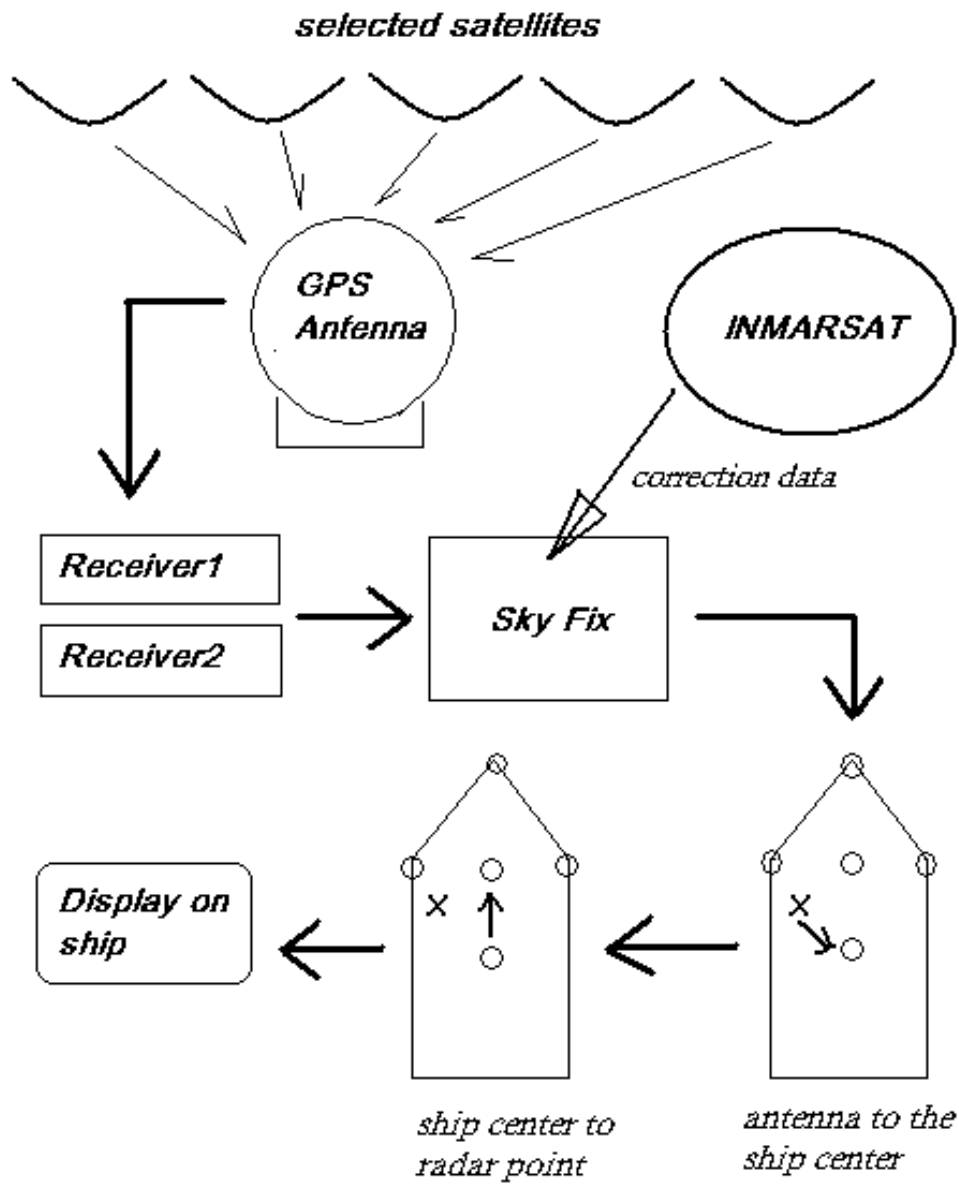# Global Positioning System Navigation

(M. Watanabe)

To locate a point in three dimensions, one needs to know the distances between the point and three other known places. The three distances are used as radii for three spheres, and the point where all three intersect is the location of the desired point. The Global Positioning System (GPS) uses instantaneous locations of three satellites for the known three points, distances being calculated by measuring the time for radio waves to arrive at the receiving point.

Information to locate the satellites is sent by radio waves, so it is important to adjust the clock of the receiving point as precisely as that of the satellite to know the time accurately. This can be challenging for many cases, so a fourth satellite is typically used to solve the problem. The fourth satellite can resolve differences in timing at each receiving point, and this information can be used to correct the three distances that are unknown. If more than four satellites are available, then an even more accurate and precise location can be obtained by using least squares. Another way to achieve precision and accuracy is to measure the location of a certain point for a long time interval, which is the same as receiving many data from several satellites.

Kairei has two independent GPS antennas. The GPS antennas are mounted on the highest open deck on the ship, and receive signals from several satellites (ideally, more than five for precise and accurate navigation). As the ship moves, its location requires correction, using signals from a fixed base point nearby. These correction data are sent by INMARSAT (International Marine Satellite Organization) to an instrument called "Sky Fix" on the *Kairei*. The precise position of the ship is defined as the middle point of the two radars located on the roof, so the signal received at the GPS antennas need to be corrected to the middle point location. First the signal is corrected to the ship's center of gravity, and then to the middle point location, which is 30 m away. Finally, the exact location of the ship is distributed to where it is needed. The information is sent every second.

selected satellites

GPS Antenna

INMARSAT

correction data

Receiver1

Receiver2

Sky Fix

Display on ship

ship center to radar point

antenna to the ship center

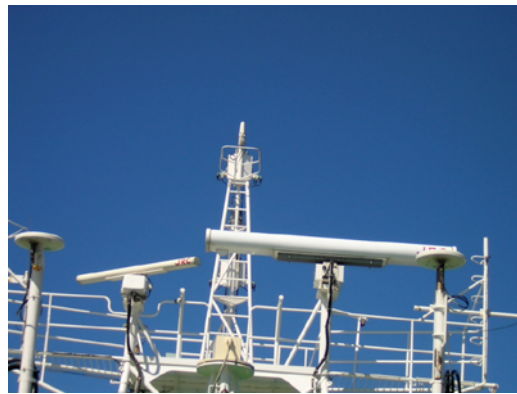Receivers 1, 2   INMARSAT antenna
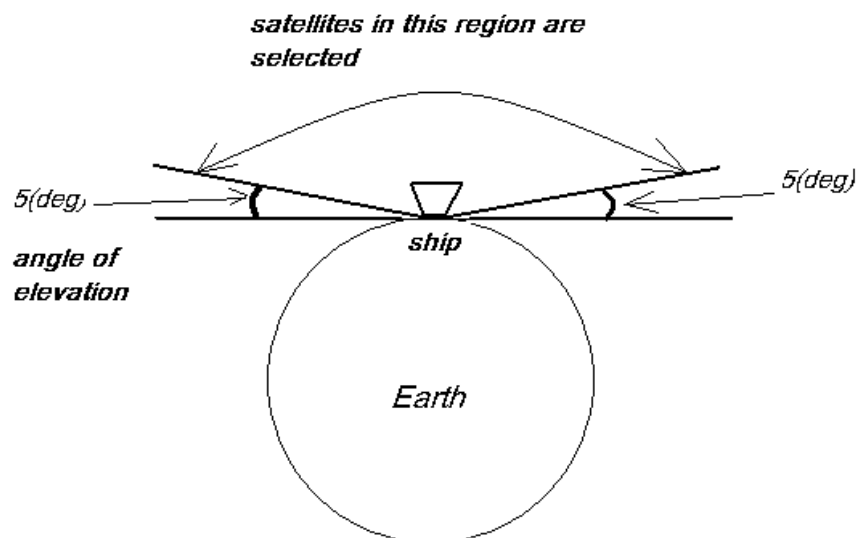
GPS antennas

Sky Fix (Demodulators)

Radars

The figure below shows the region where the satellites used for navigation are selected from around the Earth.

GPS Satellites and Signals

The constellation of 32 GPS satellites orbits the Earth at about 20,000 km from the ground. Each satellite sends out two types of carriers : Band L_1 (1.57542 GHz) and Band L_2 (1.2276 GHz). These carriers send out two signals: the code signal and the message signal. A code signal consists of the C/A code, which identifies the satellites, and the P code, which is used by the military. A message signal sends out time shift information and location of the satellite. The signals cannot penetrate through the ship's hull (metal), so the two GPS antennas are positioned on the open deck above *Kairei*'s bridge.

Navigation on *Kairei*

Kairei's primary navigation system is marine Differential-GPS (D-GPS), which typically provides geographic coordinates with a 2-3 m accuracy. The geographical limit for such accurate navigation of D-GPS, however, is ~2000 km from the nearest base point. For the KR05-01 survey of the Ontong Java Plateau, the closest (>2000 km distant) fixed receiver was the Darwin base point. The western Pacific region has too few base points for effective utilization of D-GPS, i.e., many areas are >2000 km from the nearest base point(s).

The main navigation sensors of the *Kairei* system are two D-GPS receivers, both have 12 channels. Data for differential corrections come from the SKYFIX system that uses controlled channels of INMARSAT as carriers. There are also two Demodulator/Translator instruments in the system so that the two D-GPS receivers can independently use the correction data.

The horizontal resolution varies with distance between the fixed base point and the GPS antenna. (Table 1).

Table 1. Horizontal resolution of *Kairei* GPS system

Distance [km]	Horizontal resolution [m]
<200	0.5
500	1.0
1000	3.0
1500	10.0
>2000	>20

The two D-GPS receivers are MX9400N models of Kawasaki Heavy Industries LTD. Their D-GPS input format is RTCMSC-104 Format and they have four ports (Table 2.)

Table 2. Data ports for receivers

Port 1 (CDU)	RS-232C
Port 2 (Raw data)	RS-232C
Port 3 (RTCM)	RS-232C
Port 4 (NMEA)	RS-422

The Translators, which are interfaces between INMARSAT and the Demodulators, are model 9041/H1. Their input signal frequency ranges within 195-215 MHz and 359-411 MHz.

The Demodulators exchange signals from INMARSAT and output data via RS-232C.   Their input signal frequency ranges from 60-80 MHz in 5 kHz step.

GPS Data

Data from the GPS system is sampled every second, so when *Kairei* is traveling at 15 kts, the distance traveled between GPS fixes is about 7.7 m, and at 5.5 kts (MCS survey speed) the distance is about 2.8 m. The GPS system is connected to *Kairei*'s network server by NFS, so all data are recorded in the directory (/home/hyb/DA/da/hybdata) on the server's disk. We obtained 1 s data in the SOJ format. This is available from *Kairei*'s network system, so the data can be copied onto media such as CDs. The data include information on the Date, Time and Location (latitude and longitude).

SeaBeam Bathymetry and Backscatter

(M. Watanabe)

Introduction to the system

The SeaBeam 2112 is an acoustic multi-beam survey system that generates data to produce wide-swath bathymetric contour maps and side-scan (backscatter) images. The system consists of two arrays, an array of 12 kHz projectors along the ship's keel and an orthogonal array of hydrophones across the bottom of the ship. SeaBeam 2112 transmits sonar signals from the projectors, and the signals travel through the sea water to the seafloor where they are reflected, and then return to the ship where they are received by the hydrophones. The signals are then processed by the system's electronics based on their travel times and intensities of the signal waves. This process provides bottom depths and other characteristics such as S/N ratio for echoes received across the swath. Information on the ship's position is based on GPS data and the ship's motion such as roll, pitch, and heave data originating from the Vertical Reference Unit. All data are logged to hard disks and 8 mm tapes so that they can be processed later for additional analysis. The system also includes plotters and side-scan graphic recorders to record and display the data.

Theory of operation

Sound travels in water as compressional waves and they propagate at a speed called the "local speed of sound". The local speed of sound can change depending on water properties such as salinity, pressure and temperature, but it is independent of the characteristics of the sound itself. In a typical ocean environment, the speed of sound is about 1500 m/s. When temperature, salinity, and pressure data are available, speed is calculated using the equation of Del Grosso (eq.1):

$$C = C_l + C_T + C_s + C_P + C_{TSP} \quad (1)$$

C: speed of sound in water
C_l: 1402.392 m/s
C_T: cubic equation for temperature
C_s: squared equation for salinity
C_P: cubic equation for pressure
C_{TSP}: polynomial for temperature, salinity and pressure

The SeaBeam system uses the velocity of sound in seawater to calculate range to the

31

seafloor. It is an echo sounder, which generates a ping and then listens for the echo of the pulse from the bottom. The time between transmission of a pulse and the return of its echo is the time it takes the sound to travel to the bottom and back. So the following equation yields the range to the bottom:

Range = 1/2 * velocity*echo time

In practice, we must consider some effects on the ping during its propagation in seawater. By convention, the final strength of the measured echo-return is expressed by the following equation (Fig. 1):

.

SE = SL-2TL+BS-NL+TA

(SE): Signal Excess—strength of the measured echo return.

(SL): the transmitted Source Level

(TL): Transmission Loss

(BS): Backscattering Strength

(NL): Noise Level

(TA): Target Area

① PING IS TRANSMITTED
SL

②
PING ARRIVES
AT BOTTOM
SL - TL

③
ECHO EVENT
SL - TL + BS + TA

④
ECHO ARRIVES
AT HYDROPHONE
SE = SL - 2TL + BS - NL* + TA

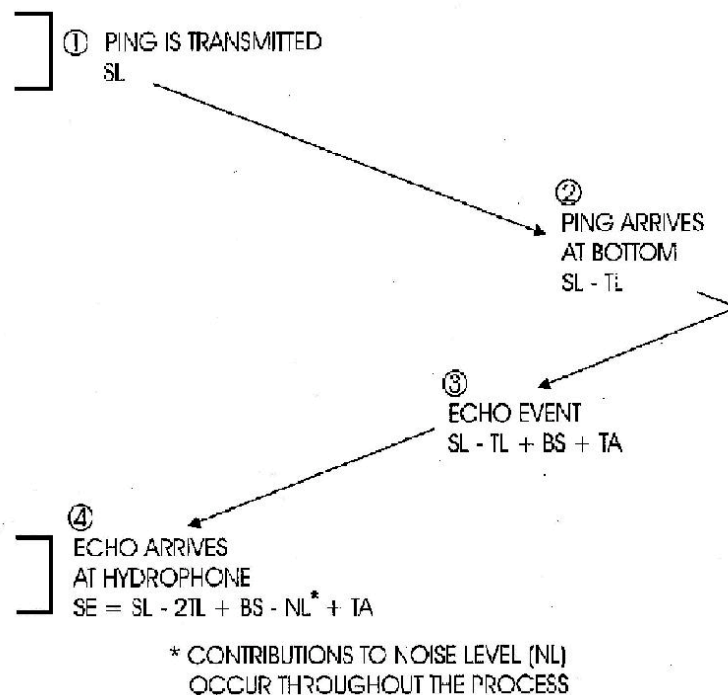* CONTRIBUTIONS TO NOISE LEVEL (NL)
OCCUR THROUGHOUT THE PROCESS

Fig. 1. Path of a ping.

Next we address how depth sounders (echo sounding devices) work, starting from the case of single-beam depth sounders to learn about their limitations. This is a prelude to

understanding multi-beam sonar (SeaBeam system).

A single-beam depth sounder consists of four components (Fig. 2): a Transmitter, a Transducer, a Receiver, and a Control and Display system.
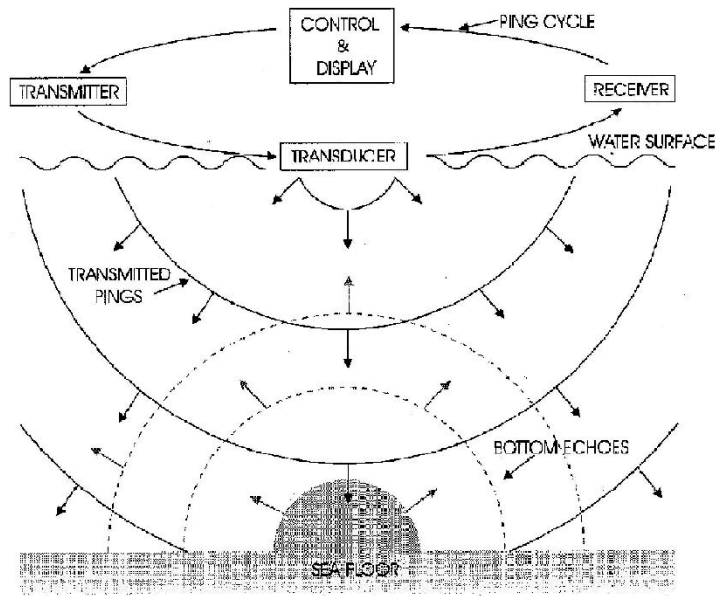

Fig. 2. Single beam depth sounder components.

In a 'ping' cycle, the Control and Display signals the Transmitter to produce a ping. The Transmitter generates an oscillating electric signal. The Transducer converts the electrical energy into sound waves. Then the oscillating electric signals are converted into mechanical vibrations that are transmitted into the water as a sound wave. Upon its return as an echo from the seafloor, the sound pulse is received and converted back into electrical signals by the Transducer. The Transducer passes on all received electrical signals to the Receiver to compute a depth. This depth is reported and recorded by the Control and Display. The Control and Display then triggers the next ping. Using this continuous 'ping cycle', depth measurements are taken and logged.

To obtain an accurate picture of the geography of the bottom, the accurate depth of many neighboring points on the seafloor must be known, with the following requirements of the sonar used: it must produce accurate depth measurement that correspond to well-defined locations on the seafloor such as latitude and longitude, and it must be able to make many such measurements in a reasonable amount of time. The single-beam echo sounder becomes inconvenient in both these points as demonstrated in the following examples.

When a survey ship is over an irregular rough seafloor, the first echo might not be from a point directly below, but from a feature behind or beside the ship that happens to be closer (Fig. 3).
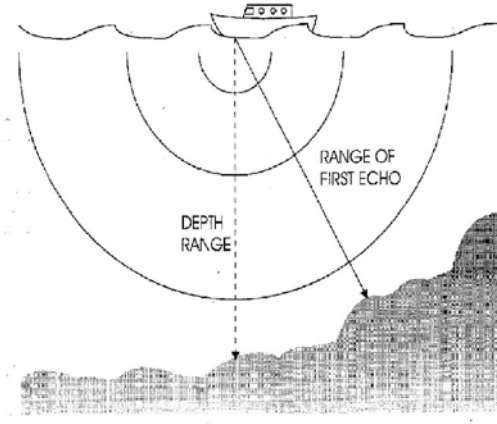

Fig. 3. Echo possibilities.

This problem can be solved by using a narrow-beam echo sounder, but two problems remain. First, because the transducers are mounted on the hull of a ship, the effect of ship motion caused by waves scatters the beams (e.g., Fig. 4). Secondly, narrow beams are made by larger, and therefore more expensive, transducers.
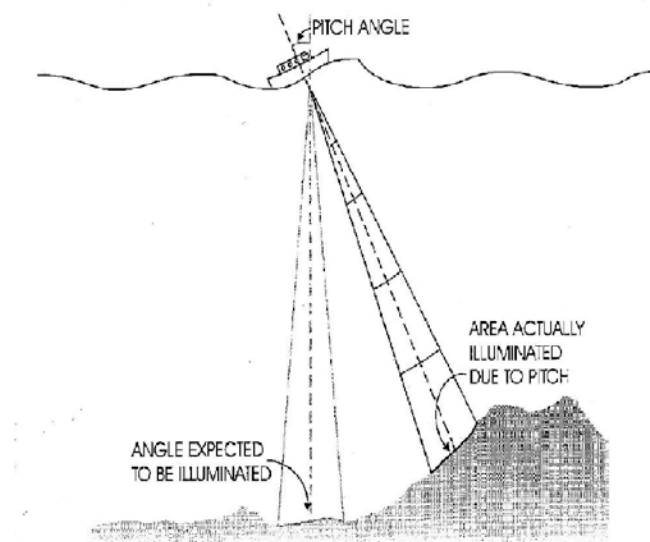

Fig. 4. Effect of ship motion.

Another problem is that the area ensonified by a fixed beam with a solid angle can change depending on water depth. The deeper a ping goes, the larger an area its angle will intersect (e.g., Fig. 5).
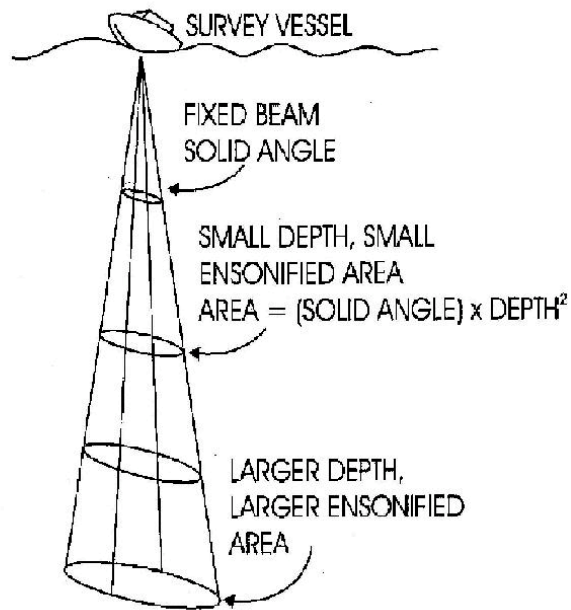
Fig. 5. Effect of depth.

A final problem is that, with a very narrow beam, mapping requires many individual measurements, thus requiring a long time.

An instrument that solves these problems is multi-beam sonar. It can map an area called a swath by performing the job of a narrow single-beam echo sounder at several different locations on the bottom at once. The dimension of the swath in the athwartship direction is called the swath width (Fig. 6).
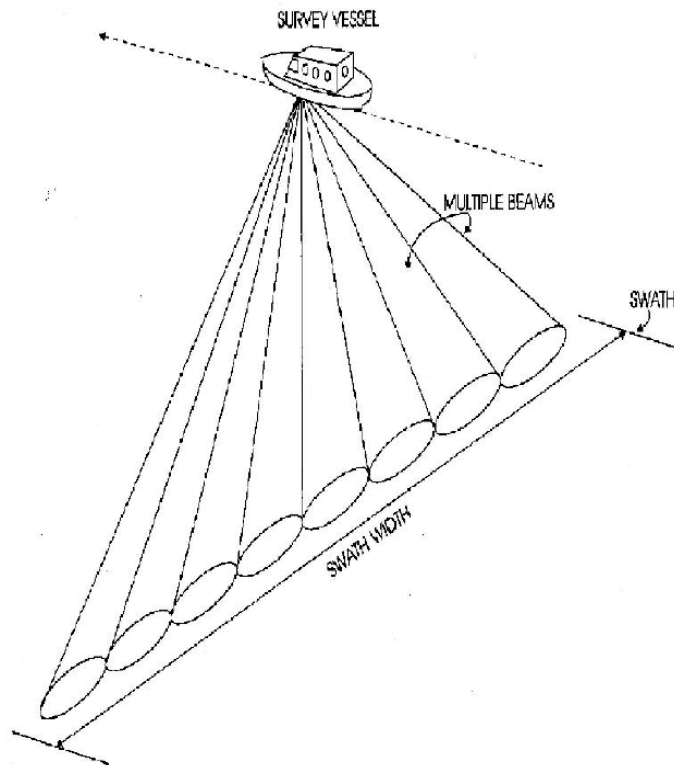
Fig. 6. Multi-beam sonar system.

The SeaBeam 2112 is a multi-beam sonar system. It maps up to 151 sounding points at $1°$ intervals with each ping, and can cover areas tens of kilometers wide in depths of a few kilometers.

Hardware Overview

The SeaBeam hardware system consists of the following major elements (Fig. 7):

● Rack assembly and all other electronics it houses (Transmitter, Echo Processor, Data Logger)
● Projector underhull assembly
● Hydrophone underhull assembly
● Vertical reference unit
● Operator control station

The projector array is a 14-foot long linear array positioned fore and aft along the *Kairei*'s keel. The receiver array detects and processes the returning echoes through stabilized multiple narrow athwartship beams in a fan shape. In the case of *Kairei*, the ship's bottom is flat, so the hydrophone array is the same shape. The system synthesizes $2°$ $*2°$ narrow

beams at an interval of $1°$, and the swath width varies, from $120°$ at depths between 1500 m and 4500 m, to $100°$ between 4500 m and 8500 m to $90°$ deeper than 8500 m. The transmit interval of the sonar signal ping increases with water depth, and is ~20 s at 6500 m. So the horizontal resolution of the bathymetry data depends on the depth and ship's speed, e.g., the across-track resolution will be 35-70 m at 2000 m depth, and 78.5-157 m at 4500 m depth. The along-track resolution depends on the ship's speed and it is ~42.4 m at 5.5 knots, and 115.75 m at 15 knots. The Fresnel Zones of each ping increase with depth, but the overlapping areas decrease with ship's speed. The accuracy of depth measurements is reported as 0.5% of the water depth.
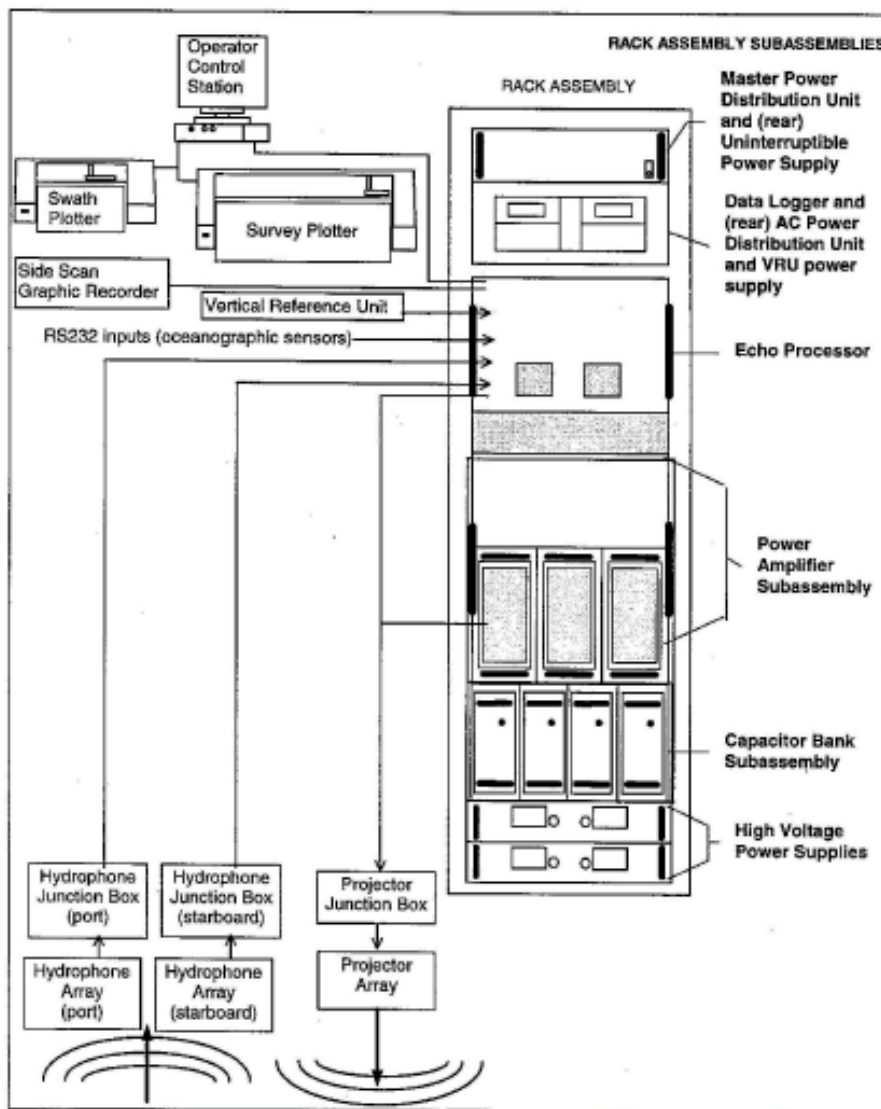

Fig. 7. SeaBeam hardware.

The Vertical Reference Unit (VRU) supplies digital roll, pitch, and digitally filtered heave data to the receiver. This data is appended to the hydrophone data records sent from the

receiver to the sonar processor. The sonar processor uses the pitch data to determine the location of the transmit beam on the seafloor, the roll data to steer the receive beams, and the heave data to correct the depth on each received beam.

The control station is where the operator performs all commands to operate the SeaBeam system.

Software Overview

The software that controls the system, Sea View, employs the Lynx Operating System and runs on Indigo work stations (SGI). The obtained raw data includes data records of each ping, nautical information (roll, pitch, and heave), and correction parameters such as water velocity structure. Post processing consists of editing raw data (deletion of bad data, correction of position, etc.), and making grid data files and various maps. The software used here is Sea View, MBSystem and GMT (Generic Mapping Tools).

Data acquisition parameters

One of the most important parameters for depth and position accuracy of bathymetric survey is sound velocity profile. The SeaBeam 2112 system uses sound velocity data not only for calculating the depth and position of each beam during the ray tracing process, but also for the beam forming process. The temperature of the surface layer is most important in this regard, and the system measures and uses surface temperature in real time. Except for the surface layer temperature, however, the user must input temperature profiles. During KR05-01, data from XBT (expendable bathy-thermograph) measurements were used to a depth of 1830 m (Table 1). The obtained sound velocity data is also shown in the tables below. For depths greater than 1830 m, data from previous CTD (conductivity-temperature-depth) measurements were used (1999, 2001, 2002, 2004). Some CTD data were obtained in different seasons, but the water temperature profile at depth was believed to be similar enough to use for this January 2005 cruise.

The salinity used for calculation throughout the measurement was 34.5 per mil.

Table 1. XBT measurements during KR05-01

	Date	Time	Latitude	Longitude
Point A	2005/01/06	22:00:00	25-08.8690N	145-29.5030E
Point B	2005/01/10	18:55:23	04-59.4598N	154-44.0037E

Point C	2005/01/15	07:10:41	02-40.0981S	157-15.5055E
Point D	2005/01/18	08:27:00	04-59.4598N	154-44.0037E
Point E	2005/01/19	05:00:00	11-19.9200N	142-12.0700E

(Point C: depth limit = 1760 m)

Sound velocity data for Point A

Depth (m)	Velocity (m/sec)	Depth (m)	Velocity (m/sec)
4.5	EXTERNAL	1000.0	1483.1
10.0	1531.7	1200.0	1483.4
20.0	1531.8	1500.0	1485.3
50.0	1532.1	1800.0	1488.4
100.0	1532.9	2000.0	1490.8
150.0	1527.1	2500.0	1497.9
200.0	1522.4	3000.0	1505.9
250.0	1519.8	3500.0	1514.3
300.0	1518.1	4000.0	1522.8
350.0	1516.8	5000.0	1540.7
400.0	1514.7	6000.0	1559.3
500.0	1506.7	7000.0	1578.2
600.0	1498.9	8000.0	1597.5
700.0	1492.2	9000.0	1617.0
800.0	1487.3	10000.0	1636.7

Sound velocity data for Point B

Depth (m)	Velocity (m/sec)	Depth (m)	Velocity (m/sec)
4.5	EXTERNAL	1000.0	1481.3
10.0	1532.7	1200.0	1481.8
20.0	1532.9	1800.0	1487.8
50.0	1533.1	2000.0	1490.8
100.0	1528.5	2500.0	1497.9
150.0	1524.8	3000.0	1505.9
200.0	1521.0	3500.0	1514.3
250.0	1516.6	4000.0	1522.8

Depth	Velocity	Depth	Velocity
300.0	1512.6	5000.0	1540.7
350.0	1509.7	6000.0	1559.3
400.0	1506.9	7000.0	1578.2
500.0	1499.8	8000.0	1597.5
600.0	1491.8	9000.0	1617.0
700.0	1486.4	10000.0	1636.7
800.0	1482.9		

Sound velocity data for Point C

Depth (m)	Velocity (m/sec)	Depth (m)	Velocity (m/sec)
4.5	EXTERNAL	1000.0	1486.3
10.0	1543.2	1200.0	1486.3
20.0	1543.4	1500.0	1487.8
50.0	1543.8	1800.0	1490.6
100.0	1537.2	2000.0	1492.7
150.0	1531.5	2500.0	1498.2
200.0	1513.7	3000.0	1505.9
250.0	1502.7	3500.0	1514.3
300.0	1493.6	4000.0	1523.0
350.0	1491.9		
400.0	1490.6		
500.0	1489.5		
600.0	1488.2		
700.0	1487.2		
800.0	1486.7		

Sound velocity data for Point D

Depth (m)	Velocity (m/sec)	Depth (m)	Velocity (m/sec)
4.5	EXTERNAL	1000.0	1486.1
10.0	1545.3	1200.0	1486.5
20.0	1545.3	1500.0	1487.8
50.0	1545.8	1800.0	1489.0

100.0	1542.7	2000.0	1490.5
150.0	1534.1	2500.0	1497.9
200.0	1519.2	3000.0	1506.0
250.0	1499.9	3500.0	1514.3
300.0	1499.6	4000.0	1523.0
350.0	1498.2	5000.0	1540.5
400.0	1497.9		
500.0	1495.1		
600.0	1491.4		
700.0	1488.2		
800.0	1486.7		

Sound velocity data for Point E

Depth (m)	Velocity (m/sec)	Depth (m)	Velocity (m/sec)
4.5	EXTERNAL	1000.0	1486.4
20.0	1551.2	1200.0	1486.0
30.0	1551.5	1500.0	1487.7
50.0	1542.7	1800.0	1490.2
100.0	1542.8	2000.0	1492.4
150.0	1523.0	2500.0	1499.0
200.0	1510.6	3000.0	1506.8
250.0	1499.4	3500.0	1515.1
300.0	1495.6	4000.0	1523.8
350.0	1491.9	5000.0	1541.6
400.0	1489.9	6000.0	1560.1
500.0	1487.7	7000.0	1579.0
600.0	1486.9	7900.0	1596.2
700.0	1486.5	9000.0	1617.5
800.0	1486.5	10000.0	1636.9

Problems with the system

When a ship turns during a SeaBeam survey, the swath pattern tends to appear radially around the turning point. This leaves a pattern when making a map with the gridded data. Another important factor is that increasing ship's speed correlates with increasing noise in

SeaBeam data, degrading both data density and quality. For regional surveys, an ideal speed for R/V *Kairei* is 10-12 kts. For local surveys, such as around a dive point, the ideal speed is 5-6 kts.
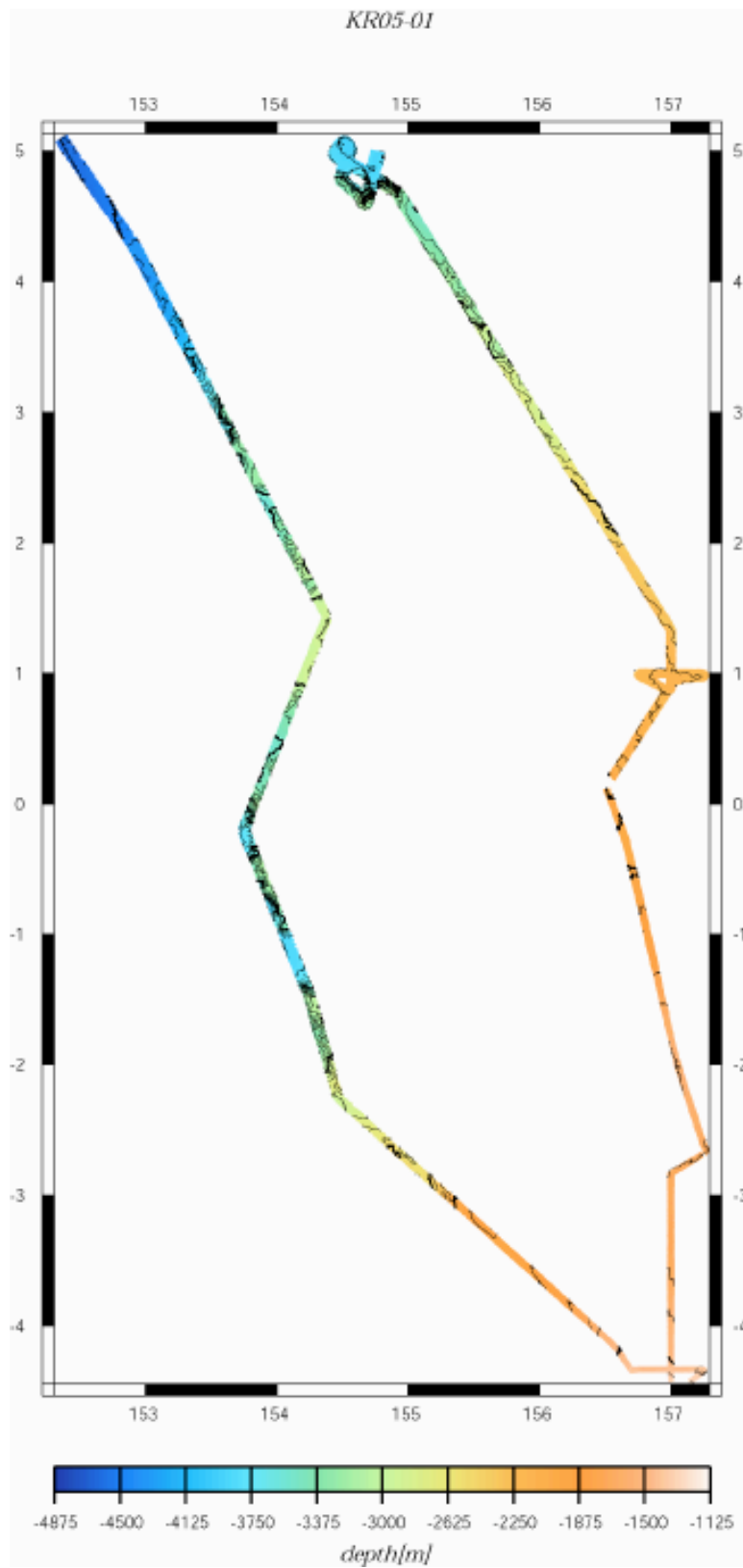
Fig. 8. KR05-01 SeaBeam image of the Ontong Java Plateau.

SeaBeam Sub-Bottom Profiler

(M. Watanabe)

Introduction to the system

The SeaBeam 2100 sub-bottom profiler system, SBP for short, is an optional system added to the SeaBeam 2112 multi-beam bathymetry system. These two systems are combined into a single system, SeaBeam 2112.004. This combined system can simultaneously collect and display SBP data and large-scale bathymetric and side-scan (reflectivity) surveys. Being able to collect these data sets at the same time is important for research on sediment type, geological activity, and detailed topographic structure. The collected data set can also be used to make plans for surveys and operations.

The following table shows the system configuration of the SBP on R/V *Kairei*.

Component or Feature	System Options Installed
Rack assembly, 4KHz	Single rack
Master power input	117VAC, 30A, 60Hz
Acoustic receiver channels	40 channels
Projector underhull assembly	4KHz
Transmit beam width, 4KHz	$5°$
Projector array, 4KHz	60 modules
Projector wet cables, 4KHz	10 wet cables
Projector junction box, 4KHz	1 junction box
Hydrophone underhull assembly	12KHz, 4KHz (same assembly used for both systems)
Receive beam width	$5°$ for 4KHz
Hydrophone wet cables	8 wet cables, 8 channels per cable (60 used, 4 spares)

Operational overview

The SBP component of the SeaBeam 2100 system is capable of acquiring data between water depths of 50 m and 11,000 m. Depth penetration varies according to bottom composition, and may be as much as 75 m.

The system uses an array of sixty TR-109 projectors to generate a projected beam. The beam

widths are $45°$ across and $5°$ along the ship. To receive sub-bottom returns by the SeaBeam 12 kHz hydrophone array (wide-aperture), a narrow normal incidence beam $5°$ wide is also generated. The hydrophone array is used together with the SBP system, so the period of the ping cycle needs to be the same so that the SBP and bathymetric data are coincident and don't interfere.

Resolution for sub-bottom sediment is higher than with standard systems owing to the SBP's narrow beam ($5°$) e.g., 175 m for 2000 m depth and 393 m for 4500 m depth. . Resolvability varies with depth and sediment type, but in most cases, it is within the range of a few tens of cm.

The system startup, parameter settings, and real time control are undertaken on an Indigo Work Station (SGI). The data are displayed on a terminal and EPC recorder, and stored on a hard disk and a data logger (EPC Thermal Graphic Recorder).

Hardware Overview

The hardware system of the SBP consists of six main elements (Fig. 1).

- Operator Control System and Data Logger
- MPDU
- Sub-Bottom Profiler(SBP) echo processor
- Spare SBP echo processor
- Surface Sound velocity (SSV) unit
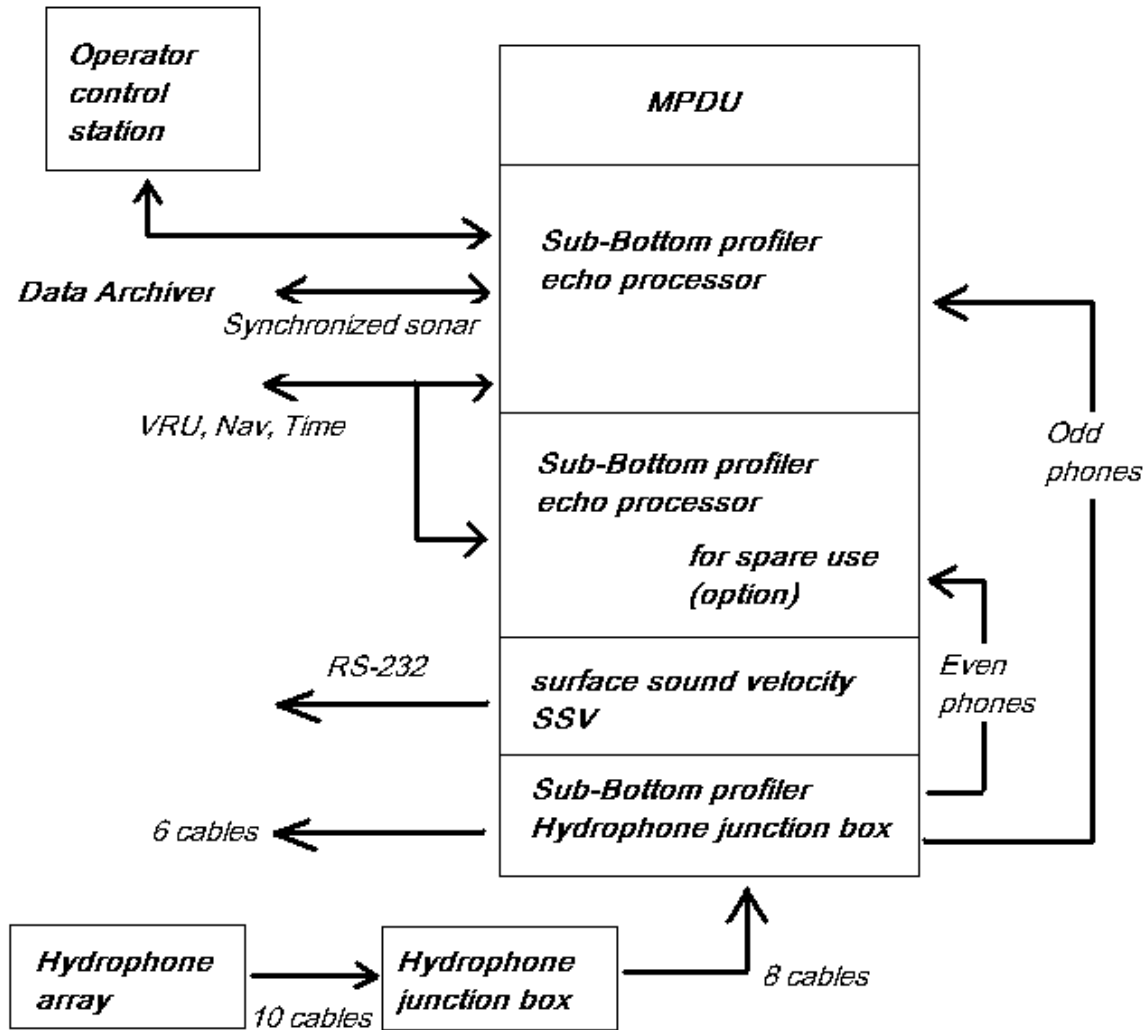- Sub-Bottom Profiler (SBP) Hydrophone junction box

Fig. 1. SBP hardware.

Problems with the system

During KR05-01, SBP data were measured below 25°N, except between 2000 and 0600 so as not to disturb humans. Data obtained during the MCS survey was of high quality, because the ship speed was around 5 kts. However, at a normal cruising speed of ~14-15 kts the SBP data were degraded by noise, and seafloor signal was occasionally lost, producing data gaps. The survey was stopped for a while when the seafloor topography was too rough. In moderate to heavy seas, many air bubbles traverse the bottom of the ship, disturbing the ping signal and its receipt, and thereby degrading the data.

ORI/ERI Multichannel Seismic Reflection System

(H. Inoue and Y. Nakamura)

Introduction to the system

This section describes the University of Tokyo Ocean Research Institute (ORI)/Earthquake Research Institute (ERI) 24-channel seismic reflection system employed during KR05-01. This section is a technical description. We collected ~20,000 shots (13 GB) of 24-channel seismic data during the cruise.

Description of Equipment

The cable reel, winch, and streamer cable were delivered to *Kairei* from ORI. The cable reel on R/V *Kairei* was positioned at the middle point of the afterdeck, approximately 21.5 m from the stern. The outer diameter of the steel drum is about 1.2 m in diameter, and its width is about 2 m. ORI's Innovative Technology Inc. (ITI) ST5 24-channel, 600 m solid streamer cable was loaded on *Kairei* at the completion of KR04-12 on 28 December 2004. Streamer diameter is 3 cm, and bulbous hydrophones every 5 m yield a 25-meter active channel. The total number of hydrophones in the 600 m streamer is 120. The outboard phone bulbs of each channel are labeled with channel numbers from 1 to 24. Each group has a single preamplifier located inside the phone bulb. These are powered by 12 v batteries in the Geology Laboratory (recording room) on R/V *Kairei*. The cable consists of a 600 m active section, a leader section 110 m long, and a tail rope 200 m long. No tail buoy is used.

Four bird coil bulbs were located at channels pre-1, 7. and 13, and post-24. The SYNTRON MultiTrak remote units (birds) consist of a depth sensor, temperature sensor, and wing angle feedback system. Each bird is accompanied by a float. Two of the birds contained a compass. The birds were connected to the MultiTrak controller SYNTRON 5814-250NSL (Fig. A) and monitored every 20 s. One of the bird floats was not available because some of its screws were rusty. Therefore, we borrowed a float from *Kairei*'s stores and used it on the pre-13 bird.

The cable has a connector at its head, and it was connected via a deck cable to the Geology Laboratory, where ORI's Geometrics Strata Visor NX data acquisition system, bird monitor, and 12 v batteries were installed. (Fig. A)

Air guns were delivered to *Kairei* from ERI. Two Bolt 1500 LL air guns, each with a 1500

in^3 chamber, were towed at equal distance (~30 m) and depth (~10 m) behind the stern from starboard and port sides. Each air gun was attached to a 'Norwegian' float. Firing cables, air hoses, and stainless wires linked the guns with *Kairei*. Each gun was shot independently using synchronized timing.

We used *Kairei'*s Leobersdorfer Maschienfabrik AG air compressors. They are located in the compressor room and connected to the air guns via air hoses. The air guns were fired at 10.9 ±0.1 MPa (~1600 psi) throughout the cruise.

Gun firing was controlled by a countdown timer. (Fig. A) A Truetime GPS clock, with an antenna on the port side of the funnel deck, was connected to the countdown timer. Shooting time was logged at a PANASONIC Loox PC. (Fig. A) A randomizer (+500 ms) was introduced to randomly shift the shot interval time, so as to mitigate against coherent previous shot energy.
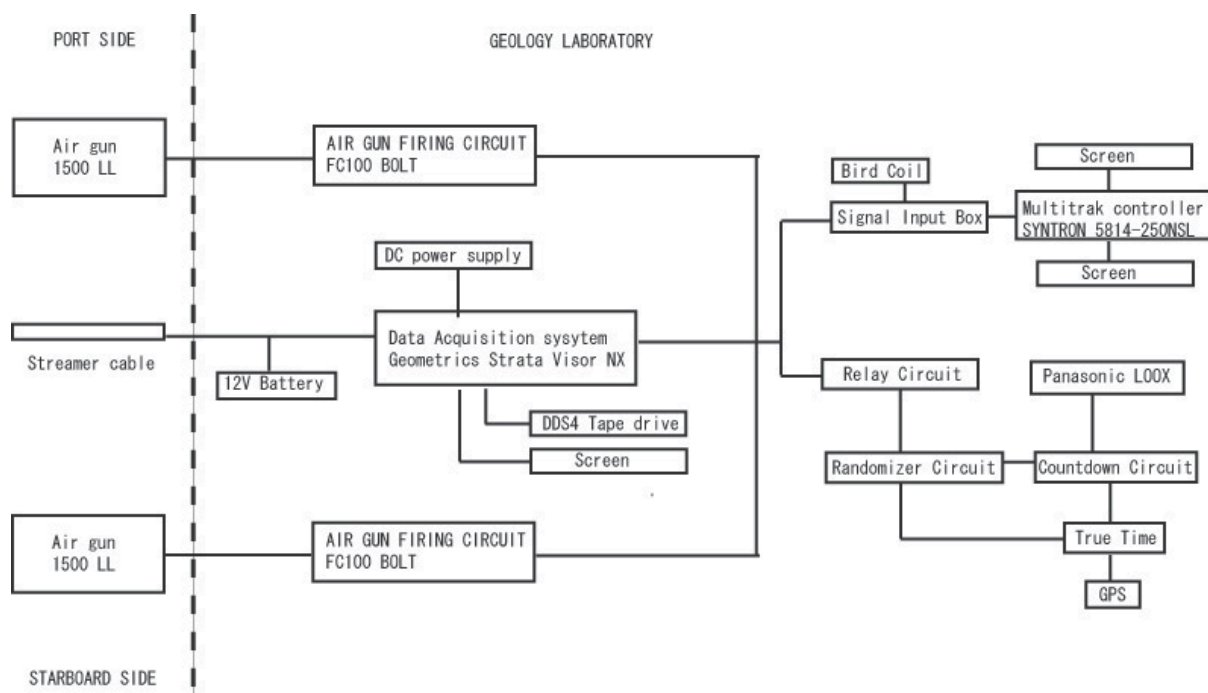

Fig. A. Diagram of air gun and streamer system.

Theory of operation

The multichannel seismic reflection (MCS) method is critical for understanding sub-seafloor geology. The main components of an MCS survey are:
1. a source of seismic energy
2. a means of detecting elastic waves traveling through the water column or in the seabed

3. a method of recording and displaying seismic waves in a readily interpretable form.

Air gun

The air gun suddenly releases compressed air into water, producing short duration and high-energy seismic waves. The air gun is made up of two high-pressure air chambers sealed by a piston (Fig. B). High-pressure air enters chambers A and B. When fired, the piston moves rapidly upward, discharging the high-pressure air from chamber B into the water through the port. After shooting the pressure difference between A and B causes the piston to descend. The firing cycle is repeated.

The dominant frequency range of the 1500 LL air gun is 12-20 Hz. This indicates vertical resolution of about 25-42 m, and vertical detection is about 12.3-21 m, assuming a sediment velocity of 2000 m/s. Vertical resolution is about 63-104 m and vertical detection is about 31-52 m, assuming a basalt velocity of 5000 m/s. Horizontal resolution based on the first Fresnel zone is about 540–707 m at 2000 m water depth, and about 774-1000 m at 4500 m water depth.
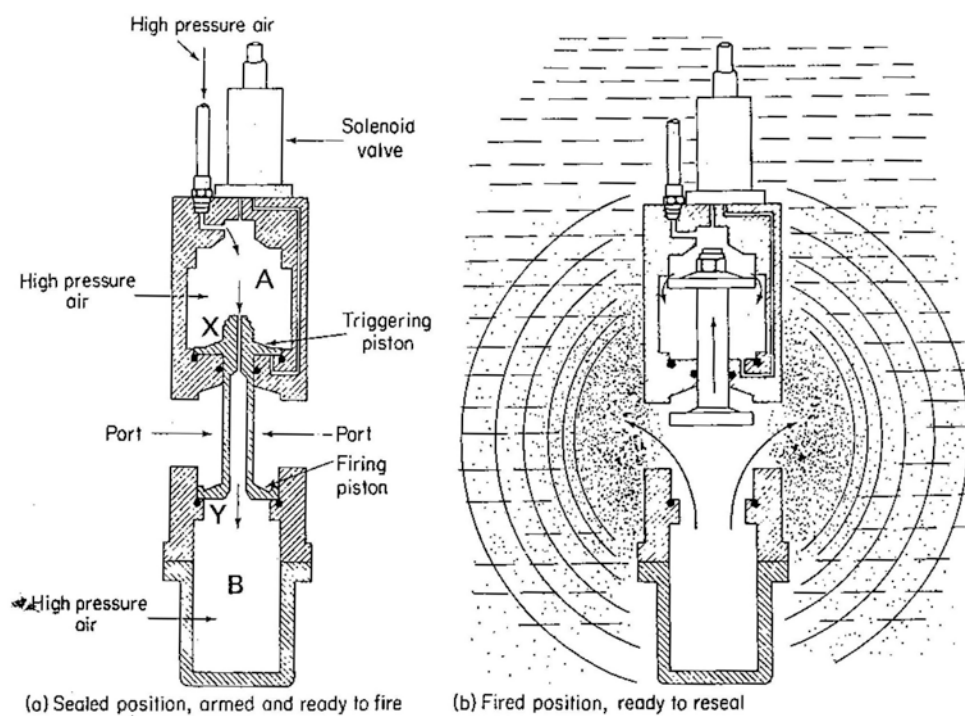

Fig. B. Air gun seismic source (from *Marine Geophysics*, E.J.W. Jones, 1999)

Streamer cable

The signal receiver used in MCS surveys is a streamer cable. This is an array of hydrophones spaced at intervals of several meters. Hydrophones are generally made from a piezoelectric material. Pressure changes in the water generate small currents in the transducer circuit. Transducer shapes are varied, and include spheres, end-capped tubes, and fine wires with sensitivities varying within the frequency range of $10 - 1000$ Hz. A streamer cable is divided into sections, with a series of hydrophones comprising a 'channel'. Analog data are transmitted through the streamer cable to the recording system.

Recording system

A recording system consists of three main parts: a seismic recording system, a navigation system, and a data logger. Seismic reflection wave data from hydrophones are monitored and recorded by the seismic recording system. This recording system consists of filters, gain-range amplifiers, analogue-to-digital converter, and digital tape recorder components. A seismic reflection survey must also record longitude, latitude, and shot time. These data are based on a GPS navigation system. Aboard *Kairei* these navigation data are logged every 5 s (see below). During KR05-01 we used the Truetime GPS clock to log shot times.

Data acquisition parameters

<div align="center">

Table of Geometry

Vessel Reference Point to stern	76.7 m	
stern to gun offset	~30 m	(see problems)
gun depth	~10 m	(see problems)
stern to first hydrophone	~110 m	(see problems)
reel to stern	21.5 m	

</div>
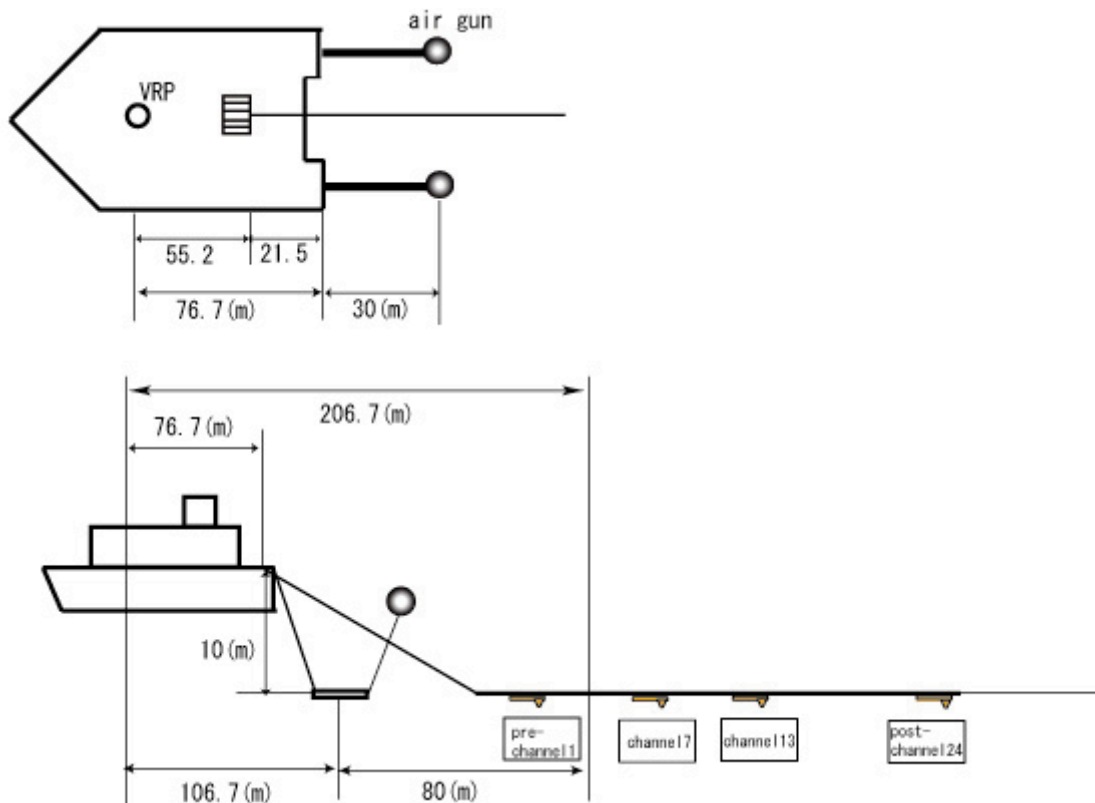
Fig. C. Location of equipment, VRP: Vessel Reference Point

Survey description and statistics

We completed the first N-S MCS transect of the Ontong Java Plateau, including two dip lines across the transition between the plateau and the adjacent Lyra Basin. In total, we obtained ~1100 km of MCS data. In addition, we conducted site surveys for proposed IODP sites ONT-1, ONT-2, ONT-3, and ONT-4. Around proposed drill site ONT-1, we acquired data on MCS lines Eastport, Moosehorn, Lubec, and Quoddy. Between ONT-1 and ONT-2, we obtained data along MCS line Roque. Around ONT-2 we obtained data on MCS lines Beals and Jonesport. Between ONT-2 to ONT-3, we acquired a cross line between MCS line 501 (KH98-01 Leg 2) and our Wass and Split lines. Between ONT-3 and ONT-4 we obtained data along seismic line Schoodic. Around ONT-4 we acquired data on seismic lines Prospect and Machias.
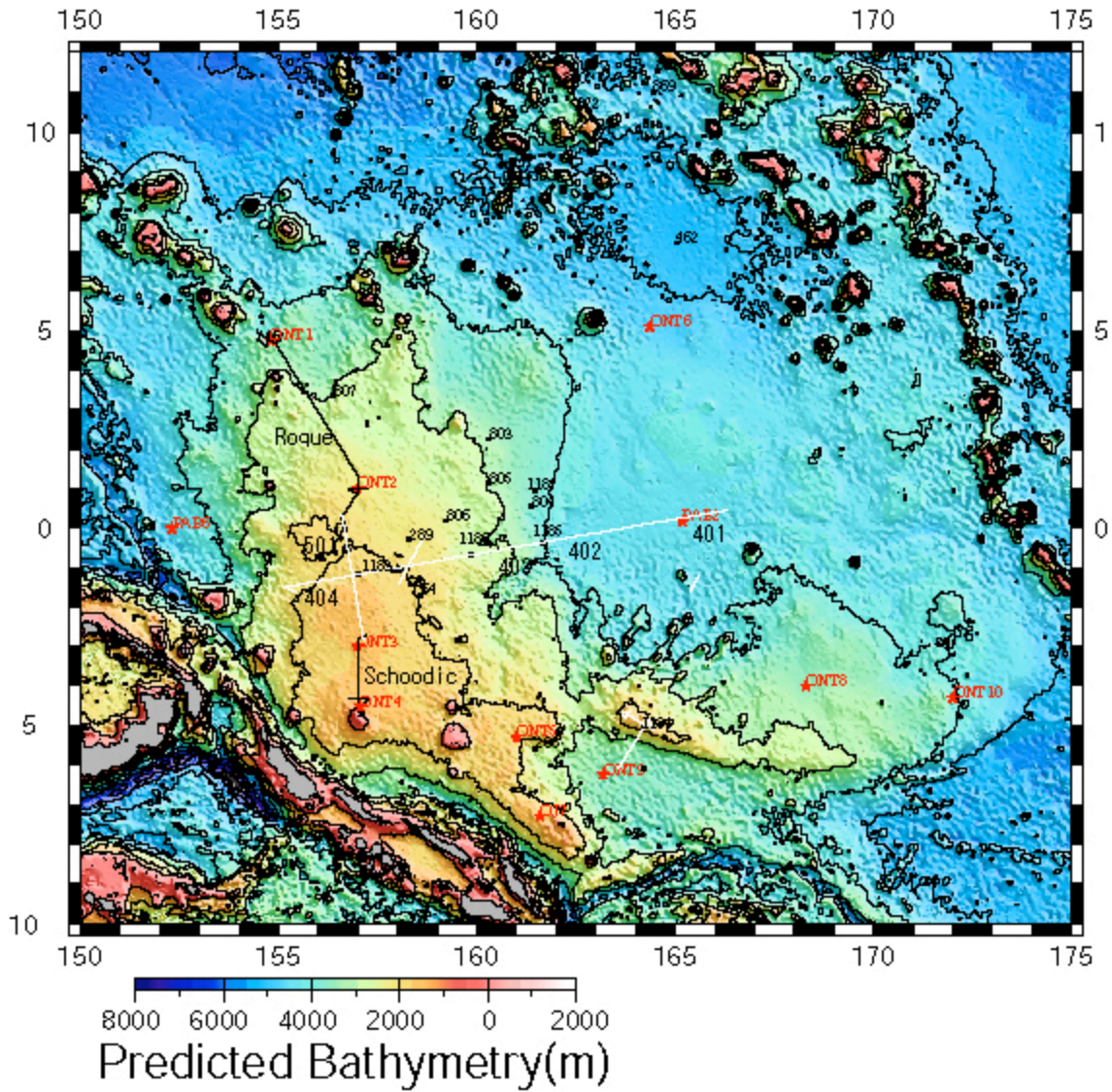
Fig. D. R/V *Kairei* KR05-01 MCS lines (black lines) and R/V *Hakuho Maru* KH98-1 Leg 2 MCS lines (white lines). Also shown are ODP/DSDP drilling sites (black circles) and proposed IODP drilling sites (red stars).
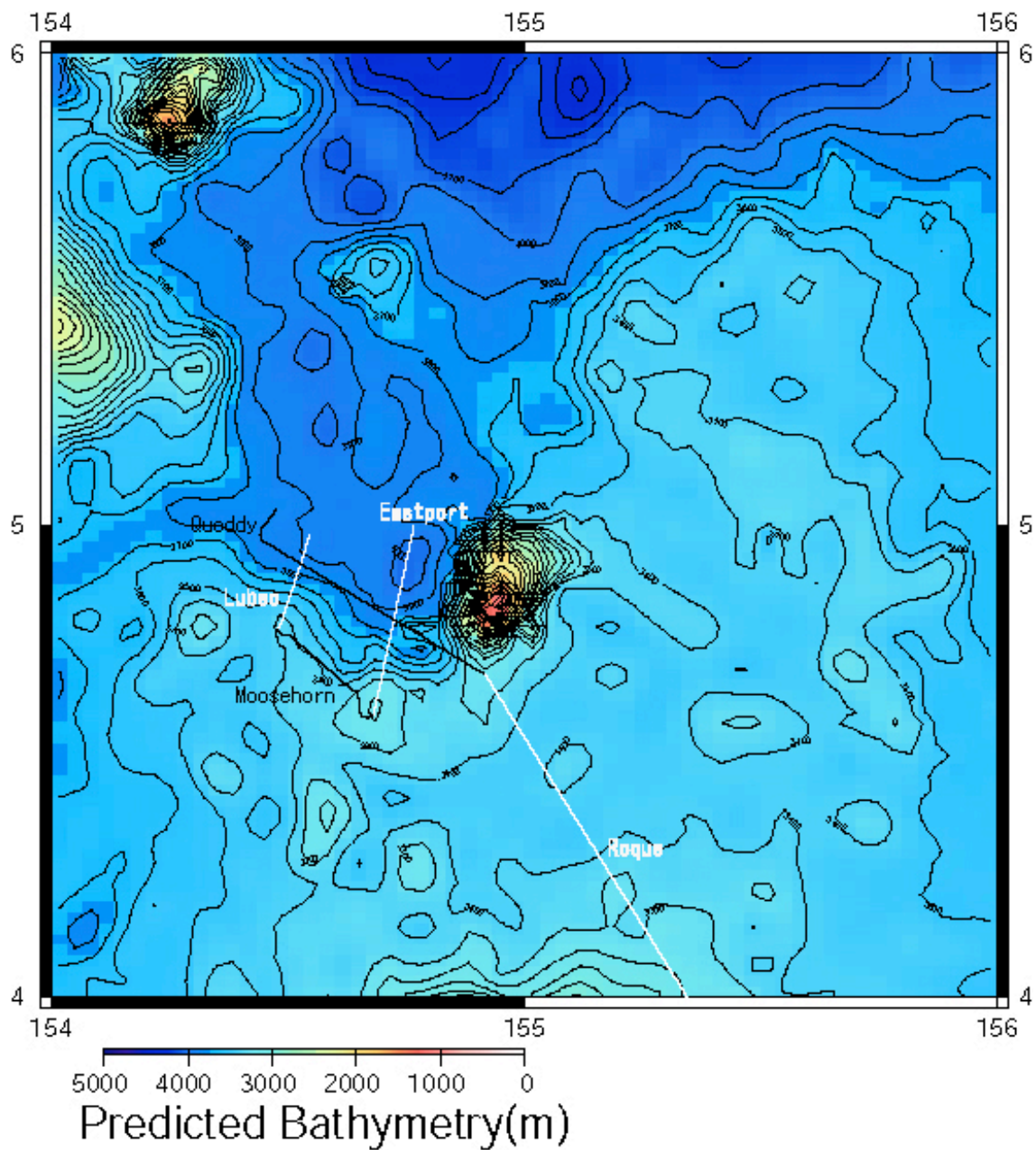
Fig. E. R/V *Kairei* KR05-01 MCS lines (black lines and white lines).
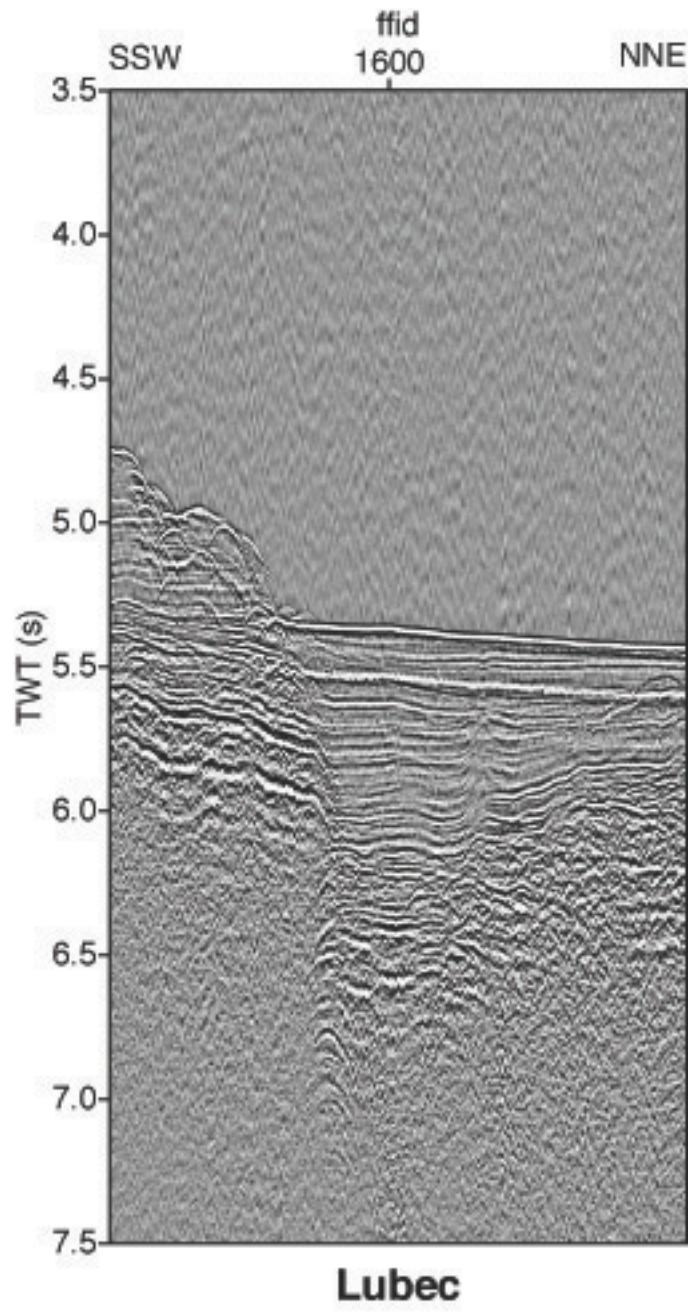
Figure F. Channel 2 plot of MCS line Lubec. See Figure E for location.
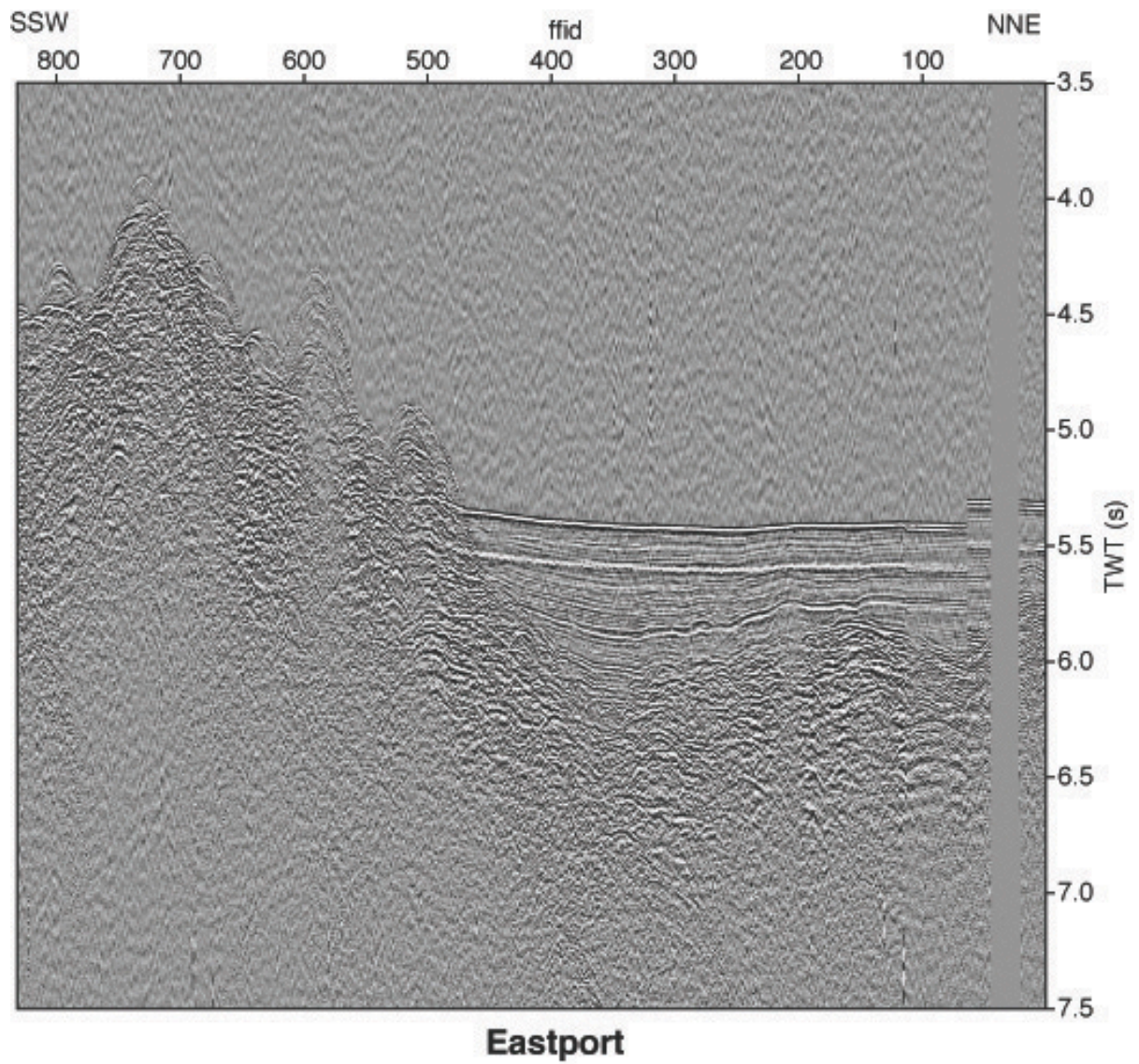
Figure G. Channel 2 plot of MCS line Eastport. See Figure E for location.
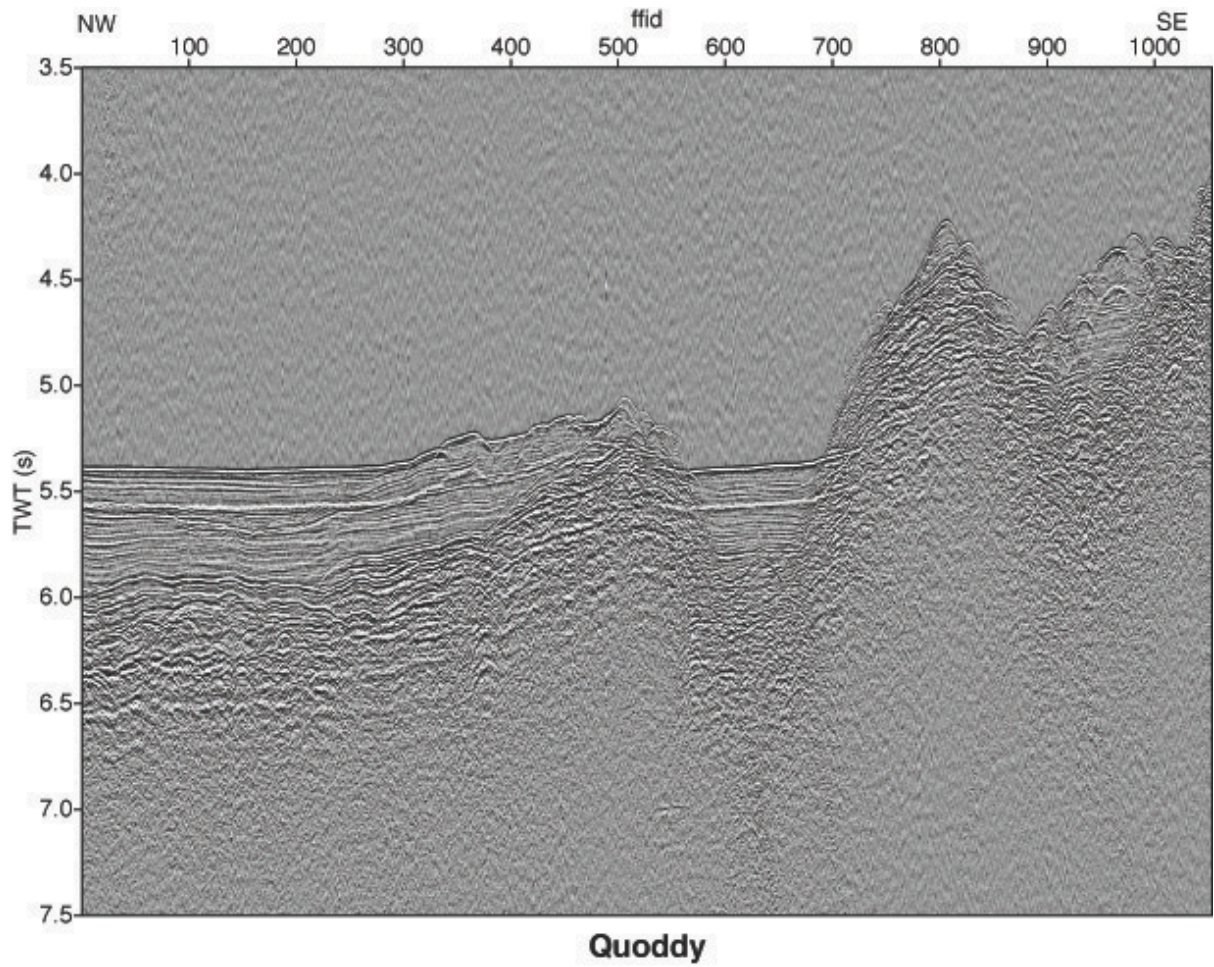
Figure H. Channel 2 plot of MCS line Quoddy. See Figure E for location.
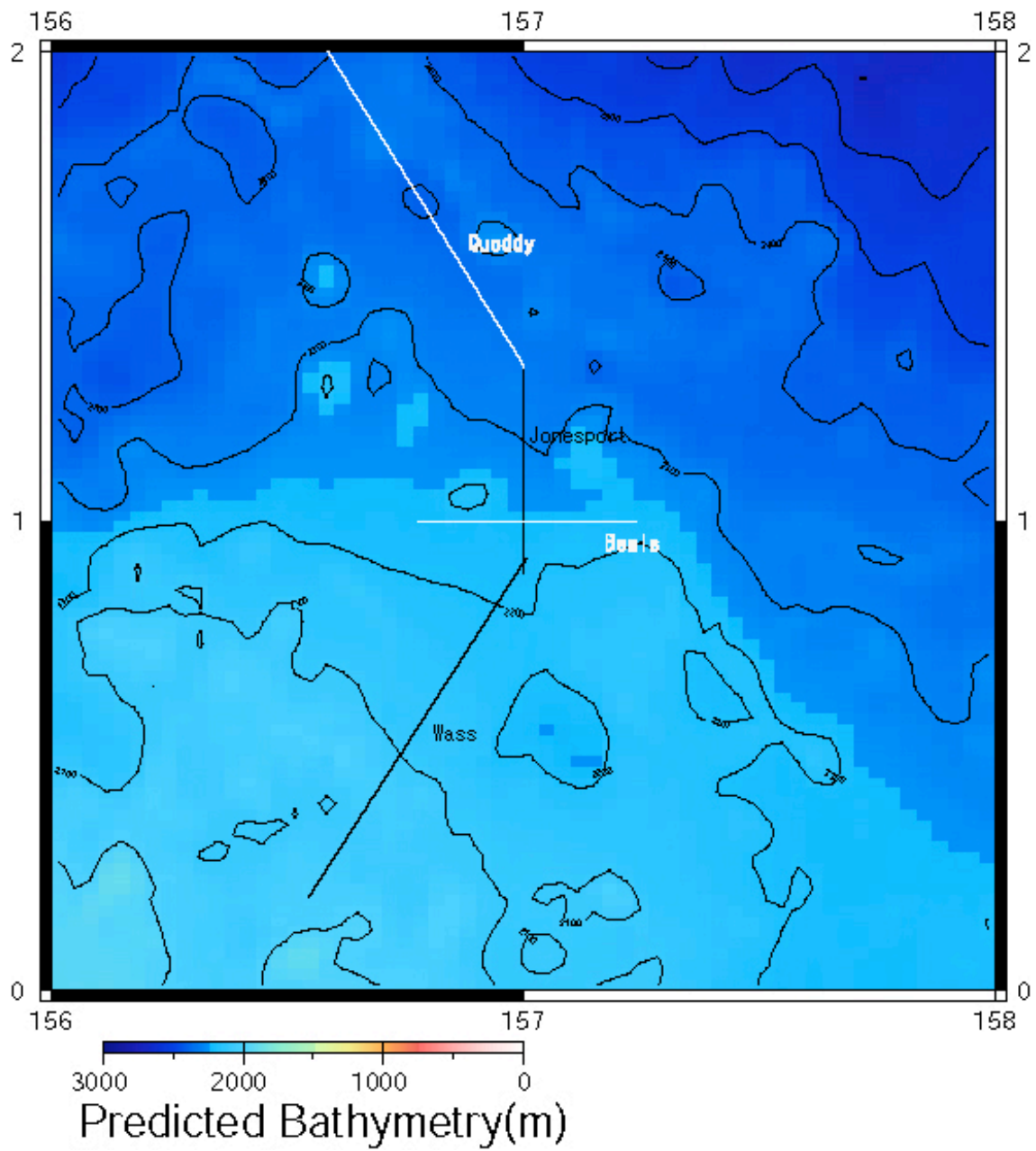
Fig. I. R/V Kairei KR05-01 MCS lines (black lines and white lines).
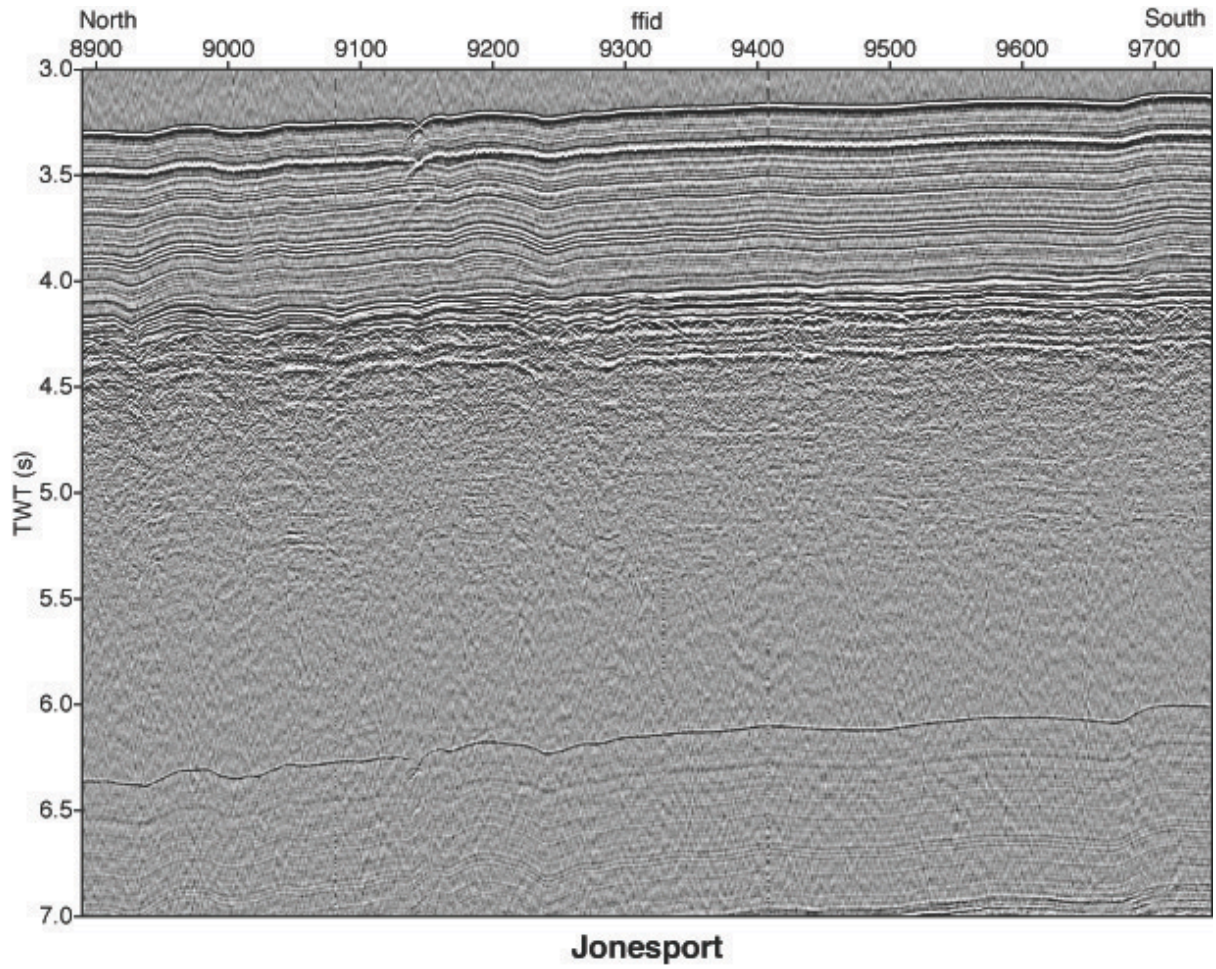
Figure J. Channel 2 plot of MCS line Jonesport. See Figure I for location.
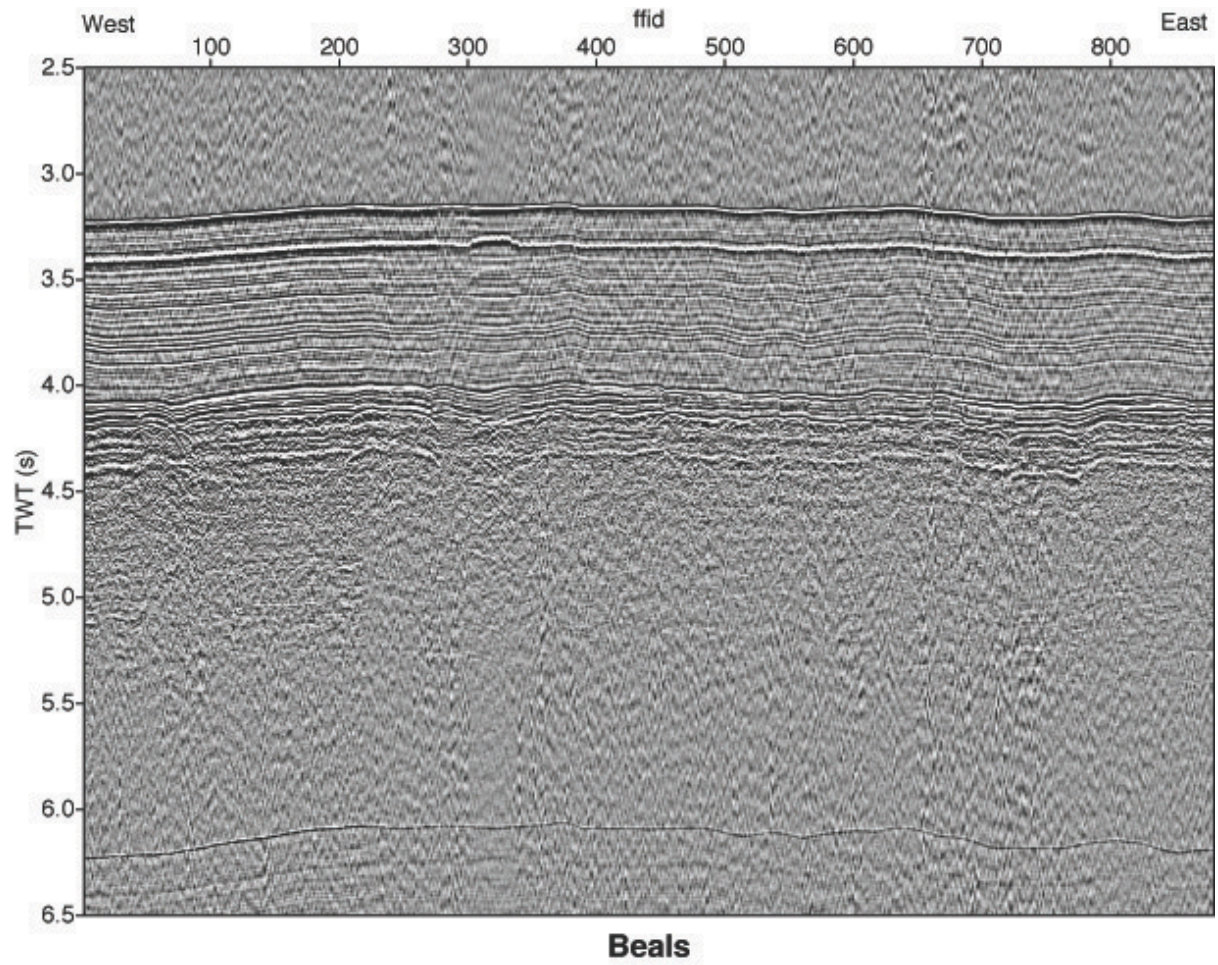
Figure K. Channel 2 plot of MCS line Beals. See Figure I for location.
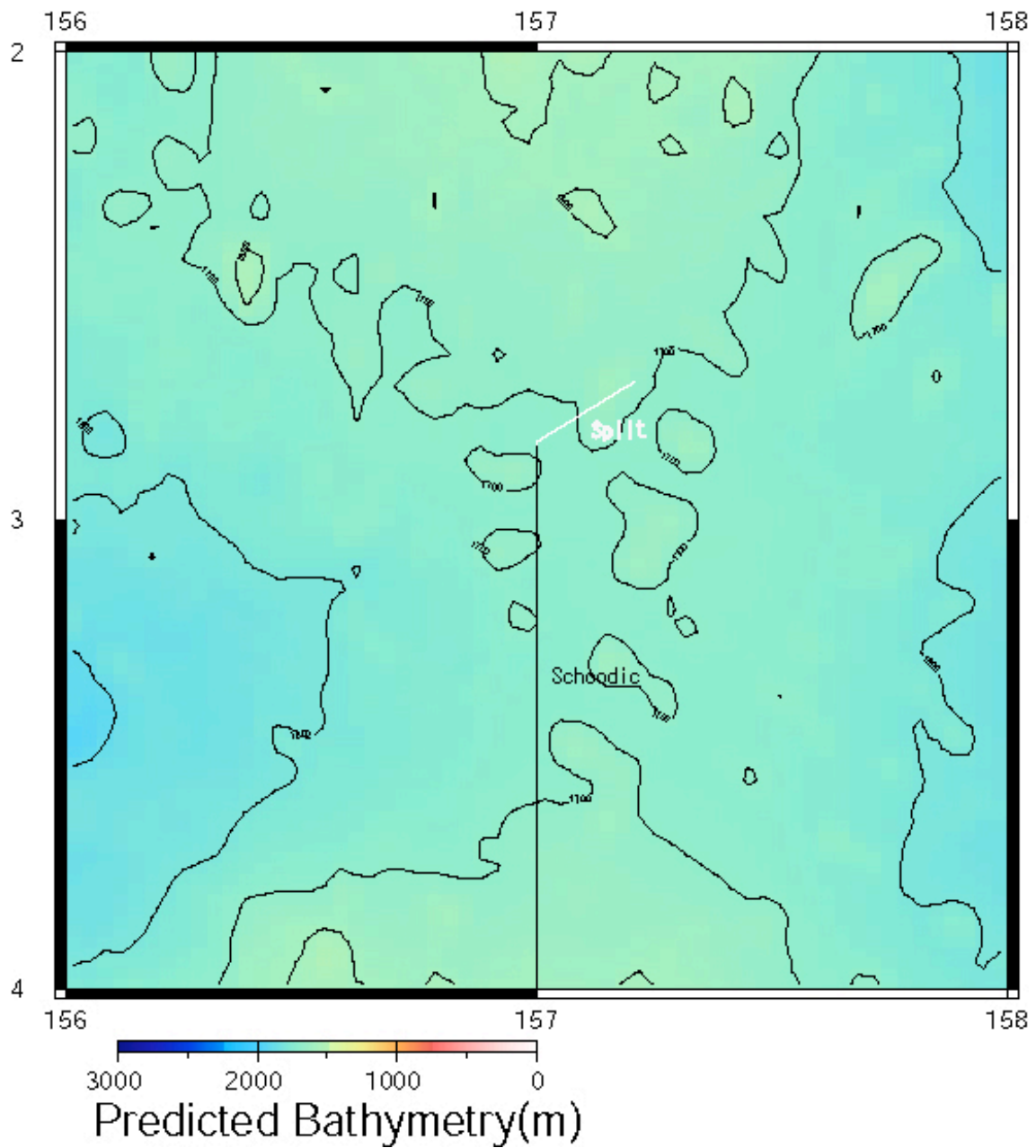
Fig. L. R/V *Kairei* KR05-01 MCS lines (black line and white line).
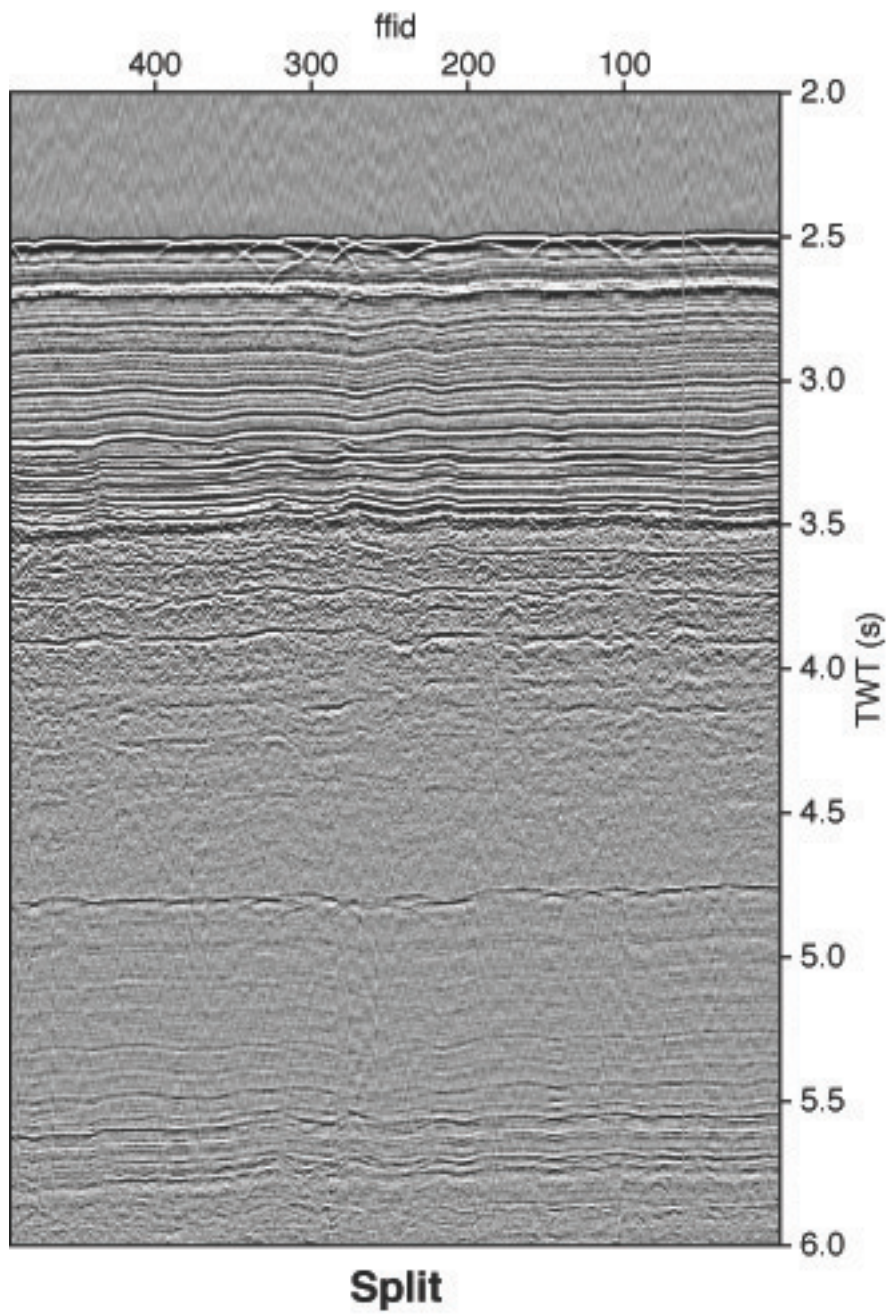
Figure M. Channel 2 plot of MCS line Split. See Figure L for location.
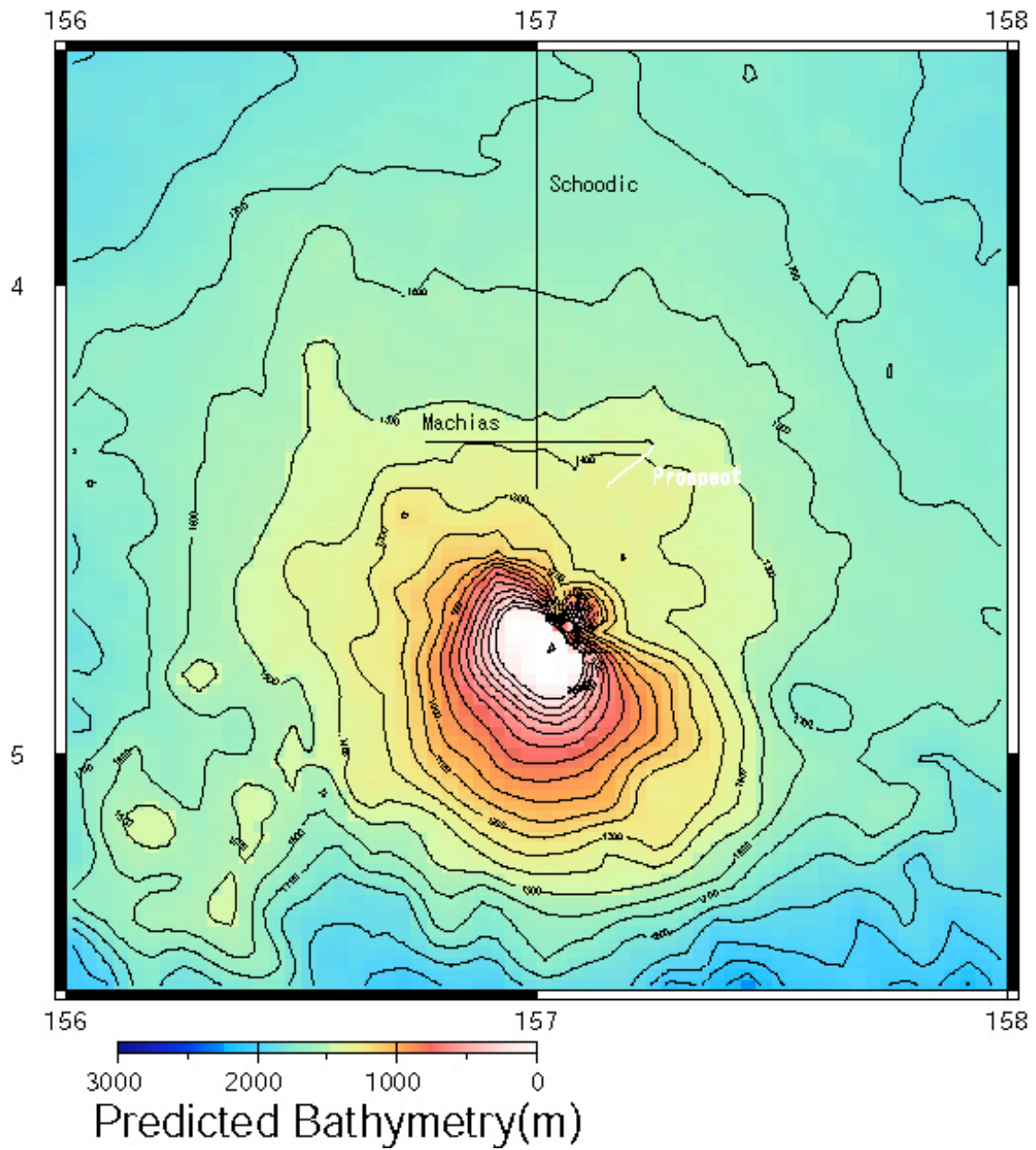
Fig. N. R/V *Kairei* KR05-01 MCS lines (black lines and white line).
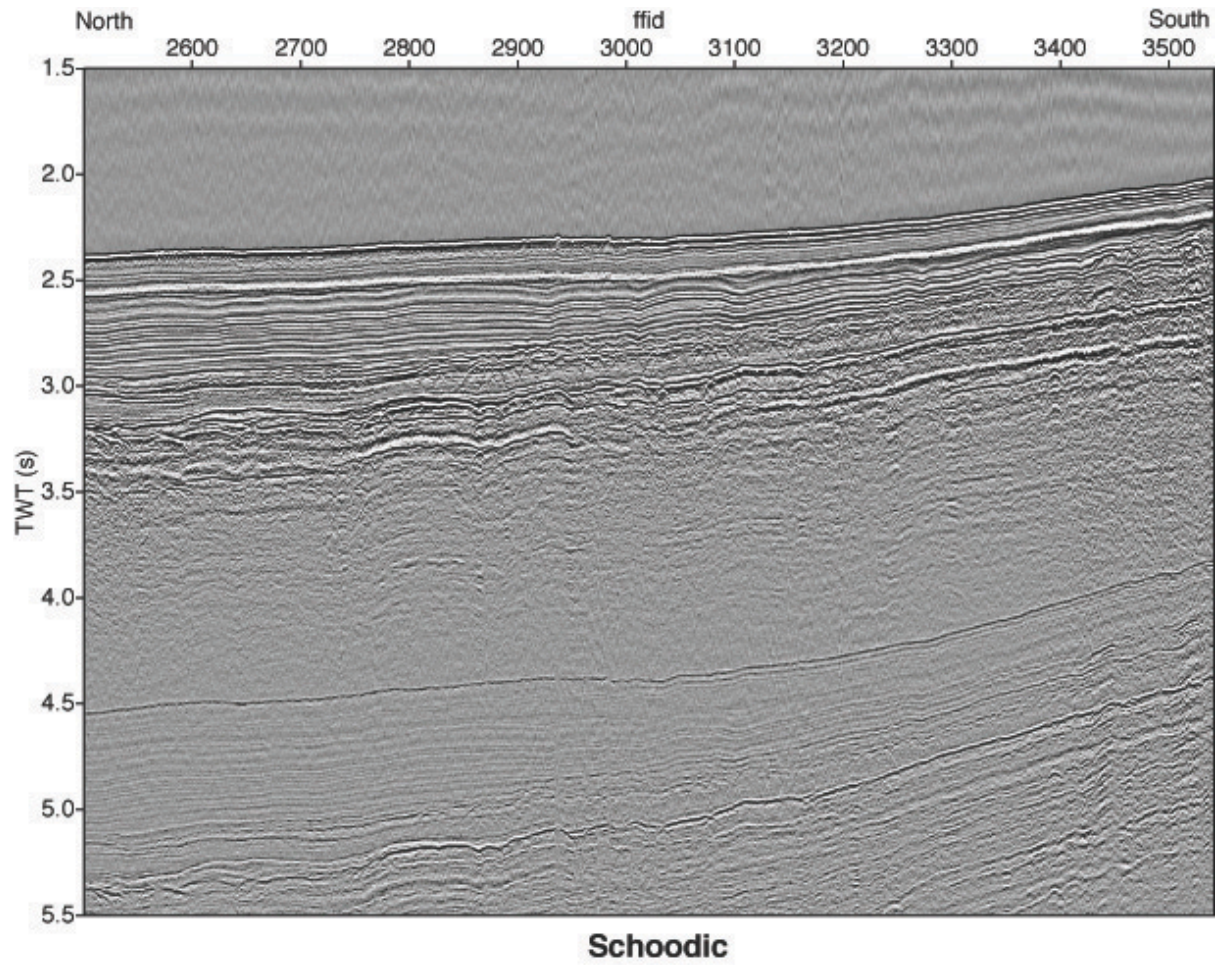
Figure O. Channel 2 plot of MCS line Schoodic. See Figure N for location.
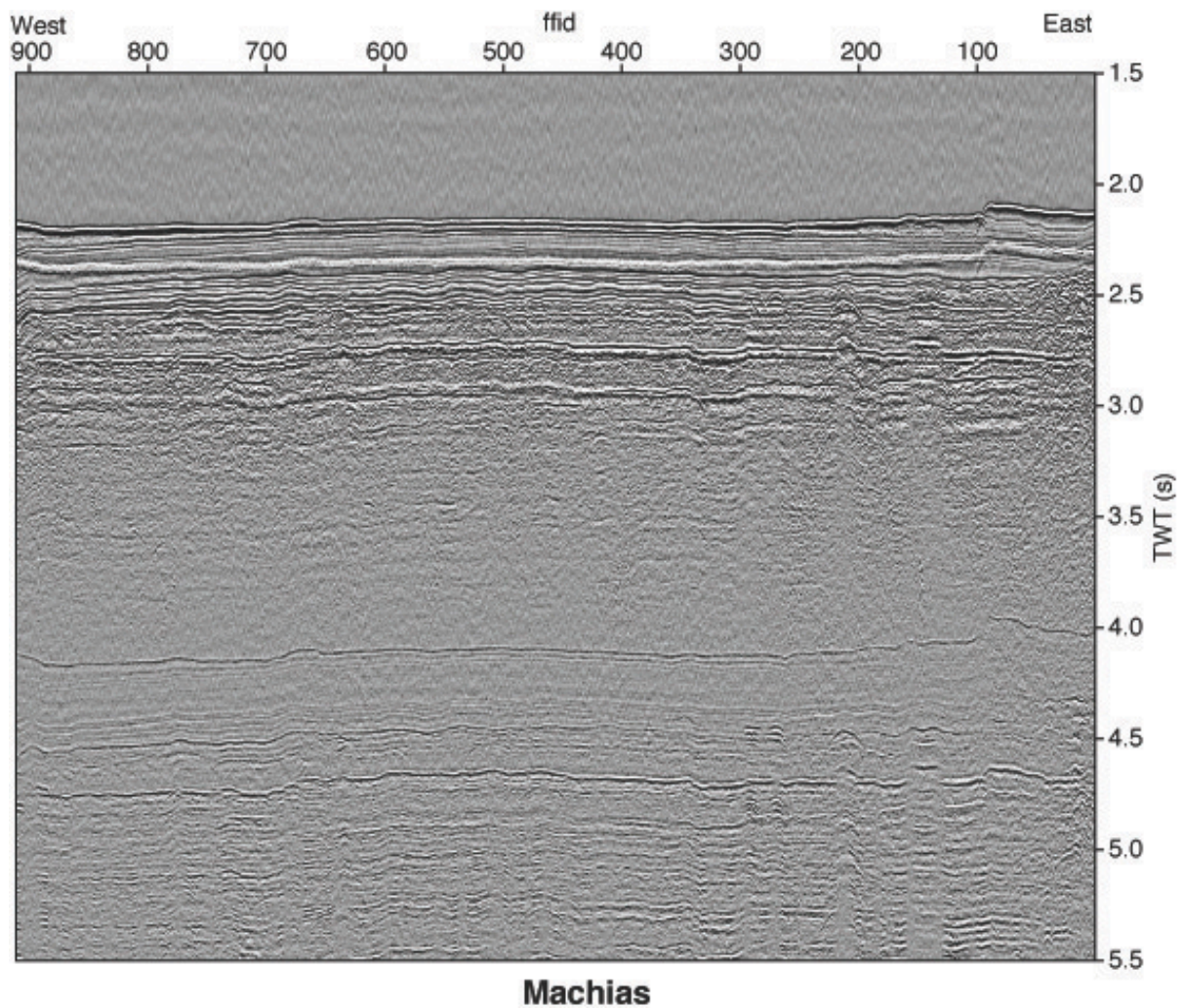
Figure P. Channel 2 plot of MCS line Machias. See Figure N for location.

Problems with the system

Cable operations

The streamer cable worked well except for channels 1, 5, 13, and 16. Channels 5 and 16 had not been working prior to KR05-01, but during the cruise channel 5 worked intermittently. Channels 1 and 16 were noisy during KR05-01. Channel 13 worked during lines Split, Schoodic, Prospect and Machias. We thought this may be related to current speed, but we don't have a good answer for the problem. Distance from the stern of the ship to the center of the first receiver channel couldn't be checked during the survey. We assume that the distance was about 80 m, but we must confirm the distance ashore.

Birds 1 and 3 did not communicate during lines Eastport, Moosehorn, and Lubec. It was difficult to control streamer depth during that time. After those lines, we tested and changed

these birds.

Ocean current speed during KR05-01 was sometimes high (maximum 1.2 knot), and it was difficult to control the depth of the streamer cable, but the quality of seismic data appeared to be good throughout the survey.

Air gun operations

Both Bolt 1500 LL air guns operated throughout KR05-01 except at ends of lines Jonesport, Beals, and Wass. Shot timing was observed on a DL1740 YOKOGAWA oscilloscope with 1 ms accuracy. At the end of line Jonesport, shot timing varied in the range of about 1-5 ms. At the end of line Beals, the port air gun's air hose developed n leak. We stopped shooting and retrieved it, and continued shooting only the starboard air gun. During line Wass the same air gun's air hose developed another leak and we continued shooting to the end of line Wass.

At the first instance of gun trouble, the air leaks developed because the air hose, the firing cable and the protective hose were chafed by a shackle during shooting (Fig. Q). We changed those, and reinforced the protecting hose, the stainless wire, and the tow harness with duct tape (Fig. R).

Between lines Beals and Wass we checked the starboard gun and discovered that the protective hose suffered from chafing against the tow harness shackle (Fig. S).   The firing cable and air hose inside the protective hose were not damaged. We reinforced the protective hose, the stainless wire, and the tow harness using duct tape.

At the second instance of gun trouble, we discovered a chafed air hose during between lines Wass and Split. This chafing was attributed entanglement of a stainless steel shackle and the retrieval wire. We changed the stainless steel shackle's orientation and reinforced the shackle with plastic tape (Fig. T).

Along the Split, Schoodic, Prospect and Machias lines, bubbles from the two air guns were not rising to the surface at the same time, but the oscilloscope indicated that the shooting times were synchronized. We must be careful when analyzing wave forms.

The distance between the air gun and a first active channel couldn't be detected with high accuracy. So, we must calculate the distance using direct waves, reflections from the seafloor, and XBT data after the cruise.

The air gun depth couldn't be detected with high accuracy, but the depth was about 10 m for our experience.

After the survey, we checked the starboard air gun, and detected that the key of the top housing was worn. (Fig. U)

Recording

We used the Geometrics Strata Visor NX system without significant trouble during the cruise. From the Eastport to Wass lines, we obtained 16 s of seismic reflection data, and from Split to Machias, we obtained 12 s of data. These data were monitored on the screen and immediately recorded onto DDS4 tapes.

Bird depths, wing angles, and temperature were logged by the SYNTRON controller. During the first part of the Schoodic line, these data weren't available.

Shot interval times were recorded by a PANASONIC Loox. But two different recordings were made by one shot because of the randomizer (about 200 ms interval). We couldn't understand the reason, and we must check the circuit to investigate how much delay was introduced.

Fig. Q. Ruptured protective sheath (left) and chafed firing line (right).

Fig. R. Reinforced protective sheath.

Fig. S. Ruptured protective air hose and firing line sheath.

Fig. T. Tangled retrieval wire and towing harness (left) and chafe-protected stainless steel snap shackle (right).
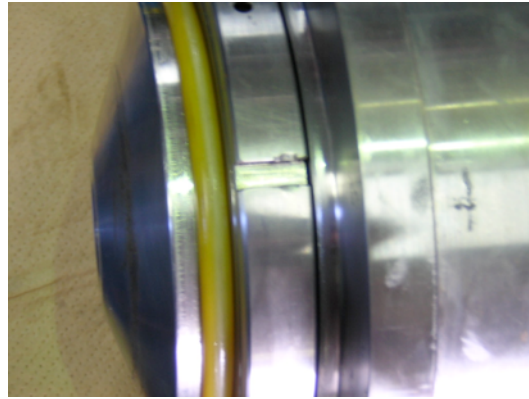
Fig. U. Worn key (left) and retainer (right).

KR05-01 Ontong Java Plateau MCS Line Summary

Streamer : ITI 600m   Source : 2xBolt 1500LL 25littres

Line	Area	course	Length	shot interva	Record length	start time (UTC)	end time (UTC)	start tape/file	end tape/file	original Line
Eastport	ONT1	SSW	70km	20s	16s	10.2259	11.0337	Tape1/1	Tape1/831	B-1
Moosehorn	ONT1	WNW	33km	20s	16s	11.0337	11.0651	Tape2/832	Tape2/1418	B-2
Lubec	ONT1	NNE	23km	20s	16s	11.0651	11.0858	Tape2/1419	Tape2/1793	B-3
Quoddy	ONT1	ESE	46km	20s	16s	11.1056	11.1750	Tape3/1	Tape3/1053	B-4
Roque	ONT1-ONT2	SE	440km	20s	16s	11.1750	13.1327	Tape3/1054	Tape5b/8889	A-1
Jonesport	ONT2	S	48km	20s	16s	13.1327	13.1812	Tape5b/8890	Tape5b/9743	A-1
Beals	ONT2	E	52km	20s	16s	13.2139	14.0232	Tape6/2	Tape6/880	C
Wass	ONT2-501	SW	96km	20s	16s	14.0624	14.1659	Tape7/1	Tape7/1906	A-1
Split	501-ONT3	SW	28km	20s	12s	15.0929	15.1213	Tape9/1	Tape9/492	A-2
Schoodic	ONT3-ONT4	S	177km	20s	12s	15.1213	16.0509	Tape9/493	Tape9/3541	A-2
Prospect	ONT4	NE	15km	20s	12s	16.0751	16.0923	Tape10/4027	Tape10/4305	I
Machias	ONT4	W	54km	20s	12s	16.0934	16.1437	Tape11/1	Tape11/911	E

KR05-01 Ontong Java Plateau MCS Tape Summary

Format: SEGD 8058

Tape No.	first file No	last file No	date.time for FF	date.time for LF	record length	sampling interval	Line name	original Line name	remarks
Tape 1	1	831	10.2259	11.0335	16s	2ms	Eastport	B-1	
Tape 2	832	1793	11.0336	11.0856	16s	2ms	Moosehorn, Lubec	B-2, B-3	
Tape 3	1	4000	11.1159	12.1012	16s	2ms	Quoddy, Roque	B-4, A-1	
Tape 4	4001	8000	12.1013	13.0826	16s	2ms	Roque	A-1	
Tape 5	8001	8230	13.0826	13.0942	16s	2ms	Roque	A-1	stopped by program down
Tape 5b	6254	6256	13.0946	13.0946	16s	2ms	Roque	A-1	misnumbered
	8231	9744	13.0948	13.1812	16s	2ms	Roque,Jonesport	A-1	
Tape 6	2	880	13.2139	14.0231	16s	2ms	Beals	C	file #1 is for test
Tape 7	1	1906	14.0624	14.1659	16s	2ms	Wass	A-1	file #1907 is for test
Tape 8	-	-	-	-	-	-	-	-	no data
Tape 9	1	3541	15.0929	16.0544	12s	2ms	Split, Schoodic	A-2	
Tape 10	4027	4305	16.0544	16.0923	12s	2ms	Prospect	I	
Tape 11	1	911	16.0934	16.1437	12s	2ms	Machias	E	file #912 is for test

KR05-01 Seismic Acquisition Recording Parameters

Line	Eastport (B-1)
Survey Number	KR05-01
Vessel	R/V KAIREI
Area	Ontong Java Plateau (ONT-1)
Sampling Interval	2.0 ms
Sampling Length	16.0 ms
Channel Interval Length	25 m
Common Mid Point	12.5 m
Seismic Channel	24 channel (1,16 dead)
First Group Offset	1 channel
Shot Interval	20 s
Ship Speed	nominal 5.5 kts
Air Gun Name/number	1500 LL/2
Air Gun Depth	normal 10 m
Randomizer	YES
Location of Birds	pre-1,7,13, post-24
Tail Rope Length	200 m
GPS Antenna to Stern Distance	76.7 m
Air gun to stern distance	30 m
Low Cut Filter	NO
High Cut Filter	NO

KR05-01 Seismic Reflection Line Log

Line	Eastport (B-1)
Vessel	R/V KAIREI
Area	Ontong Java Plateau
Survey Number	KR05-01

LINE INFORMATION	Time (UTC)	Shot Number	Tape Number
Acquisition Start	1/10　22:59	1	1
Acquisition End	1/11　03:37	831	1

LINE DETAILS	Start of Line (FSP)	End of Line (LSP)
Latitude	4° 59.886'N	4° 35.807'N
Longitude	154° 45.971'E	154° 40.767'E
Water Depth(m)	3891	3224
Log/Sog Speed (Knot)	5.3/5.2	5.9/5.4

UNDERWAY GEOPHYSICAL DATA	
SeaBeam	YES
Sub Bottom Profiler	YES
Gravity	YES
Shipboard vector anomaly magnetometer	YES

COMMENTS

Bird 3: dead

Introduce randomizer (shot point 61)

KR05-01 Seismic Acquisition Recording Parameters

Line	Moosehorn (B-2)
Survey Number	KR05-01
Vessel	R/V KAIREI
Area	Ontong Java Plateau (ONT-1)
Sampling Interval	2.0 ms
Sampling Length	16.0 ms
Channel Interval Length	25 m
Common Mid Point	12.5 m
Seismic Channel	24 channel (1.16 dead)
First Group Offset	1 channel
Shot Interval	20 s
Ship Speed	nominal 5.5 kts
Air Gun Name/number	1500 LL/2
Air Gun Depth	normal 10 m
Randomizer	YES
Location of Birds	pre-1,7,13, post-24
Tail Rope Length	200 m
GPS Antenna to Stern Distance	76.7 m
Air gun to stern distance	30 m
Low Cut Filter	NO
High Cut Filter	NO

KR05-01 Seismic Reflection Line Log

Line	Moosehorn (B-2)
Vessel	R/V KAIREI
Area	Ontong Java Plateau
Survey Number	KR05-01

LINE INFORMATION	Time (UTC)	Shot Number	Tape Number
Acquisition Start	1/11 03:37	832	2
Acquisition End	1/11 06:51	1418	2

LINE DETAILS	Start of Line (FSP)	End of Line (LSP)
Latitude	4° 35.807'N	4° 47.021'N
Longitude	154° 40.767'E	154° 28.802'E
Water Depth (m)	3224	3419
Log/Sog Speed (Knot)	5.7/5.6	5.3/5.6

UNDERWAY GEOPHYSICAL DATA	
SeaBeam	YES
Sub Bottom Profiler	YES
Gravity	YES
Shipboard vector anomaly magnetometer	YES

COMMENTS

Birds 1 and 3: dead

KR05-01 Seismic Acquisition Recording Parameters

Line	Lubec (B-3)
Survey Number	KR05-01
Vessel	R/V KAIREI
Area	Ontong Java Plateau (ONT-1)
Sampling Interval	2.0 ms
Sampling Length	16.0 ms
Channel Interval Length	25 m
Common Mid Point	12.5 m
Seismic Channel	24 channel (1.16 dead)
First Group Offset	1 channel
Shot Interval	20 s
Ship Speed	Nominal 5.5 kts
Air Gun Name/number	1500 LL/2
Air Gun Depth	normal 10 m
Randomizer	YES
Location of Birds	pre-1,7,13, post-24
Tail Rope Length	200 m
GPS Antenna to Stern Distance	76.7 m
Air gun to stern distance	30 m
Low Cut Filter	NO
High Cut Filter	NO

Line	Lubec (B- 3)
Vessel	R/V KAIREI
Area	Ontong Java Plateau
Survey Number	KR05-01

LINE INFORMATION	Time (UTC)	Shot Number	Tape Number
Acquisition Start	1/11 06:51	1418	2
Acquisition End	1/11 08:56	1791	2

LINE DETAILS	Start of Line (FSP)	End of Line (LSP)
Latitude	4° 47.028'N	4° 58.764'N
Longitude	154° 28.804'E	154° 32.760'E
Water Depth(m)	3419	3902
Log/Sog Speed (Knot)	4.8/5.8	4.2/5.3

UNDERWAY GEOPHYSICAL DATA	
SeaBeam	YES
Sub Bottom Profiler	YES
Gravity	YES
Shipboard vector anomaly magnetometer	YES

COMMENTS

Birds 1 and 3: dead

KR05-01 Seismic Acquisition Recording Parameters

Line	Quoddy (B-4)
Survey Number	KR05-01
Vessel	R/V KAIREI
Area	Ontong Java Plateau (ONT-1)
Sampling Interval	2.0 ms
Sampling Length	16.0 ms
Channel Interval Length	25 m
Common Mid Point	12.5 m
Seismic Channel	24 channel (1.16 dead)
First Group Offset	1 channel
Shot Interval	20 s
Ship Speed	Nominal 5.5 kts
Air Gun Name/number	1500 LL/2
Air Gun Depth	normal 10 m
Randomizer	YES
Location of Birds	pre-1,7,13, post-24
Tail Rope Length	200 m
GPS Antenna to Stern Distance	76.7 m
Air gun to stern distance	30 m
Low Cut Filter	NO
High Cut Filter	NO

KR05-01 Seismic Reflection Line Log

Line	Quoddy (B-4)
Vessel	R/V KAIREI
Area	Ontong Java Plateau
Survey Number	KR05-01

LINE INFORMATION	Time (UTC)	Shot Number	Tape Number
Acquisition Start	1/11 11:56	1	3
Acquisition End	1/11 17:30	1053	3

LINE DETAILS	Start of Line (FSP)	End of Line (LSP)
Latitude	5° 01.975'N	4° 41.023'N
Longitude	154° 28.537'E	154° 54.969'E
Water Depth(m)	3907	2892
Log/Sog Speed (Knot)	5.4/4.8	5.3/5.6

UNDERWAY GEOPHYSICAL DATA	
SeaBeam	YES
Sub Bottom Profiler	YES
Gravity	YES
Shipboard vector anomaly magnetometer	YES

COMMENTS

KR05-01 Seismic Acquisition Recording Parameters

Line	Roque (A-1)
Survey Number	KR05-01
Vessel	R/V KAIREI
Area	Ontong Java Plateau (ONT-1,2)
Sampling Interval	2.0 ms
Sampling Length	16.0 ms
Channel Interval Length	25 m
Common Mid Point	12.5 m
Seismic Channel	24 channel (1.5,13,16 dead)
First Group Offset	1 channel
Shot Interval	20 s
Ship Speed	Nominal 5.5 kts
Air Gun Name/number	1500 LL /2
Air Gun Depth	normal 10 m
Randomizer	YES
Location of Birds	pre-1,7,13, post-24
Tail Rope Length	200 m
GPS Antenna to Stern Distance	76.7 m
Air gun to stern distance	30 m
Low Cut Filter	NO
High Cut Filter	NO

KR05-01 Seismic Reflection Line Log

Line	Roque (A-1)
Vessel	R/V KAIREI
Area	Ontong Java Plateau
Survey Number	KR05-01

LINE INFORMATION	Time (UTC)	Shot Number	Tape Number
Acquisition Start	1/11 17:50	1054	3
Acquisition End	1/13 13:27	8889	5-B

LINE DETAILS	Start of Line (FSP)	End of Line (LSP
Latitude	4° 41.023'N	1° 19.249'N
Longitude	154° 54.963'E	156° 59.997'E
Water Depth(m)	2892	2291
Log/Sog Speed (Knot)	5.3/5.6	5.6/5.6

UNDERWAY GEOPHYSICAL DATA	
SeaBeam	YES
Sub Bottom Profiler	YES
Gravity	YES
Shipboard vector anomaly magnetometer	YES

COMMENTS

KR05-01 Seismic Acquisition Recording Parameters

Line	Jonesport (A-1)
Survey Number	KR05-01
Vessel	R/V KAIREI
Area	Ontong Java Plateau (ONT-1,2)
Sampling Interval	2.0 ms
Sampling Length	16.0 ms
Channel Interval Length	25 m
Common Mid Point	12.5 m
Seismic Channel	24 channel (1.5,13,16 dead)
First Group Offset	1 channel
Shot Interval	20 s
Ship Speed	nominal 5.5 kts
Air Gun Name/number	1500 LL /2
Air Gun Depth	normal 10 m
Randomizer	YES
Location of Birds	pre-1,6-7,12-13, post-24
Tail Rope Length	200 m
GPS Antenna to Stern Distance	76.7 m
Low Cut Filter	NO
High Cut Filter	NO
Air gun to stern distance	30 m

KR05-01 Seismic Reflection Line Log

Line	Jonesport (A-1)
Vessel	R/V KAIREI
Area	Ontong Java Plateau
Survey Number	KR05-01

LINE INFORMATION	Time (UTC)	Shot Number	Tape Number
Acquisition Start	1/13 13:27	8890	5-B
Acquisition End	1/13 18:12	9743	5-B

LINE DETAILS	Start of Line (FSP)	End of Line (LSP)
Latitude	1° 19.242'N	0° 53.325'N
Longitude	156° 59.997'E	157° 00.003'E
Water Depth(m)	2291	2158
Log/Sog Speed (Knot)	5.4/5.5	5.6/5.2

UNDERWAY GEOPHYSICAL DATA	
SeaBeam	YES
Sub Bottom Profiler	YES
Gravity	YES
Shipboard vector anomaly magnetometer	YES

COMMENTS

Data acquisition stopped between shots 8230 to 8231 (tape 5-A)

KR05-01 Seismic Acquisition Recording Parameters

Line	Beals (C)
Survey Number	KR05-01
Vessel	R/V KAIREI
Area	Ontong Java Plateau (ONT-2)
Sampling Interval	2.0 ms
Sampling Length	16.0 ms
Channel Interval Length	25 m
Common Mid Point	12.5 m
Seismic Channel	24 channel (1.5,13,16 dead)
First Group Offset	1 channel
Shot Interval	20 s
Ship Speed	Nominal 5.5 kts
Air Gun Name/number	1500 LL /2→ 1
Air Gun Depth	normal 10 m
Randomizer	YES
Location of Birds	pre-1,7,13, post-24
Tail Rope Length	200 m
GPS Antenna to Stern Distance	76,7 m
Air gun to stern distance	30 m
Low Cut Filter	NO
High Cut Filter	NO

KR05-01 Seismic Reflection Line Log

Line	Beals (C)
Vessel	R/V KAIREI
Area	Ontong Java Plateau
Survey Number	KR05-01

LINE INFORMATION	Time (UTC)	Shot Number	Tape Number
Acquisition Start	1/13 21:39	1	6
Acquisition End	1/14 02:32	880	6

LINE DETAILS	Start of Line (FSP)	End of Line (LSP)
Latitude	1° 00.003'N	0° 59.999'N
Longitude	156° 46.653'E	157° 13.999'E
Water Depth(m)	2230	2189
Log/Sog Speed (Knot)	5.3/5.6	5.4/5.8

UNDERWAY GEOPHYSICAL DATA	
SeaBeam	YES
Sub Bottom Profiler	YES
Gravity	YES
Shipboard vector anomaly magnetometer	YES

COMMENTS

Air gun (port side) stopped shooting at shot 224; retrieved.

KR05-01 Seismic Acquisition Recording Parameters

Line	Wass (A-1)
Survey Number	KR05-01
Vessel	R/V KAIREI
Area	Ontong Java Plateau (ONT-2,501)
Sampling Interval	2.0 ms
Sampling Length	16.0 ms
Channel Interval Length	25 m
Common Mid Point	12.5 m
Seismic Channel	24 channel (1.5,13,16 dead)
First Group Offset	1 channel
Shot Interval	20 s
Ship Speed	Nominal 5.5 kts
Air Gun Name/number	1500 LL /1
Air Gun Depth	normal 10 m
Randomizer	YES
Location of Birds	pre-1,7,13, post-24
Tail Rope Length	200 m
GPS Antenna to Stern Distance	76,7 m
Air gun to stern distance	30 m
Low Cut Filter	NO
High Cut Filter	NO

Line	Wass (A-1)
Vessel	R/V KAIREI
Area	Ontong Java Plateau
Survey Number	KR05-01

LINE INFORMATION	Time (UTC)	Shot Number	Tape Number
Acquisition Start	1/14 6:24	1	7
Acquisition End	1/14 16:59	1906	7

LINE DETAILS	Start of Line (FSP)	End of Line (LSP)
Latitude	0° 54.231'N	0° 11.746'N
Longitude	157° 00.4280'E	156° 32.664'E
Water Depth(m)	2177	2031
Log/Sog Speed (Knot)	5.7/4.9	3.1/3.1

UNDERWAY GEOPHYSICAL DATA	
SeaBeam	YES
Sub Bottom Profiler	YES
Gravity	YES
Shipboard vector anomaly magnetometer	YES

COMMENTS

Air gun (port side) stopped shooting at shot 1590, continued shooting with one gun to end of line.

KR05-01 Seismic Acquisition Recording Parameters

Line	Split (A-2)
Survey Number	KR05-01
Vessel	R/V KAIREI
Area	Ontong Java Plateau (501,ONT-3)
Sampling Interval	2.0 ms
Sampling Length	12.0 ms
Channel Interval Length	25 m
Common Mid Point	12.5 m
Seismic Channel	24 channel (1,5,16 dead)
First Group Offset	1 channel
Shot Interval	20 s
Ship Speed	Nominal 5.5 kts
Air Gun Name/number	1500 LL /2
Air Gun Depth	Variable (normal 10 m)
Randomizer	YES
Location of Birds	pre-1,7,13, post-24
Tail Rope Length	200 m
GPS Antenna to Stern Distance	76.7 m
Air gun to stern distance	30 m
Low Cut Filter	NO
High Cut Filter	NO

<p style="text-align: center;">KR05-01 Seismic Reflection Line Log</p>

Line	Split (A-2)
Vessel	R/V KAIREI
Area	Ontong Java Plateau
Survey Number	KR05-01

LINE INFORMATION	Time (UTC)	Shot Number	Tape Number
Acquisition Start	1/15 9:29	1	9
Acquisition End	1/15 12:13	492	9

LINE DETAILS	Start of Line (FSP)	End of Line (LSP)
Latitude	2° 42.306'S	2° 50.623'S
Longitude	157° 12.478'E	156° 59.940'E
Water Depth(m)	1692	1716
Log/Sog Speed (Knot)	4.9/5.7	4.7/4.8

UNDERWAY GEOPHYSICAL DATA	
SeaBeam	YES
Sub Bottom Profiler	YES
Gravity	YES
Shipboard vector anomaly magnetometer	YES

COMMENTS

The gun depth is variable

KR05-01 Seismic Acquisition Recording Parameters

Line	Schoodic (A-2)
Survey Number	KR05-01
Vessel	R/V KAIREI
Area	Ontong Java Plateau (ONT-3,4)
Sampling Interval	2.0 ms
Sampling Length	12.0 ms
Channel Interval Length	25 m
Common Mid Point	12.5 m
Seismic Channel	24 channel (1,5,16 dead)
First Group Offset	1 channel
Shot Interval	20 s
Ship Speed	nominal 5.5 kts
Air Gun Name/number	1500 LL /2
Air Gun Depth	variable (normal 10m)
Randomizer	YES
Location of Birds	pre-1,7,13, post-24
Tail Rope Length	200 m
GPS Antenna to Stern Distance	76.7 m
Air gun to stern distance	30 m
Low Cut Filter	NO
High Cut Filter	NO

KR05-01 Seismic Reflection Line Log

Line	Schoodic (A-2)
Vessel	R/V KAIREI
Area	Ontong Java Plateau
Survey Number	KR05-01

LINE INFORMATION	Time (UTC)	Shot Number	Tape Number
Acquisition Start	1/15 12:13	493	9
Acquisition End	1/16 05:09	3541	9

LINE DETAILS	Start of Line (FSP)	End of Line (LSP)
Latitude	2° 50.631'S	4° 25.963'N
Longitude	156° 59.940'E	156° 59.997'E
Water Depth(m)	1719	1344
Log/Sog Speed (Knot)	4.7/5.0	4.9/5.8

UNDERWAY GEOPHYSICAL DATA	
SeaBeam	YES
Sub Bottom Profiler	YES
Gravity	YES
Shipboard vector anomaly magnetometer	YES

COMMENTS

The gun depth is variable.

KR05-01 Seismic Acquisition Recording Parameters

Line	Prospect (I)
Survey Number	KR05-01
Vessel	R/V KAIREI
Area	Ontong Java Plateau (ONT-4)
Sampling Interval	2.0 ms
Sampling Length	12.0 ms
Channel Interval Length	25 m
Common Mid Point	12.5 m
Seismic Channel	24 channel (1,5,16 dead)
First Group Offset	1 channel
Shot Interval	20 s
Ship Speed	Nominal 5.5 kts
Air Gun Name/number	1500 LL /2
Air Gun Depth	Variable(normal 10 m)
Randomizer	YES
Location of Birds	pre-1,7,13, post-24
Tail Rope Length	200 m
GPS Antenna to Stern Distance	76.7 m
Air gun to stern distance	30 m
Low Cut Filter	NO
High Cut Filter	NO

Line	Prospect (I)
Vessel	R/V KAIREI
Area	Ontong Java Plateau
Survey Number	KR05-01

LINE INFORMATION	Time (UTC)	Shot Number	Tape Number
Acquisition Start	1/16 07:51	4023	10
Acquisition End	1/16 09:23	4305	10

LINE DETAILS	Start of Line (FSP)	End of Line (LSP)
Latitude	4° 25.638'S	4° 20.300'N
Longitude	157° 08.963'E	157° 14.742'E
Water Depth(m)	1311	1415
Log/Sog Speed (Knot)	4.7/5.0	4.9/5.8

UNDERWAY GEOPHYSICAL DATA	
SeaBeam	YES
Sub Bottom Profiler	YES
Gravity	YES
Shipboard vector anomaly magnetometer	YES

COMMENTS

The gun depth is variable.

KR05-01 Seismic Acquisition Recording Parameters

Line	Machias (E)
Survey Number	KR05-01
Vessel	R/V KAIREI
Area	Ontong Java Plateau (ONT-4)
Sampling Interval	2.0 ms
Sampling Length	12.0 ms
Channel Interval Length	25 m
Common Mid Point	12.5 m
Seismic Channel	24 channel (1,5,16 dead)
First Group Offset	1 channel
Shot Interval	20 s
Ship Speed	Nominal 5.5 kts
Air Gun Name/number	1500 LL /2
Air Gun Depth	Variable (normal 10 m)
Randomizer	YES
Location of Birds	pre-1,7,13, post-24
Tail Rope Length	200 m
GPS Antenna to Stern Distance	76.7 m
Air gun to stern distance	30 m
Low Cut Filter	NO
High Cut Filter	NO

KR05-01 Seismic Reflection Line Log

Line	Machias (E)
Vessel	R/V KAIREI
Area	Ontong Java Plateau
Survey Number	KR05-01

LINE INFORMATION	Time (UTC)	Shot Number	Tape Number
Acquisition Start	1/16 09:34	1	11
Acquisition End	1/16 14:37	912	11

LINE DETAILS	Start of Line (FSP)	End of Line (LSP)
Latitude	4° 19.996'S	4° 20.002'N
Longitude	157° 13.188'E	156° 45.976'E
Water Depth(m)	1418	1453
Log/Sog Speed (Knot)	5.4/5.1	5.3/5.3

UNDERWAY GEOPHYSICAL DATA	
SeaBeam	YES
Sub Bottom Profiler	YES
Gravity	YES
Shipboard vector anomaly magnetometer	YES

COMMENTS

The gun depth is variable.

Gravity Meter

(J. Sarayama)

Introduction to the system

The R/V *Kairei*'s Bodenseewerk KSS31 marine gravity meter system was used for shipboard gravity measurements during KR05-01. This system is installed in the gravity meter laboratory and consists of two main components, a platform containing a gyroscope and a gravity sensor, and an electronic circuit to determine gravity. According to the documents provided by the manufacturer, the GSS 30 gravity sensor subsystem includes the non-astatized spring-mass assembly as a basic gravity detector. The KT 31 stabilization subsystem consists of the platform and a vertical, electrically erected two-axis gyroscope. The platform stabilizes the gravity sensor for pitch and roll. This is a two-gimbal device with a two-axis gyroscope and two accelerometers. Each gimbal axis uses a DC-Torque Motor of the same size. Pitch and roll axis have an angular freedom of $\pm 40°$ each.

Gravity data were sampled every minute. During KR05-01, ship speed was about 5.5 kts and 15 kts during the MCS survey and underway geophysical survey, respectively. Therefore, differences in data density resulted, i.e., during the MCS survey, data were sampled about every 170 m, but during underway geophysical surveying, data were sampled about every 460 m.

We employed the data filter ' Seastate 2 ' for the cruise, which provides for accurate, smooth data, but which requires a delay of 76 s. When ship is in port, the data filter 'Seastate 4' will be employed. So these filters are made a choice for a state of ship's orientation.

Observed gravity data were corrected in near-real-time by the gravity meter system. Ship's position, speed, and heading derived from GPS data were used to calculate the Eotvos correction, free-air anomaly and Bouguer anomaly. The data were stored on magneto-optical media.

Gravity data were recorded from 2005/1/6/22:05 to 2005/1/19/21:15 (UTC) in the survey area.

Date (UTC)	MCS surveying or underway geophysics
1/6/22:05-1/10/22:59	Underway geophysics
1/10/22:59-1/14/16:59	MCS surveying
1/14/16:59-1/15/9:00	Underway geophysics
1/15/9:00-1/16/15:05	MCS surveying
1/16/15:05-1/19/21:15	Underway geophysics

Data acquisition parameters

(a)   Eotvos correction

Gravity is a resultant force of terrestrial gravitation and centrifugal force; therefore observed shipboard gravity contains an error caused by centrifugal force. For example, if a ship travels from west to east, the influence of centrifugal force is greater than if the ship were stationary. In this case, observed gravity is less than actual gravity. This phenomenon is called the "Eotvos Effect", and the correction for it the "Eotvos correction". Positive correction for the Eotvos Effect is required when a ship runs west to east, and negative correction is required when a ship runs east to west.

Gravity data were used for pre-processing by the gravity meter system. The formula applied for the Etovos corrected gravity was given as:

$$Eg = G \cdot K + \Delta E$$

where G is a measured gravity in mgal; K is a gravity sensor constant; and ΔE is a Eotvos correction in mgal and is given as:

$$\Delta E = 7.507 \cdot V \cdot \sin \phi \cdot \cos \lambda + (0.064498062 \cdot V)^2$$

where V is ship's speed in knots in direction of course; λ is geographical latitude; and ϕ is real course of the ship.

b)   Free-air gravity anomaly

The free-air gravity anomaly is derived from the altitude of an observation position relative to the geoid. In case of a land gravity survey, this anomaly depends on topography. However, in the case of shipboard gravity, the sea surface is an equipotential surface approximately

equivalent to the geoid, because the difference between the sea surface and geoid is not significant (< 10 m).

The formula applied for the free-air anomaly, F, was given in the system as:

$$F = (G-Gh) \cdot K + Gabs - Gn + \Delta E$$

with: G = measured gravity (actual position); Gh = measured gravity (harbor); K = Gravity sensor constant; Gabs = absolute gravity (harbor); Gn = normal gravity (actual position)

For the normal gravity, Gn, the following formula was applied:

$$Gn = 978.03185 (1 + 0.005278895 \sin^2 \lambda + 0.000023462 \sin^4 \lambda)$$

c)   Bouguer anomaly

The Bouguer anomaly, B, was also calculated by the system. At sea, the anomaly is defined as:

$$B = F + Bk$$

where Bk is Bouguer correcton, and the following formula is applied:

$$Bk = \Delta \rho \cdot Gn \cdot T \cdot 4.25976 \cdot 10^{-8}$$

With: $\Delta \rho$ = density difference between crust and sea water (1.64); Gn = normal gravity; T = water depth

d)   Other parameters

A major source of error in shipboard gravity measurement is the accuracy of position and the Eotvos effect. If a position is accurately known, the Eotvos effect can be corrected readily. Therefore, GPS position data is important for determining gravity accurately.

Shipboard gravity data must be corrected using absolute gravity data from land. For KR05-01, the shipboard gravity data were corrected using absolute gravity values obtained at the JAMSTEC pier.

Correction data

Date (UTC)	KSS31 reading (mgal)	Absolute gravity (mgal)
2005/1/4 23:10:27	-1422.39	979758.3
2005/1/25 00:00:00	-0000.00	000000.0

After the survey, a drift correction will be performed. Gravity is determined at a base point, in this case the JAMSTEC pier, at the beginning and end of a survey. The difference between the beginning and end values is divided by time and applied linearly with time to the data. After the drift correction, the free-air anomaly must be recalculated.

The Bodenseewerk KSS31 marine gravity meter system in the gravity meter room. The platform of gyro and gravity detector, and an electronic circuit to measure gravity.

Proton Precession Magnetometer

(J. Sarayama)

Introduction to the system

A PRTO10 (Kawasaki Geological Engineering) proton precession magnetometer was used for total magnetic field measurements during R/V *Kairei* cruise KR05-01. The PRTO10 magnetometer consists of two parts, the sensor and the measurement device. The sensor was towed approximately 300 m behind the ship, to reduce the effect of the ship's magnetism. This length is triple that of *Kairei*. The measurement device was placed in *Kairei*'s dry laboratory, and measurement parameters such as measurement interval, charge time, etc., could be selected. Data were displayed on a personal computer and stored on its hard disk every 20 s, including date, time, longitude, latitude, water depth, and total magnetic field strength. Accuracy of the total magnetic field data is 0.1 nT.

Theory of operation

Most protons have a magnetic moment and precess in a magnetic field. The proton precession magnetometer (PPM) utilizes these characteristics. When a magnetic moment is in a magnetic field, B, the frequency of the precession, f, is expressed as:

$$B = \frac{2\pi}{\gamma_p} f \qquad (1) \quad (nT)$$

where γ_p is a gyromagnetic ratio. Hydrogen protons, contained in the sensor of the PPM, precess in the geomagnetic field. Therefore, an electric field is induced in the coil. The frequency of electric field's signal is detected. Total magnetic field strength is calculated using equation (1).

Data acquisition parameters

Raw magnetic data consist of a geomagnetic reference field strength and a magnetic anomaly. To produce a magnetic anomaly, we must find a   reference field and subtract this from total magnetic field strength. We use the International Geomagnetic Reference Field 2003 (IAGA, 2003) in our calculations.

Survey description and statistics

This survey was carried out from 2005/1/6/22:05 to 2005/1/19/21:15 (UTC), except when MCS data were being acquired.

Data on 2005/1/19 were noisy owing to severe weather. The drogue rope attached to the sensor was lost, and measurements were intermittent until a new drogue rope could be attached.

The sensor and cable of the PRTO10 proton precession magnetometer on deck aboard R/V *Kairei*.

Reference

International Association of Geomagnetism and Aeronomy (IAGA), Division V, Working Group 8, The 9th-Generation International Geomagnetic Reference Field, Geophy. J. Int., 155, 1051-1056, 2003

Shipboard Three-component Magnetometer (STCM)

(J. Sarayama)

Introduction to the system

The shipboard three-component magnetometer system (Tierra Tecnica SFG1214) was used for three-component magnetic measurements. The Tierra Tecnica SFG1214 is a three-axis flux-gate magnetometer. The sensors with ring-core coils are fixed on the open deck above *Kairei*'s bridge. The measurement device was located in the dry laboratory.

The outputs of the sensors were digitized and sampled at 8 Hz. The ship's heading, roll, and pitch data were also sampled at 8 Hz. The ship's heading data were provided from a gyro compass, located in the bridge for navigation. Roll and pitch data were provided from an attitude sensor placed on the floor of the gravity meter room. The ship's position (GPS data) and speed data were obtained through the local area network every second. These data were stored on the hard disk of personal computer and a magneto-optical disk in ASCII format.

These measurements were recorded from 2005/1/6/22:05 to 2005/1/19/21:15 (UTC) in the survey area.

Theory of operation

Flux-gate magnetometers measure one-component of the magnetic field using saturation magnetization. A core of ferromagnetic material is wrapped with a two coils and a sinusoidal current passes through one coil. The Tierra Tecnica SFG1214 uses a ring-shaped core. Due to saturation magnetization, an alternating current passes through the second coil. Magnetic field strength in the core's direction is detected by subtracting the original sine wave frequencies. As this instrument measures a magnetic field component in the direction of the core, a magnetic field vector measurement is possible using a three-axis flux-gate magnetometer, in which the three core axes are squared respectively.

Data acquisition parameters and problems with the system

The model equation assumed for STCM data is expressed as:

$$\vec{H}_{ob} = RPY\vec{F} + ARPY\vec{F} + \vec{H}_p \qquad (1)$$

where $\vec{H}_{ob}$ is the magnetic field vector observed by the STCM (in the ship's fixed

coordinate system); $\vec{F}$ is the ambient geomagnetic field vector (in the Earth's fixed coordinates); and *R, P* and *Y* are matrices of rotation due to roll, pitch, and yaw (heading), respectively and $\vec{H}_p$ the permanent magnetic field vector of the ship. *A* is the induced magnetization matrix.

Equation (1) is also written as:

$$RPY\vec{F} = B\,\vec{H}_{ob} - \vec{H}'_p$$
$$B = (A + I)^{-1} \qquad\qquad (2)$$
$$\vec{H}'_p = B\,\vec{H}_p$$

where *I* is the unit matrix.

The effect of ship magnetization is large when utilizing a shipboard magnetometer, as observed vectors contain the ship magnetization factors. These factors must be removed using figure-eight rotation data (Isezaki, 1986). A figure-eight rotation track is two circles (a pair of left and right turns), and several are needed at different latitudes (hence magnetic inclinations) to obtain accurate coefficients for components *B* and $\vec{H}_p$. If *B* and $\vec{H}_p$ are known, the magnetic field, $\vec{F}$, can be obtained by measuring *R*, *P*, *Y* and $\vec{H}_{ob}$. Assuming that $\vec{F}$ is equal to the International Geomagnetic Reference Field at a figure-eight rotation point, *B* and $\vec{H}_p$ can be determined and the ship magnetization factors can be estimated, allowing calculation of the magnetic field vector, $\vec{F}$ (X, Y, Z). X, Y, and Z consist of a geomagnetic reference field strength and a magnetic anomaly. To produce a magnetic anomaly, we must find the three components of the International Geomagnetic Reference Field (IGRF) and subtract these from components of magnetic field strength.
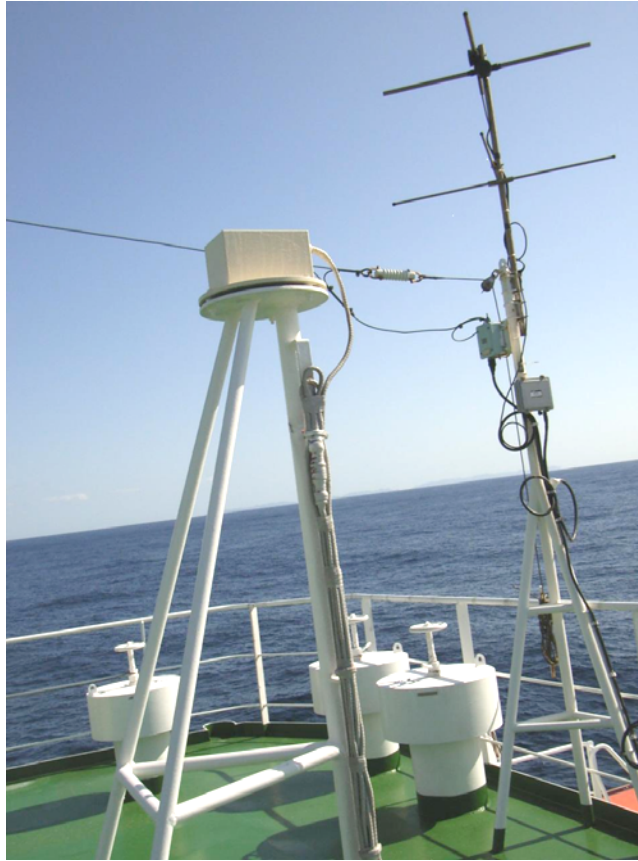
The sensors with ring-core coils of the Tierra Tecnica SFG1214 located on the open deck above *Kairei*'s bridge.

References

Isezaki, N., A new shipboard three component magnetometer, Geophysics, 51,1992-1998, 1986

International Association of Geomagnetism and Aeronomy (IAGA), Division V, Working Group 8, The 9th-Generation International Geomagnetic Reference Field, Geophy. J. Int., 155, 1051-1056, 2003